THE CHEMICAL SPECIATION OF POTENTIAL DERMALLY-ABSORBED COPPER-BASED ANTIINFLAMMATORY DRUGS

A Thesis submitted to the

UNIVERSITY OF CAPE TOWN

In fulfilment of the requirements for the degree of

DOCTOR OF PHILOSOPHY

By

LOMKHOSI MKHONTA-GAMA
B.Sc. (UNISWA), M.Sc. (UCT)

Department of Chemistry
University of Cape Town
Rondebosch
7701
South Africa

October 1999

CONTENTS Page

If anything worth doing is worth doing well
a life worth living, is worth living well

but if all hope for life is lost, is it ever too late to do anything
about the lost course of the many things

for which living is worth doing well?

Surely not! ☺

To my pillar of strength and courage-Leo, Mduduzi.
Thank-you ever so much for being there for me at all times.

ACKNOWLEDGEMENTS

The varied support of the following people during the course of this work is gratefully acknowledged.

- My supervisor Professor Graham E. Jackson for his guidance and surprisingly endless patience with me throughout my stay at UCT.

- Fellow occupants of office A121 for being themselves with me; Mr. James Maliekal, Mr. Shane Stone and Professor Phinda Songca.

- The staff and fellow students of the Chemistry Department of the University of Cape Town for giving me a sense of belonging.

- Dr. John Bacsa for helping me with the CSD.

- My close friends in the department for sharing FYT laughs with me; Winile Mavuso and Zoleka Mfono.

- My neighbour Ms. Brenda Modise for her inspiring motto " ntoa! ntoa! ntoa!..." ☺

- My daughter Nompumelelo for her company in these distant lands.

- My Teen Age friends for keeping in touch with me and believing in our lasting friendship; Thabi Magagula-Dlamini, Beauty Mazibuko-Chowa, Jabu Mthembu-Dlamini, Chris Xaba-Motsa, Nonkululeko Radebe-Dlamini, Zolile Ndlovu-Mamba, Gloria S'khondze-Manana, Naomi Tutu-Ngomane, Mprie Dlamini-Nxumalo, Goodness Nxumalo, Phumelele Fakudze, Cheryl Groening-Adams, Debbie Reid, Mariana Pullen...

- Members of my His People cell group, especially the leader Maria for not giving-up on me.

- Members of my family for their love for me; Bo-Make: Mafelokwakhe and Tfobhi, Bo-Bhuti: Mfanamkhonta, Mandla, Themba, Ambi, Zaa, Bhu, Vusi, Tutu and Gcina. Bo-Sisi: Lomathemba, Sgi, Nothando and Sanele. My nephews and nieces for their respect; Nosipho, Kelvin, Fano, Shiyabakhe, Thobile, Lindokuhle, Siboniso (Mfana), Sanele (Nana), Jabulisa and S'phamandla "president-Chiluba".

- Dr Shirley Churms for her excellent editorial contribution to this thesis.

- The University of Cape Town and the Foundation for Research Development for their financial support.

Abstract

It has been shown that increasing the amount of copper associated with low molecular weight ligands in plasma helps to alleviate the symptoms of rheumatoid arthritis (RA). Four low molecular weight ligands 1,13-*bis*(N,N-dimethyl)-5,9-dioxo-7-(N-benzyl)-1,4,7,10,13-pentaazatridecane (BID), its de-N-benzylated derivative (IDA), 1,13-*bis*(N,N-dimethyl)-5,9-dioxo-7-(N-phenethyl)-1,4,7,10,13-pentaazatridecane (DME) and its non-methylated derivative (EDA) were synthesised and characterised. The stability constants of their complexes with divalent copper, zinc and calcium complexes were determined at 25 °C in 0.15 mol dm^{-3} (Na)[Cl] by glass electrode potentiometry. The stability constants found for the copper complexes indicated that *in vitro* mobilisation of this metal ion was quite appreciable.

UV/VIS spectroscopy was used to investigate the structures of the different copper (II) solution species. Even though the degree of coordination of the different ligands varied, the coordination trend of the different species of the chemical models was similar as pH was increased from 2 to 11.

Molecular mechanics calculations were used to propose the geometry of the solution species based on the strain energy of each of the possible geometries. Out of four possible coordination geometries found, the one with the lowest strain energy was accepted as best representing the chemical systems at hand.

To investigate the feasibility of dermal absorption of the copper complexes of these ligands, octanol/water distribution coefficient experiments were performed the pH range 2 to 10.5. The results confirm that charge neutrality of a species is important for tissue solubility.

The superoxide radical the superoxide dismutase (SOD)-like activity of the copper complexes of these ligands was investigated. The results showed that the SOD-like activity of the present complex systems was too negligible for them to be considered as plausible SOD mimics.

GLOSSARY

5UM	N, N'-*bis*[(2-dimethylamino)-ethyl]ethanediamide
6UM	N, N'-*bis*[(2-dimethylamino)-propyl]ethanediamide
AMBER	A forcefield designed to handle molecular mechanics calculations associated with proteins and amino acids
BETA	ESTA task for initial estimates of stability constant values
BID	1,13-*bis*(N,N-dimethyl)-5,9-dioxo-7-N-benzyl-1,4,7,10,13-pentaazatridecane
BIOSYM	Molecular mechanics software package
BURT	ESTA task for calculating the titrant
DMARD	Disease modifying antirheumatic drugs
DME	1,13-*bis*(N,N-dimethyl)-5,9-dioxo-7-N-phenethyl-1,4,7,10,13-pentaazatridecane
Dtda	3,6,9-triazaundecanedioic acid
ECCLES	Evaluation of Constituent concentrations in Large Equilibrium Systems (a computer program)
EDA	1,4,7,10,13-pentaaza-5,9-dioxo-7-N-phenethyltridecane
ESFF	Extensible Systematic Forcefield
ESTA	Equilibrium simulation for Titration Analysis (a suite of computer programs)
ESTA2A/B	A module in ESTA program
GEP	abbr. Glass Electrode Potentiometry
IC50	Concentration of SOD-complex required to induce 50% inhibition of NBT reduction.
ZDA	1,13-*bis*(N,N-dimethyl)-5,9-dioxo-1,4,7,10,13-pentaazatridecane
INSIGHT	Molecular Mechanics program
ITIES	abbr. Interphase between Two Immiscible Electrolyte Solutions.
NBT	abbr. Nitroblue Tetrazolium
NSAID	abbr. Non-Steroidal Antiinflammatory Drugs
OBJE	ESTA task for optimising parameters with respect to emf

OBJT	ESTA task for optimising parameters with respect to reactant concentrations
P	Partition coefficient
P.M.I.	Plasma Mobilising Index
Plot Option 1	Used to obtain a observed protonation curve i.e. Observed Z_H
Plot Option 2	Used to obtain a calculated protonation curve i.e. Calculated Z_H
Plot Option 3	Used to obtain a observed complexation curve i.e. Observed Q and Z_M
Plot Option 4	Used to obtain a calculated complexation curve i.e. Calculated Q and Z_M
QBAR	ESTA task for calculating the deprotonation function
RA	abbr. Rheumatoid Arthritis
SMARD	abbr. Symptom Modifying Antirheumatic Drug
SOD	abbr. Superoxide Dismutase
TASK	Instruction card on ESTA input file
TOTL	ESTA task for calculating total concentration
Ttda	3,6,9,12-tetraazatetradecanedioic acid
VESL	ESTA task for calculating reactant concentration
ZBAR	ESTA task for calculating the formation function

LIST OF FIGURES AND TABLES

Tables

Structural Formulae of Other Ligands Discussed in this Study

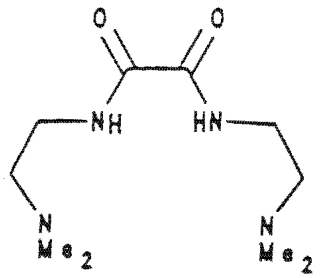

5UM

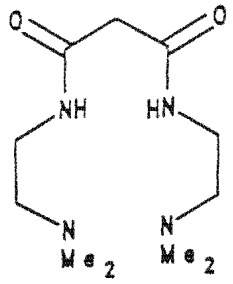

6UM

dien

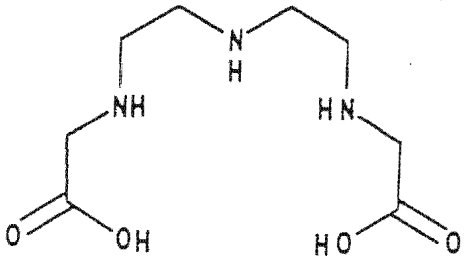

DTDA

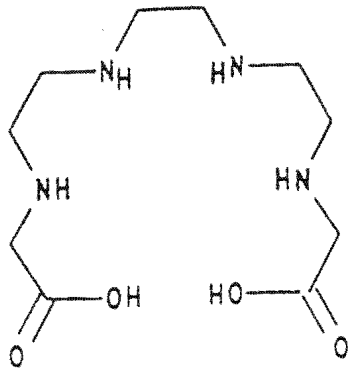

TTDA

CHAPTER ONE

1. INTRODUCTION

1.1 RHEUMATOID ARTHRITIS

Rheumatoid arthritis (RA) is a chronic inflammatory disease characterised by proliferative, erosive synovitis that erodes and destroys bone and cartilage (Aeschlimann, Simmen, Michel, 1995). It lowers the quality of life of the patient in that it affects small blood vessels, lungs, white blood cells, serosal surfaces and cardiac valves. It is a physically disabling systemic disease of unknown etiology therefore its treatment is unspecific and empiric (Brewer, 1980). This disease affects millions of people, constituting a minimum of 1-5% of the world's population. The disease is most prevalent in the 40-60 years age range and the condition occurs 2-3 times more often in women than in men. The reason for this could be that women are naturally more prone to autoimmune diseases than men are (Fischbach, 1991).

The nature of RA is such that it is relentless and so far no therapeutic agent has been capable of curing it. Sufferers have to live with morning stiffness, joint swelling and the possible development of subcutaneous nodules over bony prominences. This disease can be found in the hand, wrist, temporomandibular, ossicular, cervical, elbow, knee, hip, feet and ankle joints (Fischbach, 1991). At each of these points, the advance of the disease will create some kind of disability.

RA is a disease associated with increased mortality and significant morbidity and therefore requires highly effective therapeutic interventions (Sanz, Alboukrek; 1991). The median life expectancy is shortened by 3-7 years in women and by 4-7 years in men. RA increases the patient's chances of mortality from other diseases. This risk is further increased if the patient is undergoing treatment with immunosuppressive drugs. All the risks are increased in the 50-70 years age range. 30% of the mortality is due to RA related causes and 10% due to side effects from drug treatment (Fischbach, 1991). The whole question of the risk of mortality depends on the stage at which the disease is diagnosed and the treatment strategy that is adopted.

Upon diagnosis of RA it is usually difficult to predict the outcome of any treatment plan. Observation of a preliminary treatment over a period of about six weeks is usually necessary to detect the degree of disease advancement. From the onset of the disease, it takes about two years for irreversible damage to joints to begin. This necessitates expedient treatment of the initiating pathological reactions of the disease. Treatment may be both occupational and pharmacological and must include education of the patient about the disease through dialogue with the physician (Aeschlimann, Simmen, Michel; 1995). Studies in DNA technology may in future years be able to predict the prognosis of the disease based on the genetic predisposition of the patient to RA (Fischbach, 1991). As long as the etiology of the disease remains obscure, the approach of treatment will be based on whatever pathological evidence is present at the site of inflammation, at the time of diagnosis.

The site of the pathology of RA is the synovium. Histopathological studies report that the disease is characterised by hyperplasia in the cells of the synovial lining and the formation of many new small blood vessels (Fischbach, 1991). The amount of the different kinds of immune cells in the synovial fluid is increased. There are many pathological pathways that can perpetuate the disease.

Analysis of blood of a RA sufferer shows always some form of anemia (Older, 1991). The platelet count is increased and this correlates directly with the advancement or severity of the disease. The erythrocyte sedimentation rate (ESR) is 25% increased due to the increased concentrations of ceruloplasmin, transferrin, C3 complement, ferritin, fibrinogen and other proteins. The ESR increase is also due to the aggregation of erythrocytes brought about by an alteration in the net electrostatic charge on their surfaces (Brewer, 1980).

Also present in the blood, especially at the site of inflammation are rheumatoid factors. These are autoantibodies that are aimed at the Fc portion of immunoglobulin G (IgG). The immunoglobulin of RA patients has been found to have lower levels of galactose and higher levels of N-acetyl glucosamine and this discrepancy seems to become more

significant as the disease progresses. This attribute has also been found in patients with systemic lupus erythematosus; it is thus not specific to RA, and is believed to be characteristic of all autoimmune diseases. Other characteristics of RA are a high collagen synthesis by synovial tissue, lowered viscosity of synovial fluid and the presence of a nuclear antigen (RA33) which appears to be highly specific for RA (Fischbach, 1991).

The disease can be diagnosed at any one of the four possible disease stages (Fischbach, 1991):

In the first stage the disease is still restricted to the lining of the synovium. Here it is characterised by granulation of the fibroblasts, many new small blood vessels and a notable increase in the count of inflammatory cells. The second stage is characterised by initial fission and erosion of the joint meniscus. The third stage is identifiable by the complete tearing of the meniscus and the visibility of floating debris around the joint bag. At this stage the articular surfaces are pitted and pocked. The fourth and final stage is when the surfaces are completely eroded, with only small remnants of cartilage. In the synovial fluid there is massive structural debris. At this stage the volume of the joint-bag is incredibly reduced. The debris eroded from the meniscal surface facilitates the abrasion of the articular surfaces.

1.2 HISTORY OF RA TREATMENT

The treatment of RA has undergone a wide revolution since the disease was first diagnosed. Historically, infectious agents were suspected to cause RA, and therefore the treatment involved the removal of tonsils, decaying teeth, adenoids and appendix (Fischbach, 1991). Copper-rich foods like shellfish, nuts and cider vinegar were discovered to relieve the symptoms of the disease. Other sources of dietary copper include chocolate, animal livers, crustaceans and dried fruit (Delves, 1980). Early-day physicians also injected gold compounds into their patients and these seemed to help tremendously. RA was not proved to be hereditary but a gene sequence study was able to show that the replacement of two amino acid residues on a particular allele could reduce the person's susceptibility to RA (Fischbach, 1991).

The classical approach to the treatment of RA has been equated to a pyramid (Sanz, Alboukrek; 1991) at the base of which are the non-steroidal anti-inflammatory drugs (NSAIDS) that include aspirin and indomethacin. Drugs in this group are mainly analgesic, anti-inflammatory and antipyretic. Together with corticosteroids, antimalarials and gold, these drugs were in 1992 reclassified as symptom-modifying antirheumatic drugs (SMARDS) (Aeschlimann, Simmen, Michel; 1995). On the next level come the disease-modifying antirheumatic drugs (DMARD), where drugs like sulfasalazine and chloroquine feature. These drugs were proposed to be able to decrease inflammatory sinovitis resulting in improved joint function. The third level on the pyramid involves the immunosuppressive agents like cyclophosphamide and azathioprine. These drugs are cytotoxic. At the worst stage of the disease, total lymphatic irradiation may be used. At any point concurrently with any of these treatment strategies, low dose corticosteroids may concurrently be administered. The same goes for any of the analgesic drugs. Joint surgery may be instituted at any time if seen necessary. It is also important for the patient to be aware of the benefits of physical and occupational therapy. However, all the drugs that have been mentioned so far are foreign to the human body system and may induce a certain degree of toxicity. For this reason, the quest to mimic the natural response of the body to RA in its treatment is very important.

1.3 COPPER AND INFLAMMATION

The human body responds to inflammation, chronic or acute by the mobilisation of copper in low-molecular-weight complexes at the site of inflammation. The body gets copper from dietary sources. Biologically active oxidation states of copper are (I), (II), and (III). These oxidation states are found in copper complexes that act to transport copper to body sites where it is required. There is usually a high demand for copper and zinc atoms at sites that are affected by chronic illnesses like tissue inflammations, ulcers, cancers, convulsive spasm, diabetes, neoplasms and physiological disruptions due to harmful radiation (Weissman, 1982).

Copper is absorbed in the gut by processes other than simple diffusion (Bremner, 1980). In plasma copper is in the form of ceruloplasmin, a α_2-globulin that contains 6-8 enzyme-accessible copper atoms per molecule. Copper is mainly transported as a complex of albumin (90%) and also as complexes of histidine, threonine and glutamine (1%). All these complexes exist in equilibrium, probably as ternary complexes, which constitute 5-10% of plasma copper.

After absorption in the gut copper bound to ceruloplasmin may be deposited into bile or stored in the liver (Bremner, 1980). In the liver copper is found in the form of hepatocuprein, metallothionein and mitochondriocuprein. The copper content of metallothionein varies depending on the concentration of copper, the age of the individual and the plasma zinc status. Metallothionein is not crucial in the hepatic uptake of copper since copper still accumulates even in the absence of this. The overall metabolism of copper involves a wide variety of chemical species.

Ceruloplasmin is an antioxidant endogenous modulator of the inflammatory response. It is increased two- to three-fold in response to inflammation. Leucocytic endogenous mediator (LEM) is one of the molecules released by leukocytes during an inflammatory response (Frieden, 1980). LEM promotes the increased release of ceruloplasmin and the uptake of zinc (II), Fe (III) and amino acids by liver cells.

Copper complexes have pharmacological activity in inducing remission of inflammation. They are involved in biological tissue-repair processes and more importantly are less toxic than the current anti-inflammatory drugs. Some of the chemical compounds that are administered as antiinflammatory agents act by suppressing a normal response to inflammation or tissue injury hence preventing its progression into a fully developed disease. Other compounds act by correcting an impaired anti-inflammatory response back to normal (Sorenson, 1976). Copper complexes fall into the latter category and therefore qualify as therapeutic agents. To fulfil this role more satisfactorily, their by-products must be biodegradable either by

being substrates for other biological processes or by being easily converted to endogenous waste products.

Copper complexes were, as early as 1941, observed to be effective in the treatment of RA (Sorenson, 1976). In the early compounds, copper was in both the +1 and +2 oxidation states. The former was in a drug called Cupralene, [Cu (I)(3-allylthiouredobenzoate)] and the latter was in [Cu (II) 8-hydroxyquinoline (diethylammonium sulphonate)$_2$] also known as Dicuprene. Ontosein, a synthetic copper-based drug is a mimic of the superoxide dismutase copper-metalloenzyme. This drug was seen to have high efficacy in the treatment of RA and other tissue degradative diseases. Another historical discovery of benefit in the treatment of RA was the effect of wearing a copper bracelet, which was found to give great relief to patients. This was found to be accompanied by a 12-mg/month mass loss from the bracelet and further investigation showed that some component of sweat solubilised the bracelet and promoted dermal absorption of copper into the blood stream (Sorenson, 1976).

There are several mechanisms underlying the action of copper complexes in relieving the symptoms of RA. Copper complexes are involved in the induction of the enzyme lysyl oxidase, which has a pyridoxal-copper complex cofactor. This enzyme is responsible for the formation and maturation of collagen and elastin in the tissue repair process. Copper complexes suppress the formation of the pro-inflammatory prostaglandin (PGE2) and promote the synthesis of anti-inflammatory prostaglandin ($PGF_{2\alpha}$). The former prostaglandin is a vasodilator and the latter is a vasoconstrictor and these are two characteristics that, respectively, favor and disfavor inflammation (Sorenson, 1976).

The superoxide anion is another culprit in the initiation and perpetuation of inflammation. This free radical is disproportionated by the superoxide dismutase (SOD) enzyme (Vance and Miller, 1998) which has a copper atom at the active site and a zinc atom at another site. The active site has a distorted square pyramidal and the

zinc site, a distorted tetrahedral geometry (Reedijk, Bonomo, Driessen, Tabbi, Veldman, Spek; 1997). The availability of additional copper atoms in the form of low molecular weight (lmw) copper complexes definitely promotes the formation and activity of the SOD enzyme. Some of the anti-inflammatory lmw copper-complexes have some SOD-like activity. Copper has also been observed to stabilise the lysosomal membrane, hence reducing the level of free lysosomal enzymes, which may be destructive to tissue (Sorenson, 1976).

It has been found that the physiological effects of histamine during inflammation are enhanced if it is in the form of a copper complex. Copper complexes also have an antithrombotic effect. They have the SOD-like action of inhibiting the carboxylation of preprothrombin so that prothrombin is not formed. The copper complexes also inhibit T-lymphocyte response to inflammation, hence slowing down the perpetuation of the disease. Inflammation is also characterised by the denaturation of gamma globulin. This denaturation can be inhibited by copper complexes and hence one of the manifestations of RA is suppressed (Sorenson, 1976).

The activity of glutathione-S-transferase is lowered in the presence of copper complexes. The cupric ions are able to shift the equilibrium between free glutathione and the bound disulphide towards the disulphide; hence tissue degradation is delayed. Copper complexes are also involved in the modulation of several other enzymes. These include cytochrome-P450-mixed-function oxidase, peptide prolyl and lysyl hydroxylases, NADPH-cytochrome P-450 reductase and catechol dioxygenases. These enzyme systems are linked to other iron-dependent enzymes in the pathological destruction of tissue (Sorenson, 1976). These reactions may be de-coupled by the SOD-like activity of low molecular weight copper complexes. Copper complexes also have antimicrobial activity and if infection is involved in the aggravation of the disease, the complexes will be of therapeutic advantage in that respect.

1.4 PREVIOUS STUDIES

There are several structural features that need to be considered in the design of a ligand for coordinating to a metal ion. The metal ion involved in the present study is copper (II) and it was observed that for this metal ion as the donor atom changes from O to S to N, the copper mobilising efficiency of a ligand increases dramatically (Jackson, Kelly; 1988). Because of the toxicity of the thiol group, it is not favourable for use in the design of human therapeutic compounds. Secondly the number of coordinating atoms and their separation on the ligand is of importance to the mobilising ability of the complex. The higher the denticity of the ligand, the greater the mobilising ability; however, no increase in ability was observed with any increase in the number of coordinating atoms beyond quadradenticity (Jackson, Kelly; 1988). The separation of the donor atoms determines the size of the chelate rings that are formed after metal-ligand complexation. It was observed that ring sizes that resulted in highly strained complexes caused low copper mobilising ability in the complex. This was observed with ligands that formed three contiguous five-membered rings, as opposed to those that formed an alternating 5,6,5 chelate ring sequence upon coordination (Jackson, Kelly; 1988).

It is worth mentioning at this point that several ligands closely related to those used in the present study have been investigated in a similar quest. Even though additional metal-ion experiments may have been done, the main focus has been on the disposition of the ligands with the copper (II) ion. The results obtained in these previous studies were interesting in that they led to the choice of the present ligands. Initially it was thought that straight-chain polyamine ligands would be the best copper mobilisers. The ligands 3,6,9,12-tetra-azatetradecanedioic acid (Ttda) and 3,6,9-triazaundecanedioic acid (Dtda) were therefore investigated for their ability to mobilise copper at the RA site (Kelly, 1988). The neutrality of the copper complex was achieved by incorporating two acetate groups on the ligand. The neutral complexes of these ligands were found to be highly hydrophilic and easily excreted in urine despite being formally uncharged.

However, instead of being a candidate for copper delivery, these ligands appeared to be more suited for sequestration of the metal ion in cases of its toxicity.

Subsequently, in order to increase the lipophillicity of the complexes, it was decided to bury the charge within the ligand. Nature achieves this by using amides, which upon metal coordination lose their protons. The amide nitrogen atoms were therefore introduced in the structure of the ligand. The ligands N,N-bis[2-(dimethylamino)ethyl]ethanediamide, (5UM); N,N-bis[2(dimethylamino)ethyl] propanediamide, (6UM) and N,N-bis [2-(dimethylamino)propyl]ethanediamide (656UM) were investigated (Voye, 1993) for the same task. The copper complexes of these ligands were not neutral at physiological pH. Curves of their plasma mobilising index showed that these ligands were unable to prevent the loss of copper to endogenous ligands *in vivo*.

The present study is an advancement of the two studies summarised above. The point of interest in this study is to increase the denticity of the ligands to five in an attempt to increase the stability of the complex by the chelate effect; and to provide an extra point of alkyl substitution on the ligand chain to increase complex lipophilicity. Whilst retaining the two amide nitrogen atoms for complex charge neutrality and possessing two terminal amino nitrogen atoms, the legends of this study also include a fifth nitrogen atom donor atom at position-7 along the ligand chain.

The structure of the ligands at hand is shown in Figure 1. They resemble oligopeptides. They have special coordinating properties and are practical to deal with in the laboratory. They can lose the amide proton and bond with metals ions in their higher oxidation states. These metal ions can then be used in redox reactions hence the versatility of their oxidation states is fully utilised. This is normally the case in biological metalloenzymes whose function is to protect the body tissues from the by-products of oxygen metabolism. Complexes of these ligands with biological metal ions are models of metalloenzymes and therefore have great potential in medicinal studies (Sigel, 1981).

FIGURE 1: Ligand Structural Formula, backbone featuring five nitrogen donor atoms (two amide and three amine) with two carbon atoms between each consecutive two.

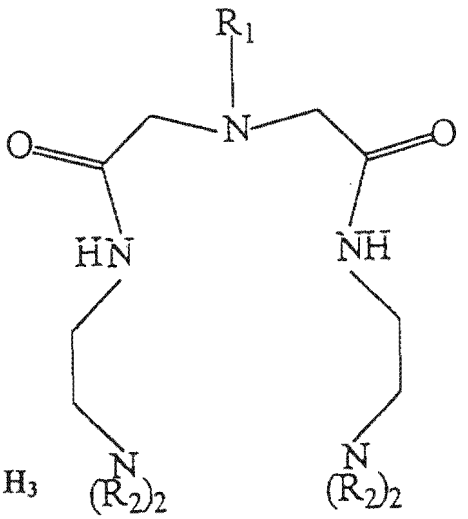

Ligand **ZDA** $R_1 = H,\ R_2 = -CH_3$

Ligand **BID** $R_1 = -CH_2C_6H_5,\ R_2 = -CH_3$

Ligand **EDA** $R_1 = -CH_2CH_2C_6H_5,\ R_2 = H$

Ligand **DME** $R_1 = -CH_2CH_2C_6H_5,\ R_2 = -CH_3$

As shown in Figure 1, the main ligand structure has different substituents at positions 1, 7 and 13, giving four different ligands. Of interest in this study is the effect of these groups on the thermodynamic stability of the copper (II) complexes of these ligands. As it would appear that dermal absorption is the most popular drug administration route nowadays, the effect of the different alkyl substituents on the partition coefficients of the copper complexes is of interest here.

Computer simulation has shown that the high *in vivo* concentrations of zinc (II) and calcium (II) makes these two metal ions important (Jackson, Kelly; 1990). For this reason stabilities of the zinc (II) and calcium (II) complexes of the present ligands were also investigated. The results of the copper plasma mobilising index calculation of the present ligands will be more comprehensive in light of their calcium (II) and zinc (II) mobilising efficiencies.

1.5 RESEARCH OBJECTIVES

In order to contribute to the understanding of the importance of drug design in the mobilisation of copper (II) at the site of inflammation, the following objectives were laid out:

1. Synthesis and characterisation of the four above named ligands by mass spectrometry, carbon-13 and proton NMR.

2. Determination of the protonation constants of the ligands and the thermodynamic stability constants of their complexes with copper (II), zinc (II) and calcium (II) in aqueous solution.

3. Determination of the structure of the copper complexes using UV/VIS spectrophotometry.

4. Use molecular mechanics calculations to investigate possible structures for the chemical species.

5. Measurement of lipophilicity of the copper complexes by measuring their octanol-water partition coefficients.

6. Finally, determination of the superoxide-dismutase (SOD)-like activity of the copper species at blood plasma pH.

1.6 THESIS STRUCTURE

This thesis consists of six chapters. The **first** chapter is the introduction in which the history and justification of the study are oulined. The experimental work is described and the results presented in chapters **two, three** and **four**. The **fifth** chapter gives the overall discussion of all the results and how they are inter-related. The conclusion, in the **sixth** chapter, is a statement of how far the objectives of the study have been met.

CHAPTER TWO

2. ORGANIC SYNTHESIS

2.1 INTRODUCTION

The basic synthetic route followed in this study was adopted from literature (Elsworth, Msimang, Jackson; 1996). Some modifications were made to suit the requirements of the synthesis of the present ligands.

2.2 SYNTHETIC SCHEME

$R^1\text{-}NH_2$ ---*(i)*→ $R^1\text{-}NH(CH_2COOCH_2CH_3)_2$ ---*(ii)* →
(1)

$(R^1)\text{-}NH(CH_2CONHCH_2CH_2N(R^2)_2)_2$ --- *(iii)* → $NH(CH_2CONHCH_2CH_2N(R^2)_2)_2$
(2) **(3)**

Reagents: *(i)* $BrCH_2CH_2COOEt$, $(Et)_3N$; *(ii)* $(CH_3)_2NCH_2CH_2NH_2$, EtOH
(iii) $H_2(g)$, EtOH, Pd/C

The ligands **4** (BID), **5** (ZDA), **6** (DME) and **7** (EDA) had the following alkyl substitutions.

	R^1, R^2	
4	$CH_2C_6H_5$, CH_3	(ligand BID)
5	H, CH_3	(ligand ZDA)
6	$CH_2CH_2C_6H_5$, CH_3	(ligand DME)
7	$CH_2CH_2C_6H_5$, H	(ligand EDA)

2.3 EXPERIMENTAL

2.3.1 *Diethyl N-benzyliminodiacetate* **1***a* *($R^1 = CH_2C_6H_5$)*

Ethyl bromoacetate (23.8g, 140.8 mmol) was added with continuous stirring to a triethylamine solution of benzylamine (7.55g, 70.4 mmol). After 30 minutes of stirring

the reaction mixture was heated under reflux for 6 h after which the mixture was concentrated on a rotary evaporator and extracted with ethylacetate. The organic phase was dried over anhydrous magnesium sulphate and evaporated to an orange residue. Column chromatography using benzene-ethanol (5:1) yielded compound **1***a* (16.4g, 78 %). NMR: (proton) δ_H ($CdCl_3$) 1.24 (2H *t*), 3.53 (4H *s*), 3.55 (2H *s*), 4.14 (4H *q*), 7.29 (5H *m*). δ_C 14.0, 47.6, 53.7, 54.1, 57.8, 60.23, 128.21, 128.63, 128.9, 138.11, 171.02

2.3.2 *Diethyl phenethyliminodiacetate* **1***b* ($R^1 = CH_2CH_2C_6H_5$)

Ethylbromoacetate (47.19g, 125.6 mmol) was added to a stirred solution of phenethylamine (7.58g, 68.2 mmol) in triethylamine (100ml). A work-up similar to that of the synthesis of compound **1***a* yielded a dark orange residue, compound **1***b* (13.9g, 69.5 %) NMR: δ_H ($CdCl_3$)1.25 (4H *t*), 2.8 (2H *t*), 3.0 (2H *t*), 3.5 (4H *s*), 4.2 (4H *q*), 7.2 (5H *m*) (carbon-13) δ_C 14.18, 34.73, 55.17, 56.22, 60.43, 126.02, 128.2, 128.6, 139.67, 171.14

2.3.3 *1,13-bis(N,N-dimethyl)-5,9-dioxo-7-(N-benzyl)- 1,4,7,10,13-pentaazatridecane* **4**

To a stirred solution of the compound **1***a* (16.4g, 57.7mmol), N,N-dimethylethylenediamine (12.4g, 140.8 mmol) was added. The reaction was heated under reflux for 36 h after which there was no residual starting material (TLC, chloroform-ethanol-ammonia, 9:5:1) The reaction mixture was then reduced to an orange intractable gum. This was then dissolved in minimum eluent. On column chromatography, with the same eluent as for TLC, product **4** was obtained (13.7g, 64.5 %). **NMR** δ_H (D_2O) 2.22 (12H *s*), 2.45 (4H *t*), 3.14 (4H *s*), 3.4 (4H *m*), 3.63 (2H *s*), 7.5 br (5H, *m*); δ_C 36.43, 45.08, 58.39, 59.53, 127.60, 128.44, 129.13, 136.88, 170.17. Analysis of hydrochloride: pale yellow, mpt = 210 -212°C, *m/z* 368 (M^+,4%), 293 (4), 272(2), 248(5), 234(10), 210(2), 130(12), 115(10), 91(30), 71(20), 58(100), 42(20), 36(25), 28(5).

2.3.4 *1,13-bis(N,N dimethyl)-5,9-dioxo-1,4,7,10,13-pentaazatridecane* **5**

Product **4** (12g, 32.6mmol) dissolved in 100m*l* absolute ethanol was hydrogenolysed at atmospheric pressure over palladium-on-carbon for 4h, monitored by TLC chloroform-ethanol-ammonia (9:5:1). Absence of the starting material close to the eluent front and appearance of a new spot in the polar region showed completion of debenzylation and the presence of *compound* **5** (6.2g, 69.6%). δ_C (D_2O) 34.5, 43.01, 47.84, 56.23, 166.6. δ_H 2.84 (12H, *s*), 3.25 (4H, *t*), 3.6 (4H,*t*), 3.94 (4H, *s*). Analysis of hydrochloride: cream white, m. pt = 226-228°C, *m/z* 273 (M^+,4%), 201(21), 158(6), 144(3), 130(8), 125(2), 111(4), 97(5), 71(53), 59(90, 42(18), 36(100), 28(29)

2.3.5 *1,13 bis(N,N-dimethyl)-5,9-dioxo-7-(N-phenethyl)-1,4,7,10,13-pentaazatridecane* **6.**

To a stirred solution of the compound **1***b* (10g, 37.2mmol), N,N-dimethylethylenediamine (6.54g, 74.3 mmol) was added. The reaction was heated under reflux for 72 h after which, there was a constant minimal residue of unchanged starting material (TLC, chloroform-ethanol-ammonia, (9:5:1). The reaction mixture was then evaporated to a brown intractable gum, which was then dissolved in minimum eluent. On column chromatography with chloroform-ethanol-ammonia (9:5:1) product **6** was obtained (11.1g, 79.6 %). NMR δ_C (D_2O)29.85, 34.68, 43.03, 55.74, 56.07, 57.60, 127.56, 128.93, 129.14, 135.46, 165.88. δ_H 2.82 (12H *s*), 3.0 (2H *t*), 3.24 (4H *t*), 3.55 (6H *m*), 4.18 (4H *s*), 7.3 (5H *m*). Analysis of hydrochloride: pale yellow, m. pt = 109-112°C, *m/z* 377 (M^+,6%), 307(6), 206(4), 262(8), 248(6), 172(3), 148(5), 134(3), 127(2), 113(2), 105(12), 85(3), 71(12), 58, 42, 36(12), 30(3).

2.3.6 *7-(N-phenethyl) -5,9-dioxo-1,4,7,10,13-pentaazatridecane* **7**

To a stirred solution of the compound **1***b* (10g, 37.2mmol), ethylenediamine (4.46g, 74.3 mmol) was added in one portion. The reaction was heated under reflux for 72 h after which, there was a constant minimal residue of unchanged starting material (TLC, chloroform-ethanol-ammonia, (9:5:1). The reaction mixture was then evaporated to an orange gum, which was then dissolved in minimum eluent. On

column chromatography with chloroform-ethanol-ammonia (9:5:1) *product* 7 was obtained (8.4g, 70.7 %). NMR δ_C (D_2O) 29.8, 36.8, 38.5, 55.5, 57.3, 127.2, 128.6, 128.8, 135.3, 165.9; δ_H 3.18 (4H, *t*), 3.57 (8H, *m*), 4.25 (4H, *s*), 7.2 (5H, *m*). Analysis of hydrochloride: pale yellow, mpt = 142- 145°C,

m/z 170(8), 152(96), 124(54), 113(2), 105(13), 91(10), 77(13), 65(5), 56(16), 42(100), 30(55).

2.3.7 *Product Hydrochloridation*

Each oily final product was dissolved in tetrahydrofuran (THF). Twenty millilitres of THF was used per gram of product. Dried HCl gas was bubbled through the stirred solution until it all precipitated out of solution and settled at the bottom of the flask. The supernatant was decanted and the rest removed by rotary evaporation. The product was then recrystallised in a hot methanol-THF solution. Product was reclaimed in 95 % yield and its identity was confirmed by mass spectrometry.

3. POTENTIOMETRIC, SPECTROPHOTOMETRIC AND MOLECULAR MECHANICS STUDIES

This chapter will report on three aspects of the study, namely glass electrode potentiometry, UV/VIS spectrophotometry and molecular mechanics. In each section theory, experimental, results and discussion will be presented in that order. The discussion at the end of each section will be of the results specific to that particular section. At the end of this chapter the results of the three sections of the chapter will be discussed in relation to each other.

3.1 GLASS ELECTRODE POTENTIOMETRY

3.1.1 Theory

3.1.1.1 Introduction

Glass electrode potentiometry (GEP), being one of the oldest instrumental methods of analysis (Kolling, 1985), has for the past four decades expanded tremendously. This has been the result of the rapid development of new electrodes and stable electronic components. For this reason, potentiometry can, today, be applied in many fields of science for the study of chemical equilibria. GEP is just one of a number of analytical tools (Martell, Motekaitis; 1988) that can be used for the determination of stability constants. It was chosen for use in this study because of its high sensitivity, its non-invasiveness and its easy accessibility. It was preferred also because of its wide use, which brings the advantage that the results obtained could be comparable to those in literature.

The structure of the glass electrode (Linder/ Torrington, 1984) is such that it has a membrane, the potential across which is reversible with respect to hydrogen ion activity. In the determination of ligand protonation constants the ligand solution is, depending on the initial pH, titrated with either acid or base in such a way that the 2 to 11 pH range is scanned. By the inclusion of a metal ion in such a titration, complexation constants may, upon data analysis, be found.

The accuracy and reproducibility (Woodward/ Redman, 1973) of GEP titrations depend on various factors. The main source of error is usually the electrochemical cell. In this regard, the electrode system has to be fully conditioned and calibrated. Conditioning entails ensuring that the reference electrode is correctly filled and that the glass electrode gives a high Nernstian response. Optimal response will always be ensured by proper use and storage of the glass electrode (Linder, Torrington, Williams; 1984).

GEP is used in the study of, among others, chemical systems of biological, environmental and geological importance. The reaction conditions of a titration used to study any of these systems have to resemble the system as closely as possible. The stability constants sought in this study were to be applied to a model of blood plasma and therefore the titrations were performed in a sodium chloride solution at an ionic strength of 0.15 mol dm^{-3}. With regard to temperature, the human physiological temperature of 37°C presents the problem of test solution evaporation during the titration. For this reason and that of the comparability of results with those found in literature, it is common to perform titrations at 25°C.

3.1.1.2 The Stability Constant

Also known as formation constant, the term "stability constant" will, in this study, be used to refer to the values obtained for the overall formation constant of a metal-ligand species. The chemical association of a ligand with protons will be referred to as the protonation constant.

For any single chemical system studied under a particular set of conditions, different workers may report a range of stability constant values. In any particular case, there may be some statistical agreement between a few of the values reported and the average of those values is normally accepted as best describing the system in question. For a set of stability constants to be comparable, they must have been measured under similar experimental conditions. In this study, the experimental conditions refer to the ionic strength (I), the temperature (T) and the nature of the background electrolyte.

The base-titration of aqueous metal-ligand equilibria involves competition between the water molecules, the ligand molecules and the hydroxide ions for the metal ion. The ligand donor sites also attract hydronium ions and metal ions (Martell, Motekaitis; 1988). For the final complex species to be formed there may be several pre-complexation processes involved. These would include the loss of a coordination water molecule from the metal ion, followed by coordination to the ligand molecule accompanied by a loss of a proton. The overall stability constant of any species is actually the product of several stepwise stability constants. Often many more species are involved in the equilibrium of a complexation reaction than are normally stated as representing the chemical system. Only the constants of the predominant chemical product species are selected to constitute the model that best describes the chemical system.

There are several criteria that can be used for the selection of a ligand donor atom for the binding of a certain metal ion (Williams, 1971). The choice of donor atom may be based firstly on Pearson's hard/soft-acid/base theory, in which the donor atom is classified as either hard or soft or intermediate between the two. Hardness is described as half the difference between the ionisation potential and the electron affinity. Softness is the reciprocal of hardness. According to this theory, a hard donor atom will prefer to bond to a hard acceptor atom and likewise a soft pair of atoms. Secondly, if the stability constant of a ligand with a metal of the Irving-Williams series ($Mg < Mn < Fe < Co < Ni < Cu > Zn$) has been measured, it can be used to predict its bonding behaviour with other metals of this series. Thirdly, the known co-ordination sphere of a metal can be used to predict the kind of species that a ligand of a particular denticity is likely to form with the metal ion, which will also determine the extent to which the complex will be aquated. The concentration ratios of the reactants also influence species that will predominate at the equilibrium. Low metal to ligand ratios favour the formation of mononuclear chemical species whilst high metal to ligand ratios promote the formation of polynuclear complexes (Nancollas, 1966).

The chemical equilibrium of a system between a metal-ion M and a protonated ligand LH is represented as:

$$M + LH <=> MLH \qquad ...(3.1)$$

It can be defined in terms of stability constants (β) in three ways (Linder, Torrington, Williams; 1984). This depends on the available parameters pertinent to the system. The stability constant can be said to be thermodynamic when described with respect to the activity of the reacting species:

$$\beta_{MLH} = a_{MLH} / a_M a_{LH} \qquad ...(3.2)$$

Thermodynamic stability constants serve best in explaining the ionic interactions in an isolated chemical system.

The stability constants may also be called stoichiometric when they are defined with respect to the concentration of the reactants;

$$\beta_{MLH} = [MLH]/[M][LH] \qquad ...(3.3)$$

The stability constants can be described as "mixed" if they are expressed in terms of both the concentration and the activities.

$$\beta_{MLH} = [MLH] /[M] a_{LH} \qquad ...(3.4)$$

Theoretically, the stability constants are called thermodynamic if they were measured at an ionic strength of zero (I = 0). Practically this is impossible because the reactant species have an ionic contribution to the reaction solution (Martell, Motekaitis; 1988) and therefore extrapolation back to infinite dilution is necessary to obtain values at zero ionic strength. This is a laborious task that can be by-passed by measuring the stability

constants in a solution of a salt at a conventionally acceptable constant ionic strength that is much higher than the ionic strength contribution of the reacting species. In this way, the effect of the varying ionic strength is negligible and "conditional" stability constants are reported.

3.1.1.3 Temperature and Ionic Strength

Salts that are commonly used to keep the ionic strength (Nancollas, 1966; Beck, Nagypal 1990) of a test solution constant include potassium chloride (KCl), sodium perchlorate ($NaClO_4$), sodium chloride (NaCl) and potassium nitrate (KNO_3). The salt selected for the purpose must be an electrolyte that yields ions that are common to the reacting acid and base, so as to eliminate the introduction of equilibria foreign to the system of study. The activity of this salt must be 100 to 1000 times greater than that of the reacting species. In essence, it is the anions of the electrolyte that are employed to maintain the ionic strength at a constant value. Of the different anions available the chloride ion, with its high electronegativity, is the least suitable for this purpose because it tends to act as a competing ligand by forming ion pairs with the reacting species. Stability constants measured in this medium are therefore highly conditional because they indirectly incorporate the chloride stability constants.

The trend (Williams, 1971) in the tendency to form ion pairs is as follows:

$$SO_4^{2-} > Cl^- > Br^- > I^- > NO_3^- > ClO_4^-.$$

Since a considerable amount of redistribution of solvent molecules takes place prior to metal-ligand complexation, it is crucial to use an electrolyte that will not complicate this pre-complexation process. If the background electrolyte also acts as a competing species the values of the stability constants are lowered. A trend (Williams, 1971) in the values of a series of stability constants measured in 3.00 M ClO_4^- was seen to be similar to the trend in stability constants measured in 0.15 M NaCl. This gives some justification to the use of sodium perchlorate as the background electrolyte in studying the trends in stability constants of biological systems. Ammonium nitrate (NH_4NO_3) at 0.15 M may

also be used as background electrolyte since the ammonium ion is isoelectric to the hydronium ion. The disadvantage of this salt, however, is that the ammonium cation is just the protonated form of ammonia, another competing ligand. Whatever salt is used as background electrolyte, it should be highly pure. This is important because, as the background electrolyte is at a concentration far higher than that of the reactants, any impurities associated with it may be as high as the concentration of the reacting species and could interfere with the equilibrium of interest.

The activity of the anion has a significant effect on the liquid junction potential. The activity ***a*** of any ion **i** is a product of its activity coefficient γ and its concentration **c**, represented as;

$$a_i = \gamma_i c_i \qquad ...(3.5)$$

Activity coefficients do not vary much in a titration where there is a high concentration of background electrolyte. The activity coefficient can be described by the equation:

$$-\log\gamma_i = (0.51\, z_i^2\sqrt{I}) / (1 + 0.33\alpha_i\sqrt{I}) \qquad ...(3.6)$$

whereby 0.51 and 0.33 are constants for water at 25°C, **z** is the charge of the ion **i**, α_i is the effective hydrated ion diameter and ***I*** is the ionic strength. The ionic strength can be represented as:

$$I = 0.5 \sum c_i z_i^2 \qquad ...(3.7)$$

where **c** and **z** are the concentration and the charge of the ion **i**, respectively.

The dielectric constant of a solvent determines the degree of electrolyte dissociation and hence concentration of the charged species. This invariably means that the activity of an ion will differ in different solvents. Once the stability constants have been found at a

certain ionic strength, the equations can be extrapolated back to find the values of the constants at infinite dilution in water at zero ionic strength.

A variation in the nature and concentration of the background electrolyte changes the nature of the liquid junction, which is described by the equation:

$$E_k^{lj} = - (RT / F) \ln (1 + d[X_H] / dI) \quad ...(3.8)$$

where X is the anion of the background electrolyte.

The stability constants of a system also change with temperature. The standard entropy (S°) and enthalpy (H°) of a chemical reaction determine its standard Gibbs free energy (G°) and are related to absolute temperature (T Kelvin) by the following equation:

$$\Delta G° = \Delta H° - T\Delta S° \quad ...(3.9)$$

Since standard Gibbs free energy is related to the gas constant (R) by the equation:

$$\Delta G° = -RT \ln K \quad ...(3.10)$$

it follows that:

$$\ln K = -\Delta H°/ RT + \Delta S°/R \quad ...(3.11)$$

Differentiation of equation 3.11 gives the Van't Hoff expression:

$$d \ln K / d (T^{-1}) = -\Delta H°/R \quad ...(3.12)$$

which can be used to adjust stability constants for changes in temperature, provided there is no change in the $\Delta H°$ of the reaction in the temperature interval between the two compared reaction conditions (Ahrland, 1967).

3.1.1.4 The Ligand Reaction Equations

Complex-formation between a metal ion M, and a weakly basic ligand molecule L may occur in several steps, one of which can be represented as

$$ML_{n-1} + L \iff ML_n \qquad ...(3.13)$$

The stepwise stability constant of this can be represented as

$$K_n = [ML_n] / [ML_{n-1}] [L] \qquad ...(3.14)$$

and the overall stability constants as:

$$\beta_{1n0} = \prod K_i \qquad ...(3.15)$$

where $\prod K_i$ indicates the product of all the stepwise stability constants up to the i*th* step.

In the absence of the metal ions, the protonation constants of a ligand in the chemical equation:

$$L + rH \iff LH_r \qquad ...(3.16)$$

may be represented as the overall stability constant:

$$\beta_{01r} = [LH_r] / [L] [H]^r \qquad ...(3.17)$$

or in the stepwise formation:

$$LH_{r-1} + H \iff LH_r \qquad ...(3.18)$$

as the stepwise stability constant:

$$K = [LH_r] / [LH_{r-1}] [H] \qquad ...(3.19)$$

The relationship between the two constants is:

$$\beta_{01r} = \prod K_{H,i} \qquad ...(3.20)$$

indicating the accumulation of the stepwise protonation constants, where $K_{H,i}$ is the constant of the protonation of the ligand by the *ith* proton.

In the analysis of data, the loss of a proton from a metal complex is viewed as similar to the gain of a hydroxide ion. The reaction equation:

$$M + L <=> MLH_{-1} + H \qquad ...(3.21)$$

whereby the overall stability constant is:

$$\beta_{11\text{-}1} = [MLH_{-1}]\,[H] / [M]\,[L] \qquad ...(3.22)$$

is, with respect to charge, equivalent to:

$$M + L + OH <=> MLOH \qquad ...(3.23)$$

whereby:

$$\beta_{MLOH} = [MLOH] / [M][L][OH] \qquad ...(3.24)$$

Since $K_w = [H][OH]$, $[H] = K_w / [OH]$ and $[OH] = K_w / [H]$.
therefore;

$$\beta_{11\text{-}1} = \beta_{MLOH}\, K_w \qquad ...(3.25)$$

Further, if $pK_w = -\log K_w$,

$$\log\beta_{11\text{-}1} = \log\beta_{MLOH} - pK_w \qquad ...(3.26)$$

3.1.1.5 The Electrode Cell

The electrode cell (May, Linder, Williams, Torrington; 1982) is the centre of any potentiometric investigation.The observed potential of the reaction cell is the result of the potential difference between the glass electrode and the reference electrode E_{ref}, the potential at the liquid junction of the reference electrode (E_{lj}) and the potential at the membrane of the glass electrode (E_g). The following cell:

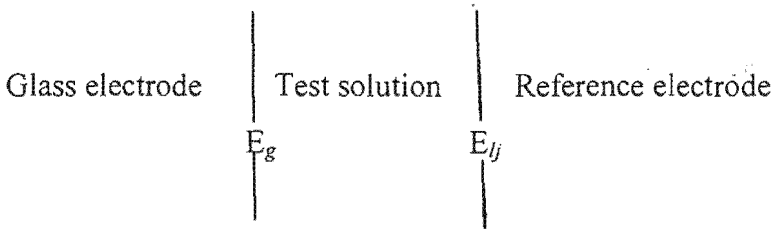

can thus be represented by the equation:

$$E_{cell} = E_{ref} + E_{lj} + E_g \qquad ...(3.27)$$

The potential at the glass electrode E_g is due to the Nernstian response of the glass electrode to the hydrogen ion activity and can be represented as:

$$E_g = E^0_g + (RT / F) \ln\{H^+\} \qquad ...(3.28)$$

where E^0_g is the standard electrode potential and $\{H^+\}$is the activity of the hydrogen ion. The cell potential then becomes:

$$E_{cell} = E_{ref} + E_{lj} + E^0_g + (RT / F) \ln\{H^+\} \qquad ...(3.29)$$

If the ionic strength is kept constant, the activity of the hydrogen ions will also be constant, therefore the concentration of the hydrogen ions, which is a measurable quantity, can be used in the definition the cell potential. Collecting all the cell constants in one term gives:

$$E_{cell} = E_{const} + s \log [H^+] \qquad ...(3.30)$$

s is the Nernstian electrode response slope and is equal to RT/F, where R is the gas constant, T is the temperature of the system and F is Faraday's constant.
Reported stability constants must be fully characterised (Tuck, 1989) with regard to the conditions under which they were obtained. The nature of the background electrolyte, the ionic strength, the units of measurement, and the temperature are all pertinent conditions that need to be specified for each set of measured stability constants. This information is useful when different stability constants have to be used to describe real chemical systems.

3.1.1.6 The glass pH electrode

The Metrohm glass pH electrode is a costly and fragile accessory of glass electrode potentiometry. The glass bulb wall is very thin and is of special composition that ensures sufficiently low electrical resistance as to allow the Nernstian response of the elctrochemical cell to emf. Prior to use, the electrode must be conditioned to give it a uniformly hydrated external surface. When not in use it must be stored in water or acidic buffer so as to ensure that the proton sensitive anionic sites on the bulb surface are kept highly charged.

As in any other analytical technique, calibration of the instrumentation used for GEP, especially the glass electrode, is of principal importance. The method used for electrode calibration must be in accordance with the test conditions in which it will be used. The activity coefficients of the reference solutions and the test solutions must not be significantly different (Choppin, Yuan-Xian, Jiang-Fen; 1996). The glass electrode is used to measure the concentration of protons under differing conditions of temperature and ionic strength. As indicated by equations (3.27) to (3.30), calibration of the cell thus involves determination of the constants E_{const} and s.

The glass electrode is calibrated with standard buffers whose pH is conventionally assigned and it is against this that the pH of the unknown is measured. It would be wiser to use acidic solutions (Davison, Woof; 1985) to calibrate electrodes but they happen to be more prone to contamination and preparation error. Common practice is

that a set of buffer solutions is used to test the reliability of the electrode. It is further advisable to have another set of buffer solutions in order to be able to check the reproducibility of the buffer line.

3.1.1.7 The electrode junction

The liquid junction of a reference electrode is the main source of error (Davison, Woof; 1985) in an electrochemical cell. A cell may be equipped with a restrained or a free diffusion junction. A restrained junction might be a ceramic, a fibre plug or a sleeved joint. Even though this type of junction is more commonly used, it is not as reliable as a free diffusion junction (Davison, Woof; 1985) especially if solutions of salts other than potassium chloride are used to fill the reference electrode.

3.1.1.8 The titration vessel

It is imperative that the temperature and pressure conditions of the titration vessel are kept constant. Although quiescent solutions give a more accurate reading of pH, in potentiometry the reaction solution must be stirred throughout the titration in order to maintain homogeneity at each addition of titre. Stirring also ensures that the message read by the electrode is representative of the whole solution. The stirring should not however, be too violent so as to avoid splattering of the solution and the introduction of gas bubbles at the surface of the electrode. Nitrogen that is free of carbon dioxide and oxygen is kept flowing through the vessel so as to maintain an inert atmosphere around the reaction.

3.1.1.9 Computer Simulation Modeling

The bio-availability of any chemical element is determined by its physicochemical identity, i.e chemical speciation. The chemical speciation of an element can be viewed in isolation as a qualitative analysis or in relation to a metabolic pathway. The latter is more applicable to biological processes as it often happens that a molecule will continually change its chemical identity in response to a biochemical reaction or an

enzyme catalyst. It therefore helps to be informed of the chemical speciation of a molecule under certain specific conditions of interest, especially in chemical pathology. The complexity of biological fluids and the difficulty, with which their equilibria can be studied with minimum disruption, make computer simulation an invaluable tool in this regard. The non-intrusive nature of computer simulation minimises any uncertainties that may be associated with drawing conclusive results on any biological fluid. Computer-aided chemical speciation modeling requires good experimental and computational technique. However, universally accepted methods and computer software have been developed to make speciation studies more accurate and much easier. In this way, computer simulation can confidently be used to confirm or disprove as well as to predict phenomena claimed to be associated with a chemical species.

3.1.1.10 Computer Data Analysis

Three kinds of data are available to the analyst (May, 1985). There are the *known* parameter values like those of the initial reaction vessel volume, the incremental volumes of added base and the temperature at which the determination is being done. There are also the parameters that are *measured,* such as the potential difference (emf) and finally, there are the *unknown* values like the stability constants. The measured emf of the reaction solution will be a function of all these parameters. The information available in the data will be extracted by the solution of mass balance equations.

The chemical reaction occurring in a system containing metal (M), ligand (L) and protons (H) can be represented by the equation:

$$pM + qL + rH <=> M_pL_qH_r \qquad ...(3.31)$$

where the coefficients p, q and r represent the number of moles of each of M, L and H in the complex. The total concentration of the metal, T_M, will be;

$$T_M = [M] + \sum [M_pL_qH_r] \qquad ...(3.32)$$

where [M] is the concentration of the free aquated metal ions and the summation is of the concentrations of all the metal-containing species which may be protonated ($r > 0$) or may not ($r < 0$). The total ligand concentration will be:

$$T_L = [L] + \sum [M_pL_qH_r] \qquad ...(3.33)$$

where [L] is the concentration of the uncomplexed ligand and the summation is of the concentrations of all the protonated or unprotonated ligand containing species.

But since the overall stability constants can be represented as

$$\beta_{MpLqHr} = [M_pL_qH_r] / [M]^p [L]^q [H]^r \qquad ...(3.34)$$

the total reactant concentrations can be expressed as

$$T_M = M + \sum i\beta[M]^p [L]^q [H]^r \qquad ...(3.35)$$

and

$$T_L = L + \sum k\beta[M]^p [L]^q [H]^r \qquad ...(3.36)$$

These mass balance equations set the mathematical limits that the computer has to adhere to whilst minimising the objective function U (May, Murray; 1988). In this minimisation the mass balance equation for the total concentration of each reactant is set equal to the analytical or real quantity and solved simultaneously to arrive at optimised values for the flagged parameters.

3.1.1.11 The Objective Function (U) (Murray, May; 1984)

During data analysis, for each titration point, the computer calculates the emf of the system and finds the difference between the calculated and observed values. These differences are then squared and summed to give a value for U, the objective function. This function may be described as the summation of all the standard deviations of the real parameter values from the calculated values.

$$U = (N - n_p)^{-1} \sum n_e^{-1} \sum w_{ni} (y_{ni}^{obs} - y_{ni}^{calc})^2 \qquad ...(3.37)$$

where N is the total number of experimental points

n_p is the number of parameters being optimised

n_e is the total number of electrodes

w_{ni} is the weight of the *ith* residual at the *nth* point and

y_{ni} is the total concentration of electrode ion i or the electrode emf of electrode i, at the *nth* titration point.

For the desired parameters to be optimum, the objective function U has to be at a minimum.

The Gauss-Newton approach to the minimisation of the objective function assumes that U is a quadratic function with respect to all the parameters, hence expressed as:

$$U = a + p^t b + (p^t H p)/2 \qquad ...(3.38)$$

where H, the Hessian is $d^2U / dp_l dp_k$ (Murray, May; 1984).

The mass balance equations are solved in an iterative Newton-Raphson manner, which requires that the set of initial estimates be very good and that the concentration of at least one of the reactants be accurately known. The rest of the input data, which includes the electrode potential, the electrode slope and the dissociation constant of water must also be reliable. Since in the solution of the mass balance equations there are more data points than unknowns, whose values are being sought, the iterative method is likely to converge at an answer that borders around the true value. The establishment and use of mass balance equations ensures that all the possible species of an element are detected.

Calculations are terminated if the resultant shift vectors are large or if the shift vector has an upward gradient. This indicates that the system input is wrong and therefore the mass balance equation cannot be solved. An upward gradient means that the minimum of the objective function has been overshot and so the shift has to be successively bisected to bring it back down to convergence. If U_{min} is not reached before shift bisection is at the

lowest possible value, then the program terminates due to failure in shift optimisation. Once the shift has been sufficiently reduced and the U_{min} is at its best possible minimum, s = the standard deviation, the Hamilton R - factor and its limit are then calculated and reported together with the optimised values of the stability constants.

3.1.1.12 The **ESTA** (*Equilibrium Simulation for Titration Analysis*) Program Library

The program ESTA (May, 1984) was intended as a flexible investigative tool for the determination of stability constants in aqueous chemical equilibria. After analysis of the potentiometric titration data, the equilibrium distribution of a well-defined system could be easily found by use of ESTA. This library of programs was also designed to perform other functions so that maximum information may be gained from the titration data. The flowchart in figure 3.0 describes the procedure for the determination of the equilibrium constants.

The ESTA program can be used to create simulated data from the experimental data. This gives a true indication of the meaning of the experimental data but it is not advisable to use it, as it does not give an indication of the quality of the initial data. It might lead to false confidence in the data. The use of simulated data is handy in the evaluation of the accuracy of the initial experimental data.

The ESTA program calculates two important functions (May/ Murray, 1984) from the titration data. These functions define the kind of equilibria that are present in a chemical system. They are the formation function (Z) and the deprotonation function (Q). These functions are defined differently for the ligand, the binary and the ternary systems. This is because the kinds of equilibria taking place in the different systems will vary depending on the number of components that constitute each system.

For the ligand system, the proton formation function is expressed as:

$$Z_H = (T_H^* - H + OH) / T_L \qquad ...(3.39)$$

where T_H^* is the total hydrogen ion concentration, T_L is the total ligand concentration and $OH = K_w / [H]$. The Z_H function is plotted against pH. In simple terms, Z_H is the average number of hydrogen ions bound to the ligand at each pH.

The Z function can also be defined for metal complexation titration data, as:

$$Z_M = [T_L - A(1 + \sum\beta_{LHn}H^n)] / T_M \qquad ...(3.40)$$

where $A = (T_H - H + OH) / (\sum n\beta_{LHn}H^n)$

and T_M is the total metal concentration. This function is plotted against pL, i.e. -log[L]. It indicates the average number of ligand molecules bound to each metal ion at each concentration of ligand.

On the other hand, the deprotonation function, Q can be expressed as;

$$Q = (T_H^* - T_H)/ T_M \qquad ...(3.41)$$

where T_H^* is the total calculated proton concentration in the absence of the metal ions, T_H is the observed concentration of the protons in the reaction system and T_M is the total metal ion concentration. Before the deprotonation function can be calculated the computer first has to solve the two following mass balance equations;

$$T_H^* = H - OH + \sum r[M_pL_qH_r] \qquad ...(3.42)$$

$$T_L = L = + \sum q[M_pL_qH_r] \qquad ...(3.43)$$

where $p = 0$ and $OH = K_w /H$

In binary systems, a formation function representing the number of protons **n** that would be on the ligand in the absence of the metal ion, is simultaneously defined as;

$$n = (T_H - H + OH) /T_L \qquad ...(3.44)$$

The difference between **n** and Q gives the number of protons on the complex. This can be represented as:

$$\mathbf{r} = (\mathbf{q} \times \mathbf{n}) - (Q \times \mathbf{p}) \qquad ...(3.45)$$

where **p** and **q** are the stoichiometric coefficients of the metal and the ligand respectively. It is possible that $\mathbf{r} < 0$, in which case either the deprotonation of the complex formed or the formation of hydroxo species is envisaged.

The ESTA programs also have limitations. Tasks (see glossary) like OBJT cannot make corrections for the activity coefficient, electrode selectivity and the liquid junction potential. With tasks like TOTL, VESL, BURT and SPEC, (see glossary) the mass balance equations are solved without the consideration of the charge balance of the system. This has an insignificant effect on the numerical values obtained but in itself it is a disadvantage of ESTA.

ESTA is one of the many programs that are available for use in the analysis of titration data. Though it has limitations, it has the advantage of a multi-directional approach to optimisation. However, of more importance to proper model selection are the errors in the analytical concentrations, the accuracy of predetermined stability constants and electrode calibration. With the ESTA programs, these attributes of data analysis have been understood and hence the ability to avoid them has improved. This has resulted in the improvement of the agreement between different analysts in published sets of stability constants describing any aqueous chemical equilibrium system.

3.1.1.13 DATA ERROR ANALYSIS

Before any stability constant measurement can be made, a thorough examination of the typical error inherent in the system has to be made. This may be done by studying a well-known system for instrumentally generated error, or by varying the reaction conditions for a particular system and observing its reproducibility. The insertion of randomly generated error would provide the variation of experimental conditions for subsequent calculations.

3.1.1.13.1 *Weighting*

Error weighting (May, Murray; 1988) in percentage is applied to each of the parameters of titration data in accordance with the gravity of its role on the global error of the system. This is done so that the information obtained from the data is not biased toward any of the parameters. Any error that may be associated with whatever parameter that is held constant during an optimisation manifests itself differently at different regions of the data. The effect of such error has to be reduced at the regions of the data at which the source parameter is less influential and only stressed where the parameter is most influential. Mathematically, the weight is the reciprocal of the variance of the residual between the real and calculated data. The weight of the *ith* residual at the *nth* titration point is:

$$w_{ni} = [\, \Sigma \, (\, d(\, y_{ni}^{\,o} - y_{ni}^{\,c} \,) \, / \, dp)^2 \, \sigma_p^{\,2}]^{-1} \qquad ...(3.46)$$

where *p* is the parameter being optimised and σ_p is the standard deviation in p.

Weights may be calculated either once off at the beginning of the optimisation or at each Gauss-Newton cycle of the optimisation. If, however, the initial estimates are not good, then convergence is less likely, but if calculated at each cycle, the weights are based on a more correct value each time and are therefore much more reliable and informative. In this study, the weights are calculated at each cycle; since the ESTA2A rather than the ESTA2B module (May, 1977) is used for optimisation of parameters. Weighting is more important when optimising with respect to the emf (task OBJE) than when optimising

with respect to the analytical concentration (task OBJT). The reason for this is the wider variation of emf during the titration compared with that observed in the analytical concentration, which is much narrower. Weighting is beneficial if systematic errors are present in a set of data because, otherwise, significantly different values of stability constants would be found.

At the end of an optimisation of weighted data, the goodness-of-fit between the experimental and the calculated value of a refined parameter is indicated by the Hamiltonian R-factor. It is represented by the expression:

$$R_H = [\, U / \Sigma n_e^{-1} \Sigma w_{ni} (y_{ni}^{obs})^2]^{1/2} \qquad \ldots(3.47)$$

The R-factor is normally provided together with the R-limit which indicates the optimum fit. It is calculated from the lowest estimates of experimental error (Meloun, Havel, Hogfeldt; 1988) and is expressed as:

$$R_{lim} = [\, N / \Sigma n_e^{-1} \Sigma w_{ni} (y_{ni}^{obs})^2]^{1/2} \qquad \ldots(3.48)$$

where N is the total number of experimental titration points.
Optimistically, the R-factor should be equal to the R-limit but since titration data contain errors that are other than just random, this is hardly achievable.

3.1.1.13.2 *The Monte Carlo Analysis of Error Propagation*

The Monte Carlo (May/ Murray, 1988) simulation method is used in error analysis of potentiometric data, both calibrative and titrimetric (Meier, 1985; Horvai, Pungor; 1988). In such data, only the random as opposed to systematic errors can be calculated by the least-squares approach. The effect of any error due to a parameter, on the final optimisation result, will be proportional to the importance of that parameter to the data. If the errors do not cancel out even when they are of equal and opposite magnitude then they can be said to be systematic. Systematic errors may affect the data in either a local or a global manner. In a set of titration data being analysed together, local errors are

those that are associated with a particular titration, such as errors in analytical concentrations and volumes as well as in the electrode calibration for that titration. Global errors are those associated with fixed predetermined parameters, like the dissociation constant of water and the ligand protonation constants. The magnitude of systematic errors is never apparent and therefore a good experimental technique is always advisable. The least squares method of quantifying error in stability constants becomes highly inadequate when applied to systematic errors and may indicate untrue degrees of accuracy. In such a case, the Monte Carlo approach then becomes a better method to use.

The Monte Carlo technique applies random error to all the optimised parameters in a Gaussian distribution manner and, in a number of cycles, repeatedly calculates the objective function in an attempt to minimise it. The parameters that describe titration data are mathematically related, so that whatever error is associated with any parameter that is held constant will be propagated to a related parameter that is being optimised. The Monte Carlo technique minimises the objective function with respect to the standard deviation of the optimised and fixed parameters. This approach makes it easy to identify which parameters are better fixed during an optimisation and how much a particular optimised parameter is affected by error in the fixed parameters. This inter-parameter error effect is called correlation. The correlation coefficient between two parameters can be quantified using the equation:

$$r_{ij} = -G_{ij} / (\sqrt{G_{ii}G_{jj}})^{1/2} \qquad ...(3.49)$$

where G is the reciprocal of the Hessian (1/H) (see equation 3.38).

Correlation (May/ Murray 1988) in the parameters is inevitable and therefore a way has to be found to reduce it so that as much independent analysis of each parameter error as is possible is achieved. The degree of correlation between the fixed and the optimised parameters will determine how much the errors in the fixed parameters will distort the optimisation. Correlation is not guaranteed by the mathematical relationship between the

parameters but may be greatly influenced by the number and the spread of the data points in the analytical range. Even though it is true that the wider the range of the spread of experimental points the better the independence of optimisation of parameters, the danger lies in the fact that a wider range has a higher probability of inheriting systematic error. The chances of parameter correlation are even higher. This, however, is a chance that has to be taken in order to have more confidence in the stability constants obtained from the analysis of the data. In all this, the matter still rests on the quest for high quality experimental data.

In order to quantify the correlation associated with stability constant determination, the way the error is carried through in the calculation of the objective function will be indicated as a standard deviation at the convergence of the optimisation. Different combinations of freed and fixed parameters give different Monte Carlo spreads as would be reflected in the reported standard deviation. However some different combinations of freed and fixed parameters give the same standard deviations, so that it becomes necessary for the analyst to use chemical intuition and experimental experience to explain such observations and to use only the appropriate parameters in the determination of the best chemical model.

When a parameter is fixed, all those that are optimised will be based on this parameter and its associated error, therefore it is preferable to optimise more parameters rather than less. This opens more room for correlation and widens the Monte Carlo spread, but gives higher precision for the stability constant determination at each Monte Carlo cycle. There has to be a balance between systematic error associated with fixed parameters and deviation from the true stability constants due to higher correlation and error propagation between optimised and fixed parameters. Since the true stability constants of any system can never be known exactly, an average has to be found by the comparison of various stability constant values, measured under similar conditions for the same system, as reported by different analysts. This would at least indicate the range in which the true stability constants might lie. In addition to high quality experimental data, a good choice

of parameters to optimise and the application of appropriate weighting measures would ensure that this range is minimised as much as possible.

3.1.2 Experimental

In this study the titrations were performed in a cell with a glass pH electrode and a silver/silver chloride reference electrode. The cell was calibrated in terms of proton concentrations at 25°C with the dissociation constant (pK_w) of water at 13.77. The emf was monitored by the use of a Radiometer pH meter. The reaction mixture was kept at a constant temperature of 25°C by circulating thermostated water and purified nitrogen was bubbled through the cell throughout all titrations. Titres of sodium hydroxide solution were dispensed from a Metrohm 645-Dosimat burette.

All titrations were performed under an inert condition of purified nitrogen. The nitrogen was purified by passing it through a train of bottles containing 50% potassium hydroxide to remove carbon dioxide, Fieser's solution (Vogel, 1984) to remove oxygen and background electrolyte solution to humidify the reaction chamber.

3.1.2.1 The Titration Solutions

All solutions were made with a solution of recrystallised NaCl as background electrolyte, at an ionic strength of 0.15 mol dm^{-3}. The NaCl crystals had been dried in an oven for at least 24 hours. This solution will be referred to as background electrolyte in the sections that will follow.

3.1.2.1.1 *Preparation of Ligand Batch Solution*

The hydrochloride salt of each of the four ligands ZDA, BID, EDA and DME (glossary) were dissolved in background electrolyte to make each batch of ligand solution. An estimated concentration of the batch solution was calculated based on the dry mass of the ligand hydrochloride salt. All batch solutions were made to a concentration of approximately 0.1 M.

3.1.2.1.2 *Stock Acid Solution(HCl)*

Acid solution was made to a concentration of 0.035M from Merck ampoules (1.09973-Titrisol) in background electrolyte. They were standardised against recrystallised sodium tetraborate decahydrate, (borax), $Na_2B_4O_7 \bullet 10H_2O$.

3.1.2.1.3 *Stock Base Solution (NaOH)*

NaOH solutions were made from a Merck ampoule (1.09959-Titrisol) in a glove box under nitrogen to reduce CO_2 contamination. Solutions were stored in high-density polypropylene bottles fitted with CO_2 traps. The solutions were standardised against recrystallised potassium hydrogen phthalate as well as against standardised HCl solution by the Gran method (Rossotti, Rossotti; 1965).

3.1.2.1.4 *Metal Ion Solutions*

Copper: A Merck copper chloride ampoule (1.09987-Titrisol) containing an equivalent of 1g of copper was used to prepare 1*l* of a copper ion solution. This solution was standardised against EDTA using Fast Sulphon Black F indicator (Vogel, 1978).

Zinc: A zinc (II) standard solution ampoule supplied by Merck (1.09953-Titrisol) was used to prepare 500 m*l* of stock metal solution.

Calcium: A calcium (II) standard solution ampoule supplied by Merck (1.09943-Titrisol) was used to prepared 500 m*l* stock metal solution.

3.1.2.1.5 *Metal Solution Acid Determination*

Acid is added to the metal ion solution in the ampoules to prevent the hydrolysis of the metal ions. This concentration of acid has to be quantified to ascertain the acid contribution of the metal solution to the titrant solution. To determine the amount of this acid, a 15-ml volume of the metal ion batch solution was titrated potentiometrically with a 0.015 M HCl solution. The data obtained was analysed by the Gran function (ϕ) for free acid. This gave an indication of the concentration of free acid in the metal ion solution.

The acid titration of the metal solution gives a better indication of the free acid concentration in the metal ion solution than a base titration would because of the possible problem of metal hydroxide formation in the latter case. This would give an unreliable reflection of the concentration of hydrogen ions present in the metal ion solution.

3.1.2.2 The Titrations

3.1.2.2.1 *Protonation Constant Titration*

The protonation constant titration data was also used to standardise the ligand solutions. A 15-ml aliquot of the batch ligand solution was dispensed into the titration vessel by a piston burette. A 1-ml aliquot of the standardised HCl solution was added to the vessel from another burette, to ensure that the ligand was completely protonated. The electrodes completed the reaction cell and the solution was allowed to reach the working temperature. The titration was then followed potentiometrically with the glass electrode at 0.05-ml standard-base addition increments. Data obtained consisted of the volume of titre added and the corresponding emf values of the system at each titration point.

3.1.2.3 Data Analysis

3.1.2.3.1 *Ligand Protonation*

The following formulae for the Gran function (Rossotti, Rossotti; 1965) were applied to the data to produce two sets of data.

$$\phi = (V_i) \times 10^{-pH} \qquad ...(3.50)$$

$$\phi' = (V_0 + V_i) \times 10^{pH} \qquad ...(3.51)$$

where ϕ and ϕ' are the two Gran functions, V_0 is the initial reaction vessel volume and V_i is the volume of added base at *ith* point of the titration. The pH values used in the Gran function at each titration point were calculated using the equation;

$$pH = -(E - E_0 / s) \qquad ...(3.52)$$

The concentration of the hydrogen ion before and after the end point was calculated by the Gran equations (3.50) and (3.51) respectively. A plot of the Gran functions against the volume of base added showed two different graphs for these two functions. The point where ϕ intersects the x-axis shows the endpoint volume of base for the free acid titration while ϕ' intersects the x-axis at the end-point of the titration of the total acid. This was done for each set of titration data. For replicate titrations, the average of the two sets of hydrogen ion concentration was used for computer simulation calculations.

The difference between these two endpoint volumes of base indicates the volume of base that was used to completely deprotonate the ligand. Depending on the number of ionisable protons assumed to be present on each ligand molecule, the concentration of the ligand in the reaction solution could be found by dividing the total concentration of the acid associated with the ligand by that number of protons. The concentration of acid, the concentration of ligand and the electrode potential were then used as input into an ESTA file template for the determination of the protonation constants. Each set of replicate titrations was analysed together for the determination of the stability constants.

The value of the dissociation constant of water used, obtained from the optimisation of the acid/base internal calibration (May, Williams, Linder, Torrington; 1982) titrations, was 13.77. Using the concentrations obtained in the Gran calculations, the $ZBAR_H$ task plot options 1 and 2 (see glossary) yielded observed and calculated curves respectively. These curves were not in agreement in that they did not completely overlap. Optimisation of the concentrations by task OBJE resulted in good agreement between the observed and calculated formation curves. The acid concentration and protonation constant values obtained as output of the optimisation were then used for the Z_H plots. If this yielded complete overlap of the calculated and observed Z_{bar} plots, the protonation constants were accepted as true for the ligand. The corresponding values of the concentrations of the ligand and the proton were then used for the standardisation of the batch ligand solution.

Adjustments to experimental concentrations were necessary in order to obtain data that were suitable for analyis with the ESTA program. Several different titrations were performed, each with slightly different initial concentrations of ligand. Data analysis was aimed at obtaining a system that converged after fewer cycles and whose standard deviations of the optimised parameters were minimal.

3.1.2.3.2 *Complexometric Titrations*

The titration data for each of the pairs of titrations carried out at three different metal to ligand ratios were first analysed separately as pairs and then all together as bulk data. In each case, the input data included the protonation constants, the calculated concentrations of metal, ligand and hydrogen ion. Also included were the standard electrode potential, (E°), calculated using a strong acid reading taken immediately prior to the titration by equation (3.30) in section 3.1.1.5, the dissociation constant of water and the titration data. The constants for the hydrolysis (Baes, Mesmer, 1976) of the different metals were included in the speciation models.

For copper,

$$Cu^{2+} + H_2O <=> [Cu\,(OH)]^{+}; \qquad \log K = -8.0 \qquad ...(3.53)$$

$$2Cu^{2+} + 2H_2O <=> [Cu_2\,(OH)_2]^{2+} \qquad \log K = -10.6 \qquad ...(3.54)$$

For the hydrolysis of zinc

$$Zn^{2+} + H_2O <=> Zn(OH)^{+} \qquad \log K = -8.37 \qquad ...(3.55)$$

$$Zn^{2+} + 2H_2O <=> Zn(OH)_2 \qquad \log K = -16.9 \qquad ...(3.56)$$

$$Zn^{2+} + 3H_2O <=> Zn(OH)_3^{-} \qquad \log K = -28.4 \qquad ...(3.57)$$

$$Zn^{2+} + 4H_2O <=> Zn(OH)_4^{2-} \qquad \log K = -41.2 \qquad ...(3.58)$$

$$2Zn^{2+} + H_2O <=> Zn_2(OH)^{3+} \qquad \log K = -9.07 \qquad ...(3.59)$$

For the hydrolysis of calcium

$$Ca^{2+} + H_2O <=> Ca(OH)^+ \qquad \log K = -12.84 \qquad ...(3.60)$$

Initial guesses of the complex species and their stability constants were entered into the input file and evaluated by the BETA task (glossary), with all guessed stability constants marked with the *2* symbol for a more general adjustment. The output gave modified values of the stability constants. Subsequently, the initial guesses were replaced by the modified guesses and marked with the symbol 1 (one) for a final modification. The output values and the acid concentration were optimised by the OBJE task to give the final values of the stability constants and the acid concentration describing the system

The values found for the stability constants were then used in a QBAR task to check if the model selected fitted the system, i.e. if the species that were assumed to be in the reaction system were really there. If the calculated and the observed QBAR plots overlap, then the model selected is correct. Two types of deviation are possible in the appearances of the observed and the calculated QBAR plots. They might have the same shape but not overlap, which means that the model is correct but there is an under- or over-estimation of one of the stability constants reported. The other possibility is that the shape of the observed plot is totally different from the shape of the calculated plot, indicating that the model is completely wrong. It may be that there is a species missing or that there is a species that has to be omitted. Once there is total overlap of the observed and the calculated QBAR plots, it can be concluded that the model is correct.

The $ZBAR_M$ task (indicated by plot options 3 and 4 (see glossary)), which gives a plot indicating the average number of ligands per metal ion, can also be used to check if the model is correct. Even here, coincidence of the observed and calculated plots is required for the confirmation of the correctness of the model.

Species distribution plots were calculated by the task SPEC of the ESTA1 module. This plot shows the distribution and the percentage of the different species of the chemical model along the pH scale.

Figure 3.0 is a flowchart summarising the procedure followed in the computer analysis of titration data in quest of the protonation and complexation constants. These are then entered into the ECCLES model of blood plasma to determine the metal ion plasma mobilising indexes of the ligands under investigation.

The plasma mobilising index is described as:

$$\text{p.m.i.} = \frac{\text{(total concentration of low-molecular-weight copper (II) complexes in the presence of the drug)}}{\text{(total concentration of low-molecular-weight copper (II) complexes in normal plasma)}}$$

Figure 3.0: Flow chart, describing procedure for the determination of protonation and complexation constants.

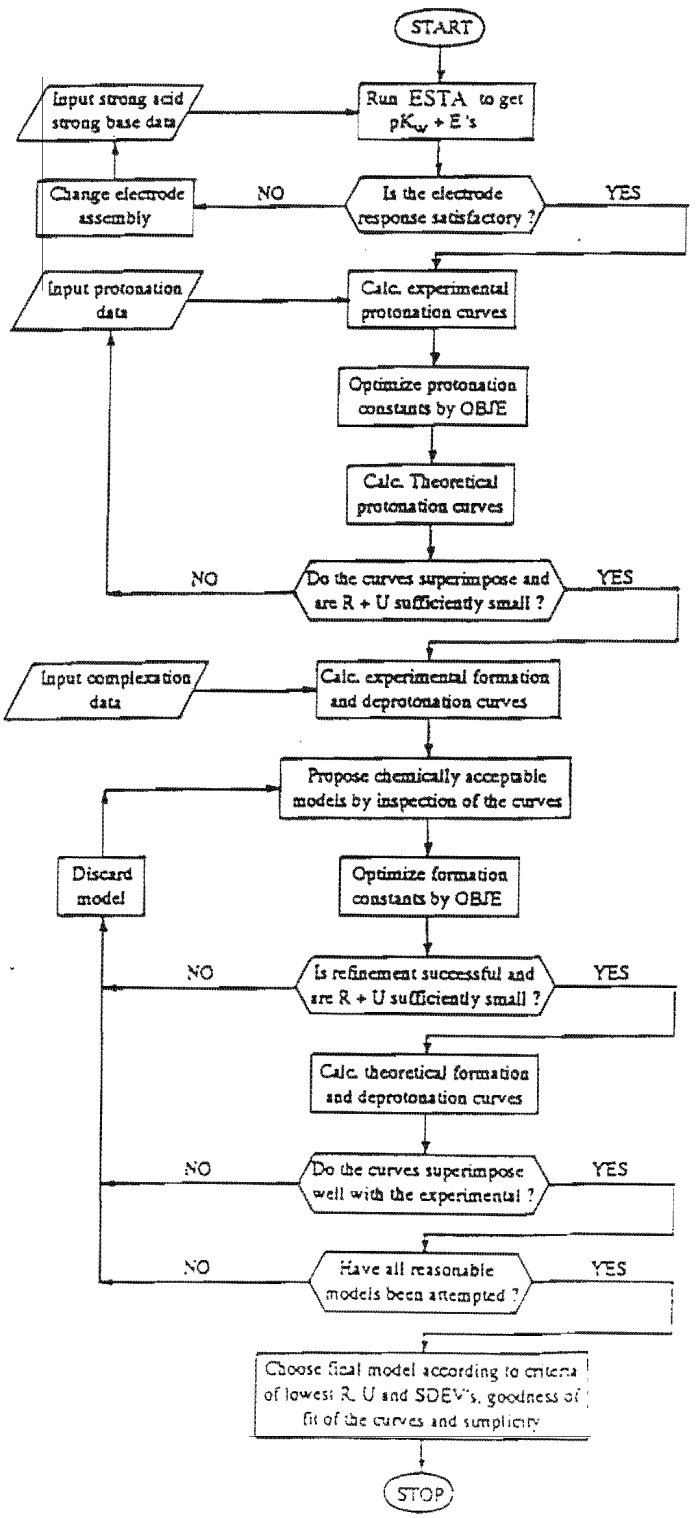

3.1.3 **RESULTS**

In this section numerical results for all four ligands will be presented. Since the chemical speciation of all the ligand systems is similar and for the sake of clarity, only the plots of Cu/EDA system will be discussed. The plots of the other Cu/Ligand systems will appear as an appendix to the thesis. Ligand EDA is chosen because of its high potential for use in further work.

3.1.3.1 Protonation

Table 3.1.3a: Logarithms of overall protonation constants (log β_{01r}) of present ligands, measured at 25°C in 0.15 mol dm^{-3} (Na)[Cl]. S.dev = standard deviation, n_T = number of replicate titrations, n_P = number of titration points, R_H = Hamilton R factor, R_{lim} =Hamilton R limit.

Ligand	Species	log β	s.dev	logK	n_T	n_P	pH	R_H	R_{lim}
ZDA	011	8.88	0.003	8.88	2	239	2-10	.017	.021
	012	17.7	0.005	8.78					
	013	22.2	0.009	4.53					
BID	011	8.80	0.005	8.80	2	417	2-10	.018	.01
	012	16.8	0.006	7.47					
	013	19.9	0.01	3.21					
EDA	011	9.41	0.004	9.41	3	663	2-11	.12	.13
	012	17.9	0.005	8.55					
	013	21.6	0.009	3.63					
DME	011	8.73	0.003	8.73	3	924	2-11	.12	.12
	012	16.7	0.003	7.98					
	013	20.2	0.007	3.44					

The overall protonation constants in Table 3.1.3a were confirmed to be accurate by the complete overlap of the calculated and the observed Z_H plots (see Figure 3.1.3a. This is also indicated by the close approach of the Hamilton R-factor to its limit. The low

standard deviation of less than 0.01 makes these values acceptable within the confidence range.

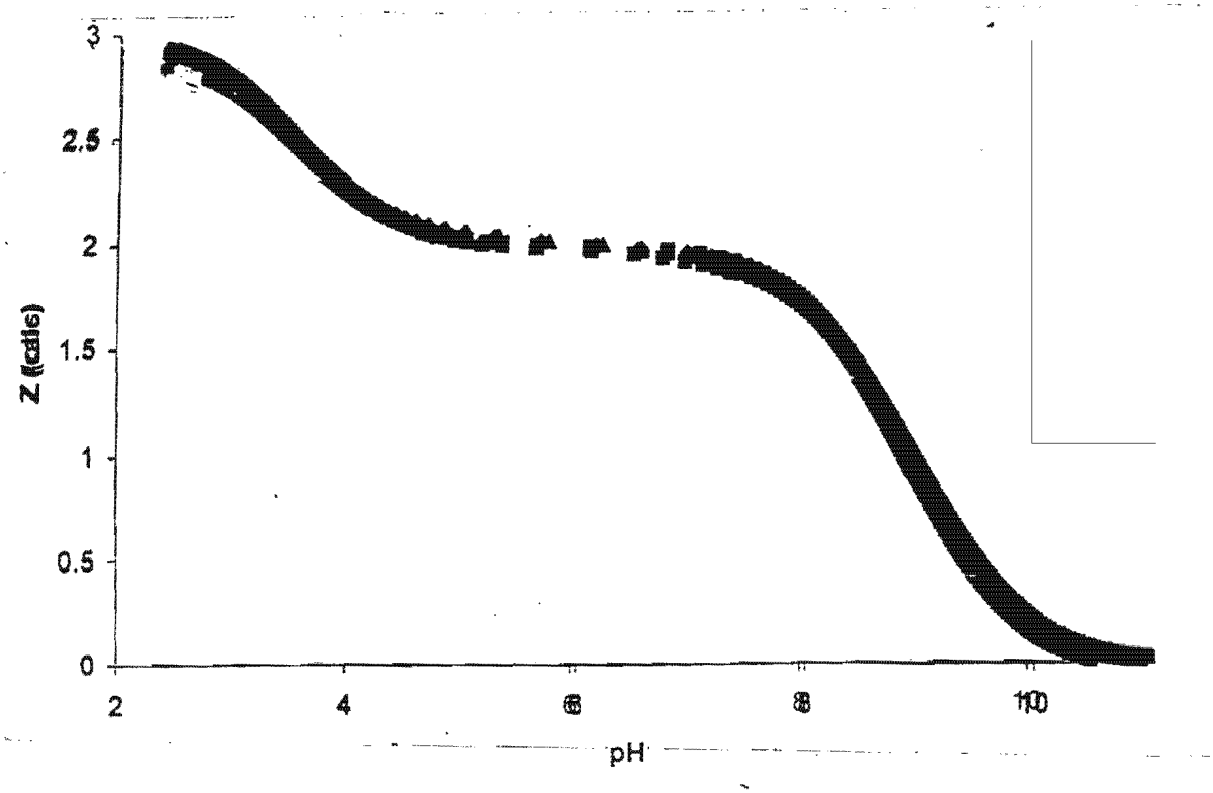

Figure 3.1.3a: Protonation Function Curve (Z_H) curve (Ligand EDA) at 25°C in 0.15 mol dm^{-3} (Na)[Cl].

Comment: This plot shows the average number of protons on the ligand as pH changes. The plot of Z_H versus pH shows an approach to a maximum at $Z_H = 3$ in the low pH region. This indicates that the ligand possesses three sites of protonation i.e at a pH of about 2, there are three dissociable protons on the ligand. The three titrations, each with a different starting concentration of ligand, performed for the determination of the protonation constants are well superimposable. This indicates high experimental accuracy and reproducibility of the titrations. This therefore lends greater confidence in the protonation constants found. The poor overlap observed in the pH regions below 2.5 and above 9 is due to poor electrode response in these regions.

Table 3.1.3a shows that the values of the first two protonation constants are close to each other and these correspond to the protonation of the two terminal amino groups. The value of the third protonation constant is much lower than those of the other two and corresponds to the protonation of the central amino group.

Figure 3.1.3b shows the distribution of the different species of protonated ligand. It shows that for quite a sizeable range of pH (4 to 8), a hundred percent of the ligand present in solution is doubly protonated. The singly protonated LH has a very short pH span as completely deprotonated ligand predominates above pH 9.5. This plot further illustrates the Z_H curve in that it shows the pH regions in which the different protonated species occur together.

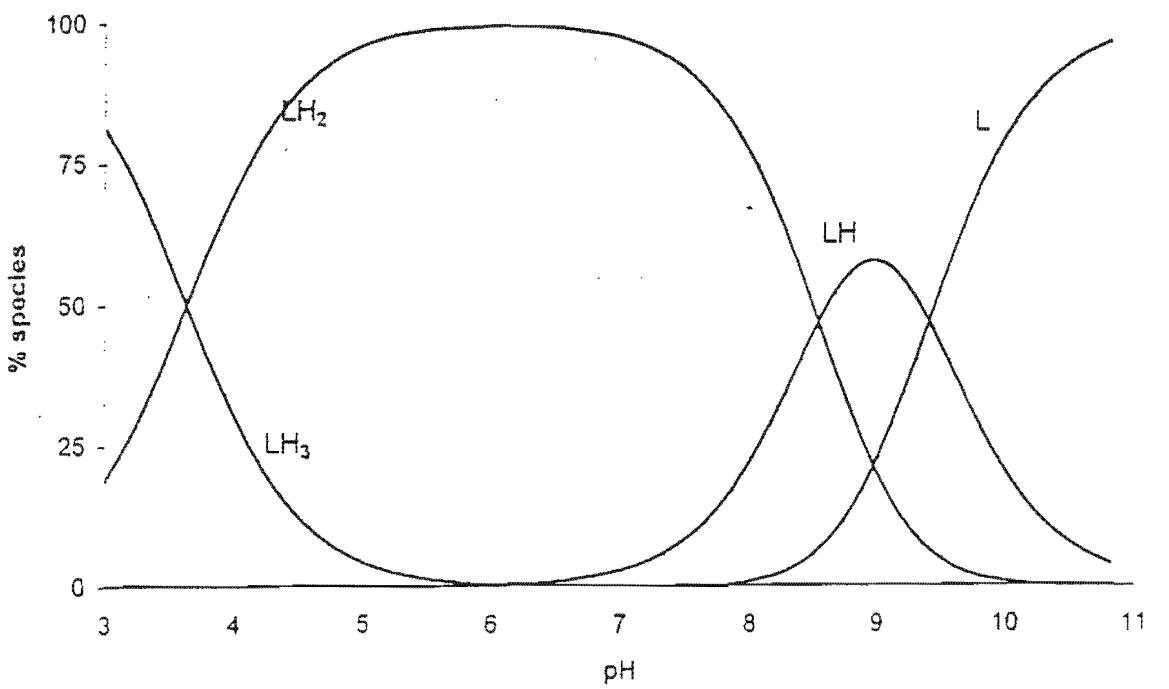

Figure 3.1.3b: Protonated species distribution diagram (Ligand EDA)

3.1.3.2 Copper complexation

Table 3.1.3b: Logarithms of the overall stability constants ($\log \beta_{pqr}$) of copper (II) species of present ligands at 25°C in 0.15 mol dm^{-3} (Na)[Cl]. S.dev = standard deviation, n_T = number of titrations, n_P = number of titration points, R_H = Hamilton R factor, R_{lim} =Hamilton R limit.

Ligand	pqr	$\log\beta_{pqr}$	s.dev	n_T	n_p	R_H	R_{lim}
ZDA	111	15.79	0.01	6	607	.021	.02
	110	10.77	0.02				
	11-1	2.87	0.03				
	11-2	-6.46	0.04				
BID	111	14.04	0.04	6	981	.02	.02
	110	10.03	0.01				
	11-1	2.07	0.01				
	11-2	-7.28	0.01				
EDA	111	15.06	0.04	6	561	.02	.01
	110	10.54	0.04				
	11-1	3.51	0.01				
	11-2	-6.36	0.01				
DME	111	15.74	0.02	6	779	.07	.01
	110	9.22	0.02				
	11-1	1.09	0.03				
	11-2	-9.26	0.03				

Discussion: Considering the fact that the Gran function that is used in the analysis of the protonation titration data is biased towards strong acid/ strong base titrations (and the present ligands are weak acids), the present protonation constants are accepted because the Hamilton R-factor is close to its limit and is acceptably low. The low standard deviations in the overall stability constants show their accuracy. This is

supported by the fairly good overlap of the calculated and observed Q and Z_M plots (figures 3.1.3c and 3.1.3d).

All four ligands favour the same chemical model in that the same species are reported for each ligand system. However, the different proficiencies of the different ligands to coordinate with the copper (II) ion is shown by the stability of their complexes.

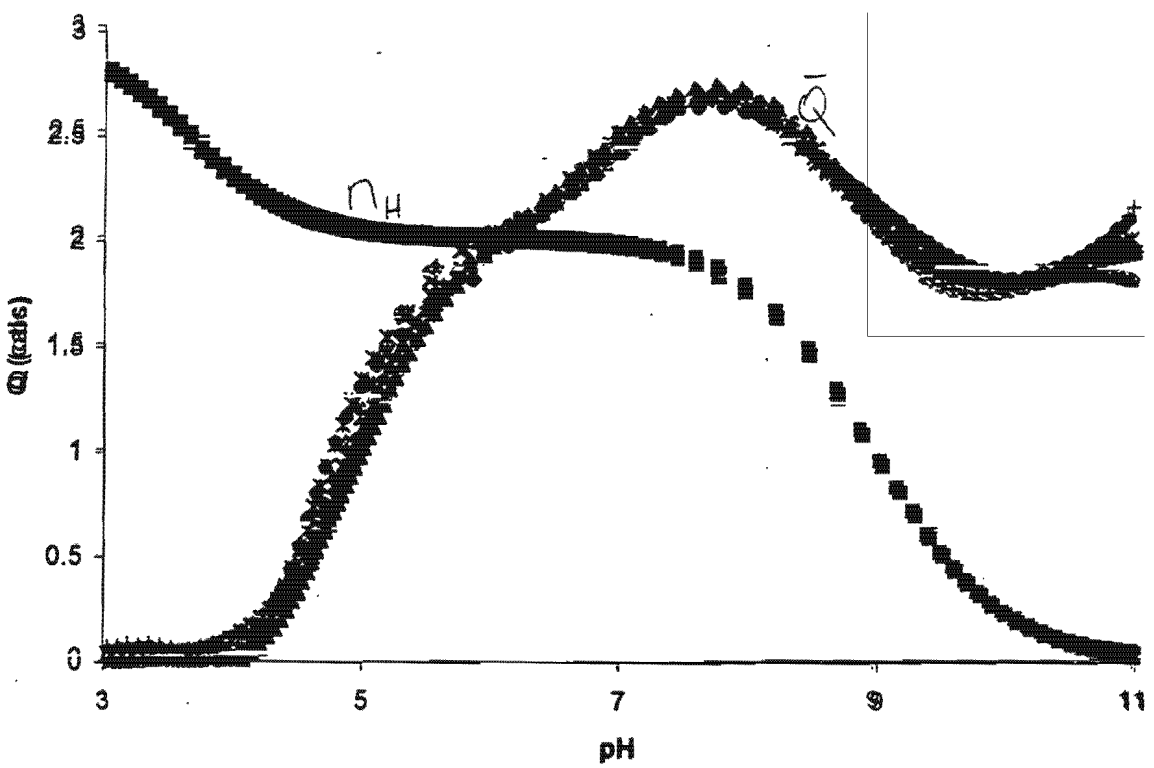

Figure 3.1.3c Deprotonation function curve (Q_M) for Cu^{2+}-EDA system at 25°C in 0.15 mol dm^{-3} (Na)[Cl]. n_H is the possible number of dissociable protons on the ligand and Q is the average number of protons released by the ligand due to complexation.

Comment: The n_H curve that is plotted with the deprotonation function curve shows the number of protons on the ligand as a function of pH. Figure 3.1.3c shows that deprotonation begins at a pH of 4 as indicated by the increase in Q. At any pH, the

number of protons on the ligand are calculated by the difference between the value of n_H and that of Q. This can be expressed as:

$r = (q \times n) - (Q \times p)$ where p and q are the complex stoichiometric coefficients of the metal and the ligand respectively.

As will be shown by the species distribution diagram of this system, at pH 4.5 the MLH species is approaching its maximum percent formation and the Q-curve shows that there are 1.5 protons on the ligand. At pH 6, the deprotonation function curve intersects the n_H indicating that there are no protons on the complex, $(n_H - Q) = (2-2) = 0$. This is the pH at which the ML species predominates.

At pH 7.8 the Q-curve peaks to 2.8, at which point the n_H curve reads 1.8. The value of $n_H - Q$ is at this point –1 and as the speciation diagram shows, the 11-1 species predominates from this pH to about pH 10. Throughout this region, the Q-curve runs parallel to the n_H curve indicating that there is no further deprotonation occurring.

Above pH 10, the plot shows a further increase in deprotonation. This leads to the fomation of the 11-2 species. Evidence of this is the predominance of the 11-2 species above pH 10.

The poor response of the glass electrode in the extreme pH regions (< 2.5 and >9) causes the observed poor overlap of the Q plots.

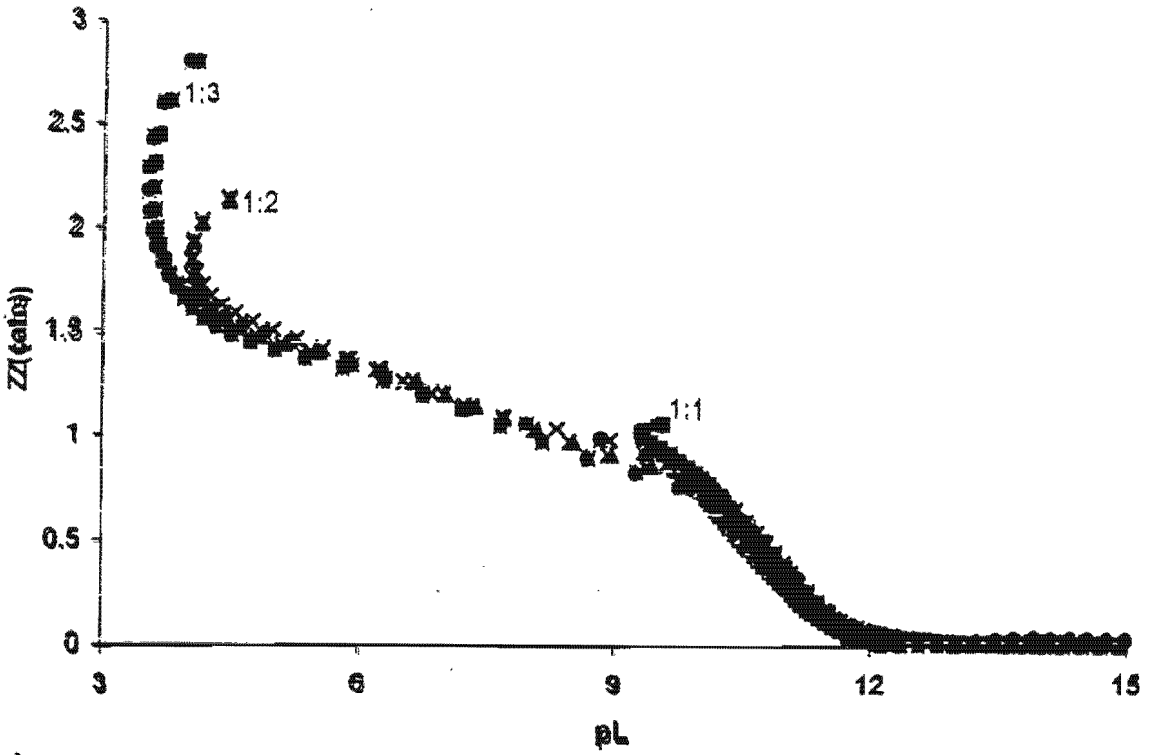

Figure 3.1.3d Formation Function (Z_M) curve (Ligand EDA) at 25°C in 0.15 mol dm^{-3} (Na)[Cl].

Comment: As the formation function shows the average number of ligand molecules bound to each metal ion, Figure 3.1.3d shows that high ligand to metal ratios are required to form the ML_n complex species in which n >1. The three plots on the graph each fan back as lower pL values are approached. This indicates the formation of hydroxo or deprotonated species. In the present case this is observed because of the deprotonation of the amide nitrogen atoms as complexation occurs. These protons are not observed as dissociable protons in the protonation constant investigation because they can be removed only at very high pH.

The levelling of the plots at $Z_M = 1$, immediately followed by the fanning back, indicates that, on average, each metal ion in the system is chelated by one molecule of ligand, followed by the formation of hydroxy or deprotonated complex species.

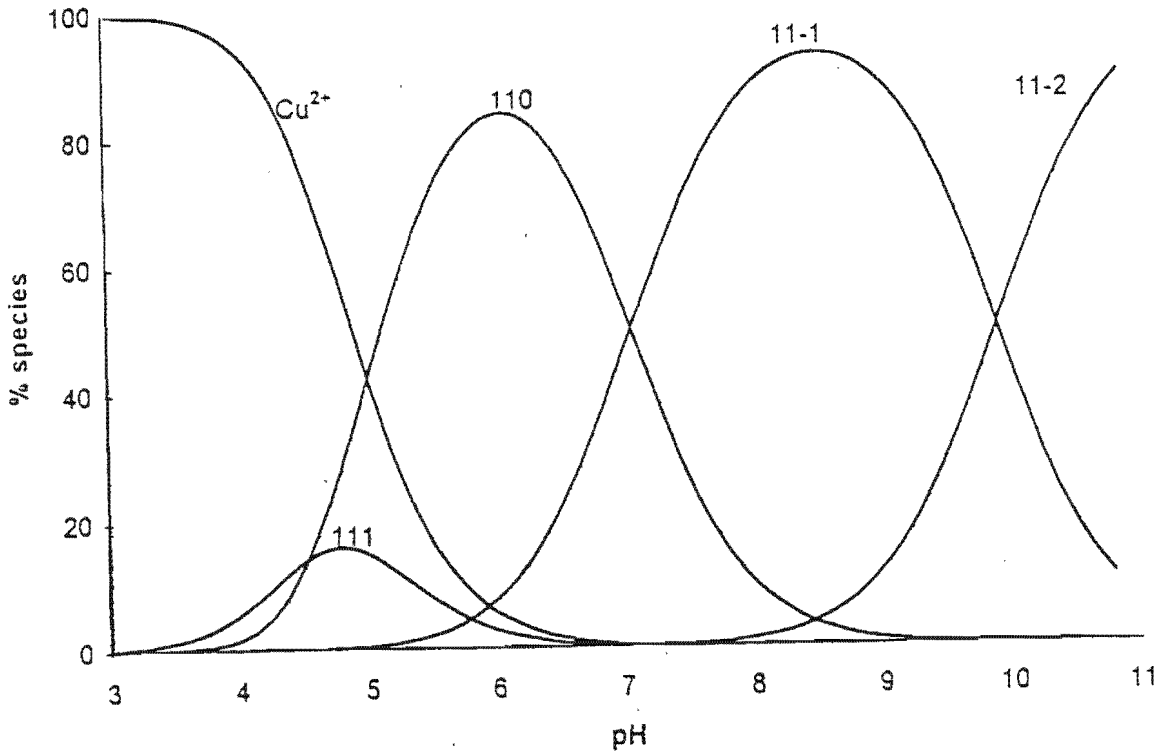

Figure 3.1.3e Copper (II)-EDA Species Distribution Diagram at 0.007 M, in a 1:1, metal to ligand ratio.

Comment: The different species of the chemical model predominate at different regions of the pH scale. The protonated 111 species occurs at the low pH region where the protonation of the ligand donor atoms is more marked, the non-protonated species is at neutral pH and the deprotonated 11-1 and 11-2 species are at the upper end of the pH scale. This spread of species along the pH scale becomes useful in the determination of the structures of the species.

3.1.3.3 Zinc

Tabulated in this section will be the stability constants of the zinc complexes of the present ligands. The Z_M, Q and species distribution diagram of only one of the ligands will be presented and those of the others will appear in the appendix.

3.1.3.3.1 Zinc Complexation

Table 3.1.3.3a: Logarithms of the overall stability constants (log β_{pqr}) of zinc (II) species of present ligands at 25°C in 0.15 mol dm^{-3} NaCl. S.dev = standard deviation, n_T = number of titrations, n_P = number of titration points, R_H = Hamilton R factor, R_{lim} =Hamilton R limit.

	Log β	s.dev	R_H	R_{lim}	Nt	Np
ZDA						
11-1	-2.71	0.073	0.067	0.13	6	726
11-2	-11.15	0.044				
123	33.61	0.037				
133	39.36	0.057				
130	15.78	0.072				
13-2	-1.67	0.083				
13-3	-10.95	0.080				
13-4	-21.47	0.082				
BID						
133	36.69	0.099	0.034	0.014	6	977
112	18.67	0.038				
11-1	-2.18	0.021				
11-2	-10.54	0.030				
11-3	-18.94	0.021				
11-4	-29.81	0.029				
123	32.56	0.018				
12-2	-6.06	0.031				
13-4	-19.79	0.083				
12-4	-23.67	0.063				
12-5	-33.81	0.059				
13-5	-28.57	0.046				
13-6	-38.40	0.038				

Table 3.1.3.3a continued

EDA						
111	13.65	0.021	0.030	0.014	5	694
112	20.94	0.014				
110	6.12	0.027				
11-1	-1.53	0.016				
11-2	-10.63	0.016				
11-3	-21.64	0.019				
120	9.79	0.378				
130	13.87	0.177				
13-1	5.11	0.111				
13-2	-3.94	0.045				
13-3	-14.37	0.050				
13-5	-36.33	0.052				
DME						
111	11.92	0.037	0.045	0.014	6	622
112	19.19	0.031				
11-1	-3.26	0.043				
11-2	-11.34	0.026				
11-3	-22.32	0.035				
21-2	-7.54	0.068				
13-3	-16.97	0.091				

The results in table 3.1.3.3a show that the ligands (ZDA and EDA) have more species in their chemical models than the ligands (BID and DME). Notable in the zinc systems is the high number of hydroxy species. The stability constants of the zinc complexes, were accepted as correct because of the superimposability of the calculated and observed formation and deprotonation function curves (see also appendix A). For the zinc system, the Zn/BID curves will be presented. (Figures 3.1.3.3a-c)

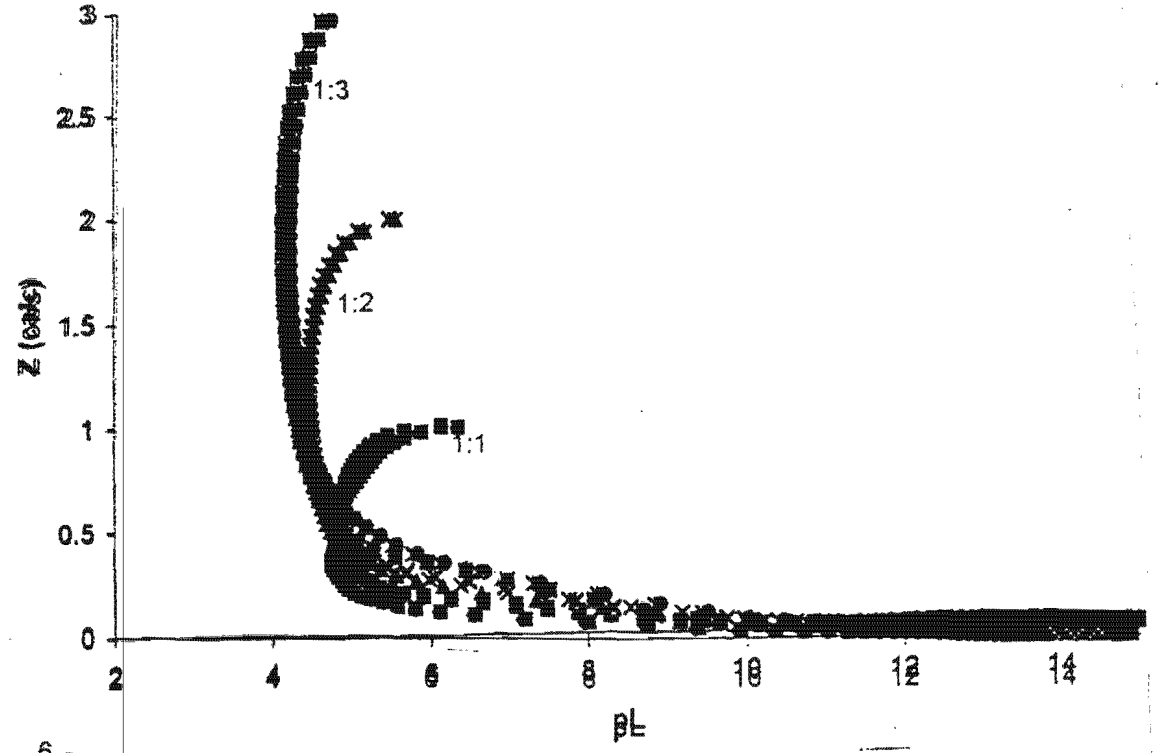

Figure 3.1.3.3a: Formation function curve for Zn/BID system at 25°C in 0.15 mol dm-3 (Na)[Cl].

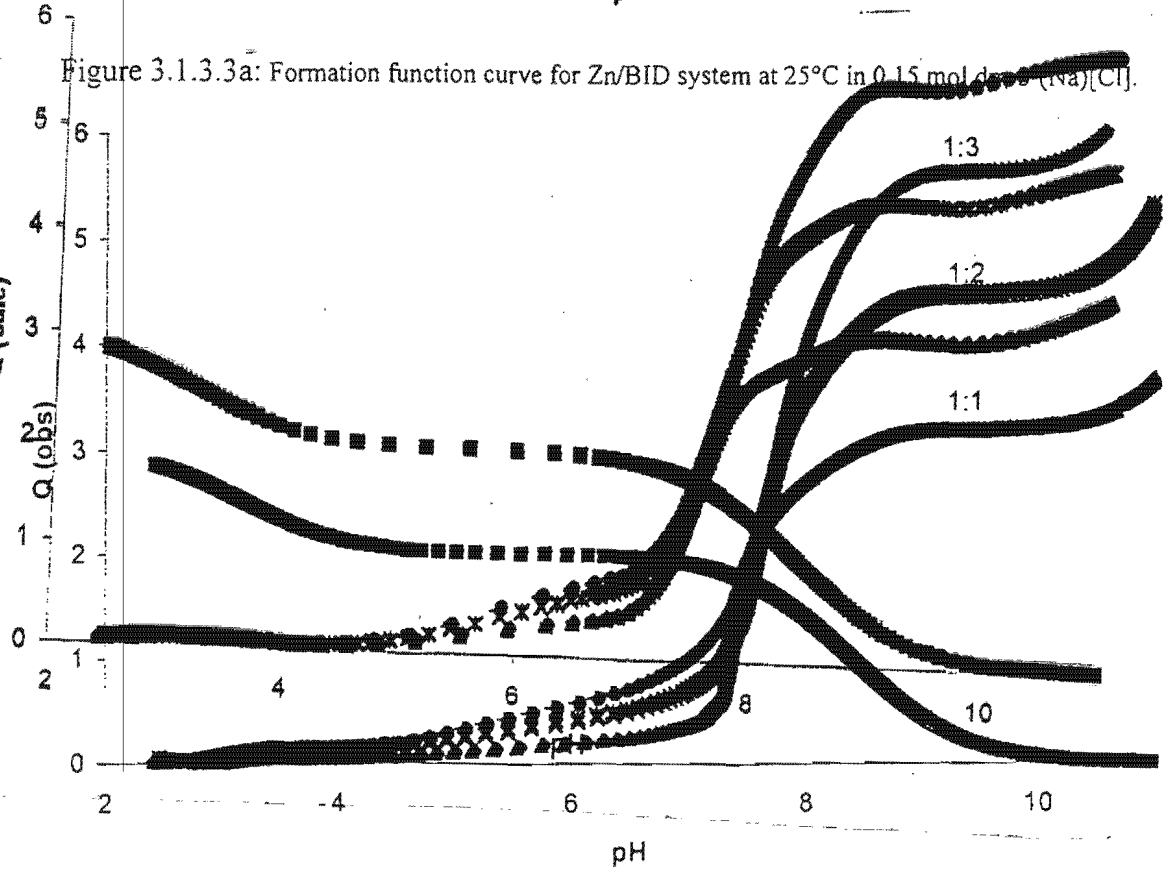

Figure 3.1.3.3b: Deprotonation function curve for Zn/BID system at 25°C in 0.15 mol dm-3 (Na)[Cl].

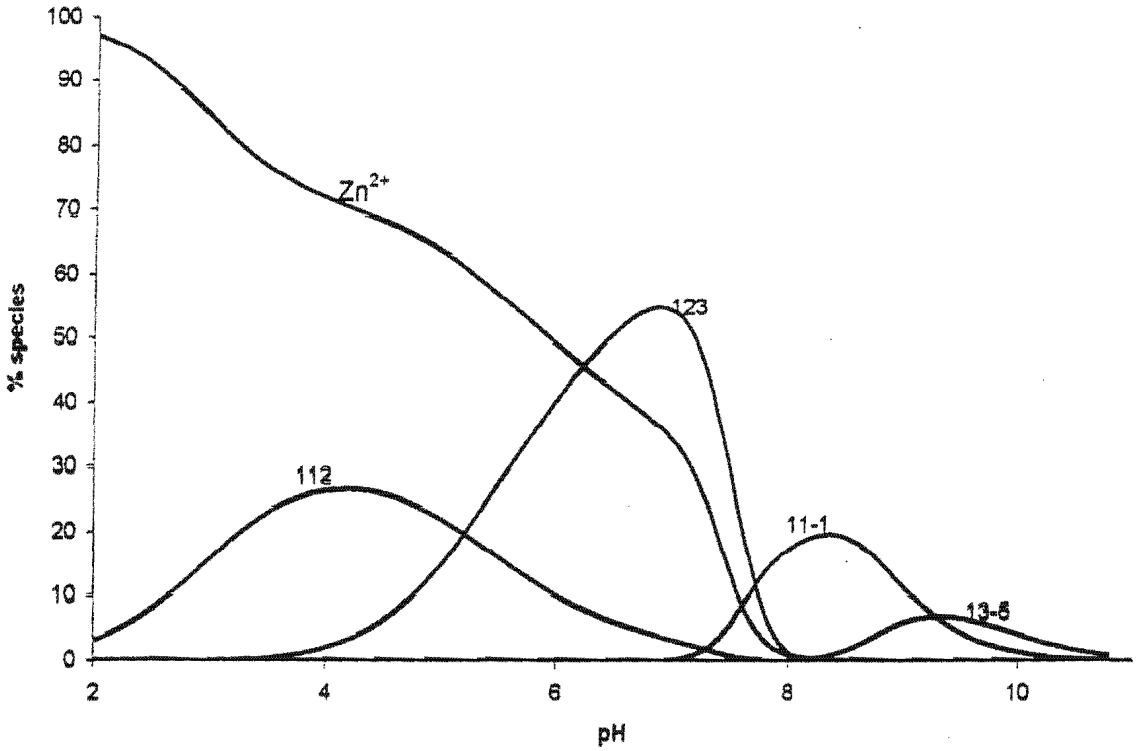

Figure 3.1.3.3c: Species Distribution Diagram for Zn/BID system at 0.007M, in a 1:1, BID:Zn ratio.

3.1.3.3.2 **Calcium**

In this section are the stability constants of the calcium complexes of the four ligands of this study. The formation, deprotonation and species distribution diagram of only the Ca/ZDA system will be presented and the plots of the other ligand systems will be in the appendix.

Table 3.1.3.3b: Logarithms of the overall stability constants (log β_{pqr}) of calcium (II) species of present ligands at 25°C in 0.15 mol dm^{-3} (Na)[Cl]. S.dev = standard deviation, n_T = number of titrations, n_P = number of titration points, R_H = Hamilton R factor, R_{lim} =Hamilton R limit.

	Log β	s. dev.	R_H	Rlim	Nt	Np
ZDA						
123	34.03	0.019	0.039	0.012	6	820
122	26.50	0.017				
120	9.28	0.082				
12-1	0.995	0.084				
12-2	-10.94	0.123				
131	23.17	0.034				
13-1	5.43	0.039				
13-2	-4.73	0.043				
13-4	-27.21	0.053				
BID						
112	19.21	0.035	0.056	0.011	6	591
111	11.58	0.043				
121	14.55	0.034				
12-3	-28.92	0.076				
EDA						
123	32.55	0.014	0.019	0.012	6	860
122	23.74	0.052				
121	15.51	0.016				
130	9.14	0.019				
13-1	-1.45	0.019				
13-4	-35.54	0.025				

Table 3.1.3.3b continued

DME						
123	30.10	0.025	0.025	0.016	6	369
122	22.32	0.033				
121	13.86	0.043				
120	5.53	0.016				
13-1	-2.14	0.019				

Discussion: The superimposability of the calculated and observed deprotonation and formation function curves of the different ligand systems lent acceptability to the chemical speciation models. Figures 3.1.3.3d and 3.1.3.3e show the kind of goodness-of-fit that was observed for the calcium complexation systems.

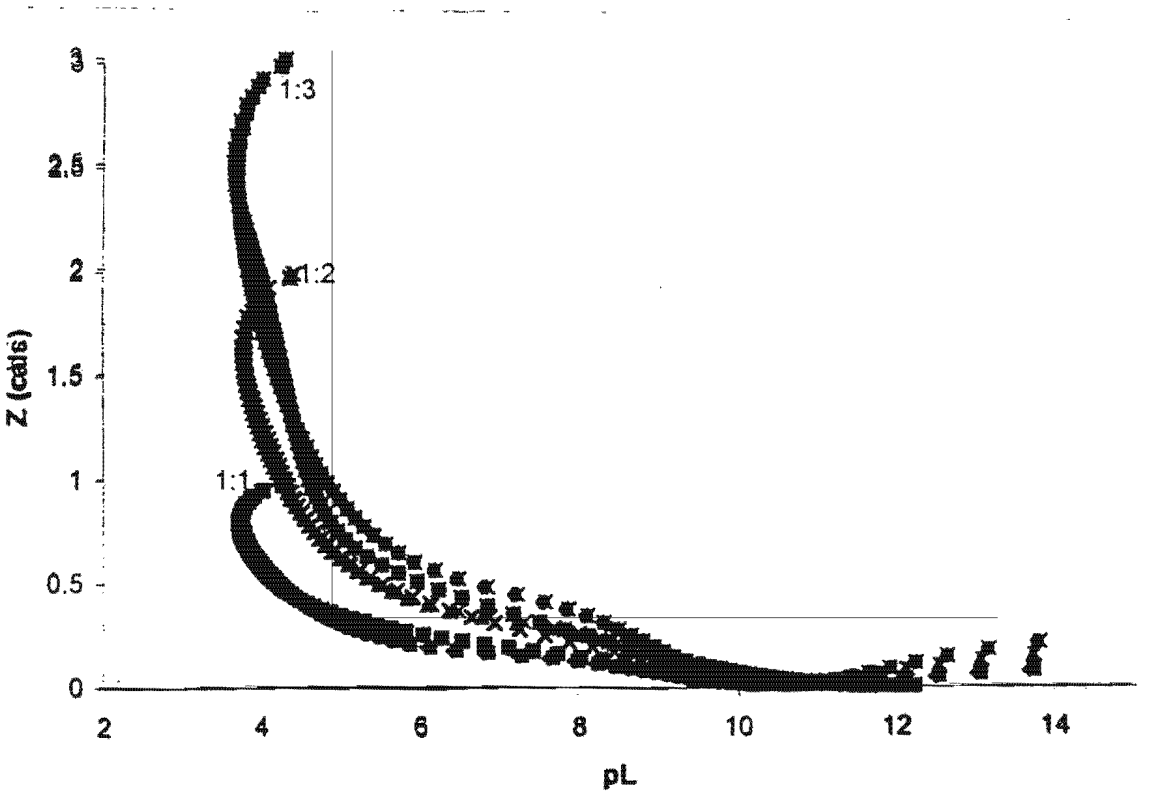

Figure 3.1.3.3d: Formation function curve for the Ca:ZDA system at 25°C in 0.15 mol dm-3 (Na)[Cl].

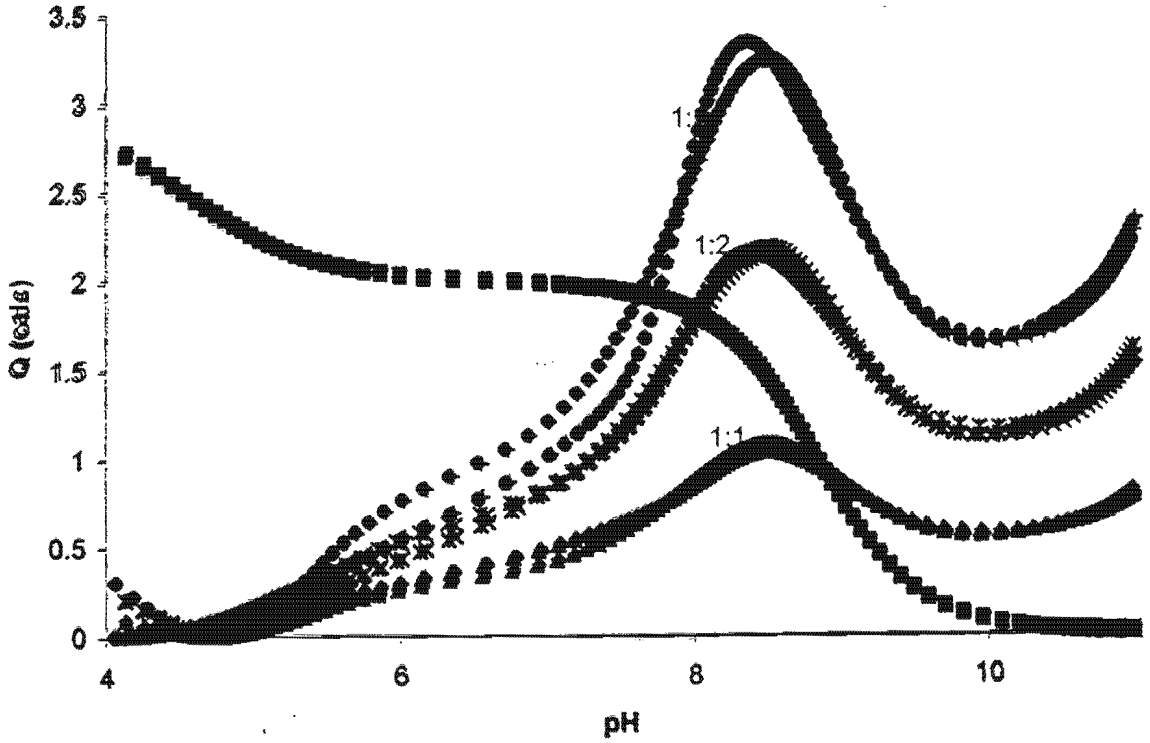

Figure 3.1.3.3e: Deprotonation function curve for the Ca/ZDA system at 25°C in 0.15 mol dm-3 (Na)[Cl].

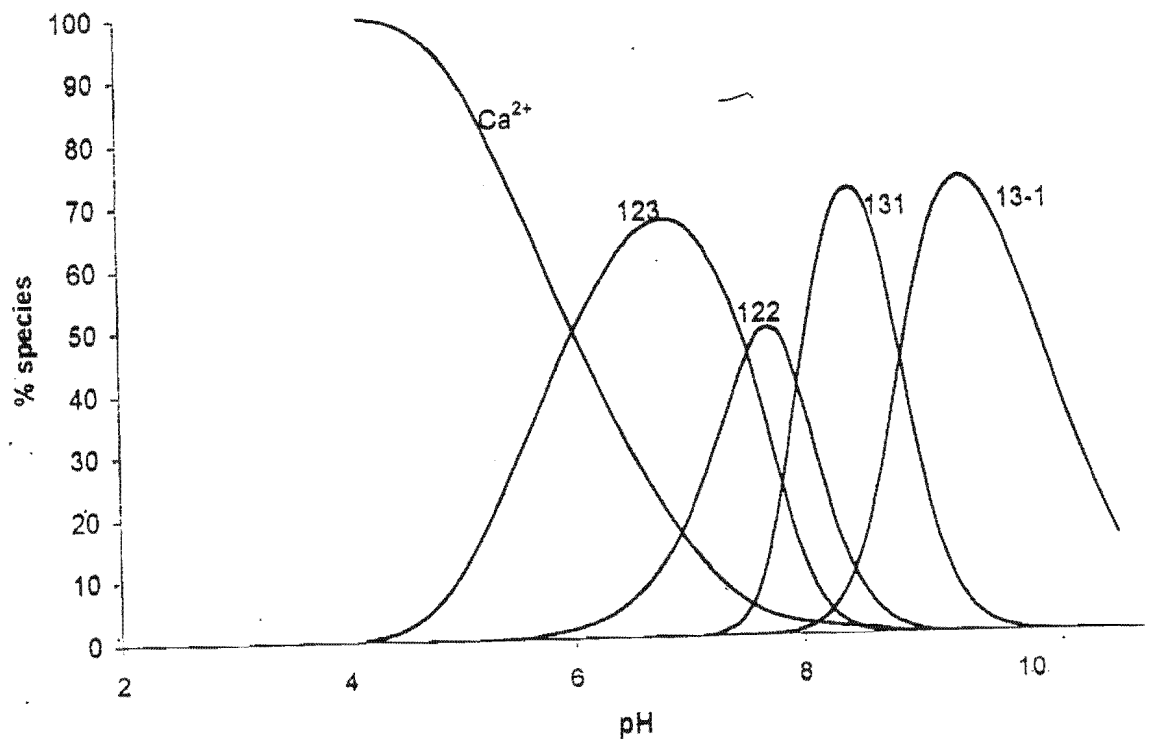

Figure 3.1.3.3f: Species distribution Diagram for the Ca/ZDA system in 0.007M 1:3, calcium (II) to ligand ratio.

3.1.4 Discussion

In this section the metal complexation of the present ligands will be discussed in relation to that of related ligands. In subsection 3.1.4.1 the simple ligand dien has been selected as a basis for comparison because of its possession of three protonation sites. Also included are the ligands that have been investigated in previous studies in this area. In subsection 3.1.4.2, the simple ligand trien has been chosen for comparison because of its quadradentate nature (Martell/ Smith, 1975).

3.1.4.1 Protonation

Table 3.1.5.1. Comparison of present Stepwise Protonation Constants with those of related ligands

	ZDA	BID	EDA	DME	6UM	Ttda	Dien
pKa_1	8.88	8.80	9.41	8.73	8.83	9.7	9.84
pKa_2	8.78	7.47	8.55	7.98	8.08	8.9	9.02
pKa_3	4.53	3.21	3.63	3.44		6.35	4.23

The order of protonation observed for the ligands of this study is a result of the different inductive effects of the constituent alkyl groups of each ligand. Most observable is the difference in the pKa of the central nitrogen atom of the ZDA ligand and that of the other three. According to Perrin, Dempsey and Sarjeant, (1981) the benzene ring reduced the pKa of the nitrogen atom by 1.4 log units when attached to a carbon α- to it. In the ZDA to BID structural modification a 1.32 log unit is observed. It is also stated that a 0.8 log unit reduction is expected if the benzene ring is attached to a β-carbon. In the ZDA to DME structural modification a 1.09 log unit reduction is observed. These observed -ΔpKa values are close to those stated in literature.

In addition to the effect of the alkyl substitution, the central amine nitrogen of the present ligands also suffers the base weakening effect of the amide group. This effect is lower for the terminal amine nitrogen atoms because the amide group is further from

these that the central amine nitrogen atom. The trend in the basicity of the terminal nitrogen in relation to that of the central nitrogen atom observed for dien is also seen in the present ligands.

The central nitrogen atom of ligand ZDA is a secondary amine nitrogen as is that of dien hence the comparable basicity. It would be expected that the central nitrogen of ligands BID, EDA and DME show higher basicity because of their tertiary nature, but the basicity trend $NR_3 > NR_2H > NRH_2$ observed in the gas phase does not apply in solution. In solution, tertiary amines are the least basic followed by primary amines, with the secondary amines being the most basic. This is clearly depicted by the one log unit difference between the protonation constants ($logK_1$, $logK_2$) of BID and Ttda.
The pKa_1 value of EDA comparable to that of dien and is higher than that of the other ligands of the present study because it has primary terminal amines. Protonation of the alkyl substituted terminal amines results in internal strain in the cation causing weakening of the base (Perrin and Clark, 1964)

3.1.4.2 Complexation

a) Copper

Table 3.1.4.2 Stability constants of copper complexes of present ligands and that of related ligands

Pqr	ZDA	BID	EDA	DME	Ttda	Dtda	6UM	Trien
111	15.8	14.0	15.1	15.7	24.9	19.2		
110	10.8	10.0	10.5	9.22	21.3	21.3	6.51	20.1
11-1	2.87	2.07	3.51	1.09	8.24	8.24	-1.54	
11-2	-6.5	-7.3	-6.4	-9.3			-8.94	

Discussion: The ligands of the present study have a chemical model that is common to all of them. The complexation reactions of these ligands with copper are fast at the present working temperature of 25°C and the reaction mixture changes colour from blue to deep blue to purple. According to the stability constants for copper complexes shown in table 3.1.4.2, the present ligands do not exhibit the same affinity for copper

as that of Ttda, Dtda and 6UM. This behaviour is a direct result of the differences in donor atom basicity, denticity, steric and inductive effects that exist between the ligands. Because of the high basicity of the coordinating atoms of the Ttda and Dtda ligands as opposed to that of 6UM and the present ligands, they tend to form more stable complexes.

For each of the present metal-ligand systems, the stability constant varies in the order 111>110>11-1>11-2. As pH increases, the number of atoms coordinated to the central metal cation also increases. This shows that steric strain is an important factor influencing stability of these copper complexes. A direct result of the increase in the number of chelate rings around the metal ion is the increase in girdle strain (Chung, Liu, 1984) in the equatorial plane. Generally, a combination of high steric strain and low donor atom basicity results in low complex stability.

The higher complexing ability of the present ligands compared to that of 6UM stems from the presence of the extra coordinating nitrogen atom positioned midway between the two amide groups. Smaller chelate rings have more rigidity which is a factor that reduces the entropy of the molecule; and often, the higher the number of chelate rings on the complex, the higher the stability. Also important is the sequence of the sizes of contiguous chelate rings around the central metal ion. The sequences 6,6,6 or 5,5,5 tend to be less favourable for complex stability than the alternating 6,5,6 or 5,6,5 sequences. Of the alternating sequences, the latter is even more conducive to complex stability.

The copper (II) ion can induce the ionisation of the amide protons of the ligand. It is expected that at low pH, the carbonyl oxygen of the amide group is coordinated to the metal ion. With increase in pH there will be a transition from a Cu—O to a Cu—N coordination arrangement (Chung, Liu, 1984).

For each of the species found in the chemical model of the present ligands there are many different ways in which the ligand may be coordinated to the metal ion. For each

species, several possible coordination rearrangements will be presented and discussed with the aim of selecting the most likely coordination based on thermodynamic evidence.

The 111 Species

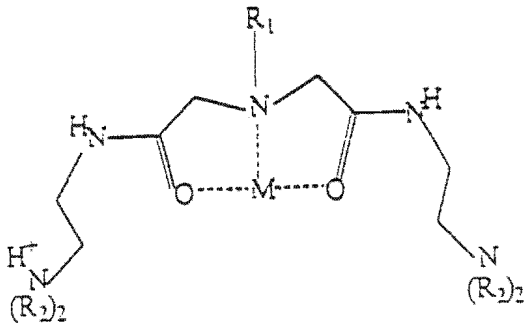

Figure 1

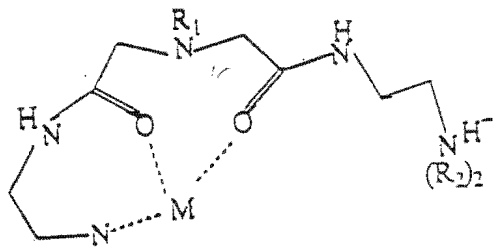

Figure 2

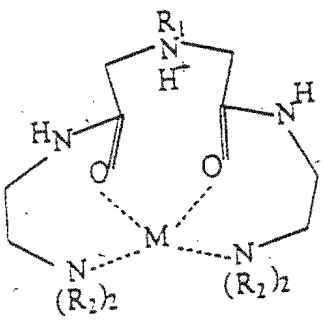

Figure 3

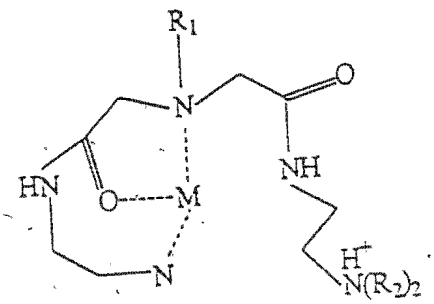

Figure 4

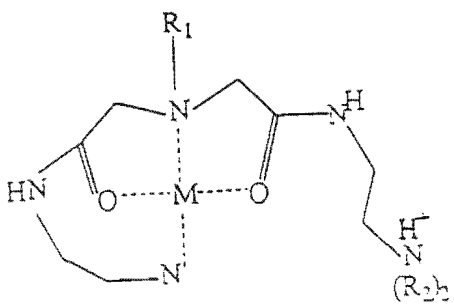

Figure 5

Clearly in the pH range in which this species predominates (3 - 6) the central nitrogen atom would be deprotonated and the terminal nitrogen atom protonated unless coordinated to the metal ion. The coordination of both amide oxygen atoms is possible in the low pH region, hence the 111 species can be represented as figure **1**, with protonation of one of the terminal nitrogen atoms. The protonation of only one of the terminal amine nitrogen atoms could be a result of the charge influence of the divalent metal cation present in the complex formed.

In figure **2** the uncoordinated terminal nitrogen is protonated but the large chelate rings of the structure are not favourable for a high complex stability. This structure is therefore unlikely to represent this stoichiometry.

Figure **3** shows coordination of both oxygen and both terminal nitrogen atoms, with protonation of the central nitrogen atom. As already stated, this species is unlikely as because of the low pK_a value of this nitrogen atom. Even though figure **3** has more chelate rings than figure **2**, they are too large and flexible to confer the high complex stability associated with this species.

This species can also be represented by figures **4** and **5** in which the central amine nitrogen is coordinated simultaneously with either one or both carbonyl oxygen atoms and one terminal amine nitrogen atom. These structures have two and three chelate rings respectively, with one protonated uncoordinated terminal nitrogen atom. Figure **5** is more strained than figure **4**, therefore it is more likely that figure **4** would best represents this species.

The 110 Species

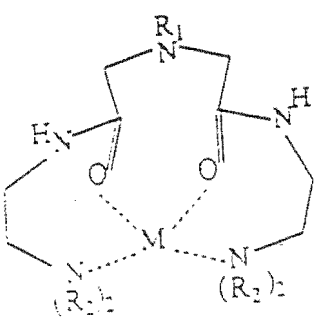

Figure 6

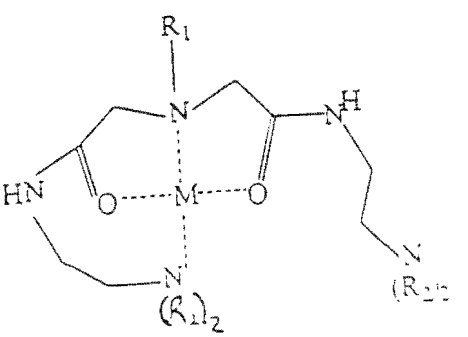

Figure 7

This species occurs in the pH range of 5 to 8 in which the central nitrogen atom is deprotonated. The terminal amine is protonated at pH 5. It could be that the 111 to 110 speciation is just a loss of a proton from the terminal amine and nothing more. This is possible since the presence of the copper dication would decrease the pK_a of the terminal amine. This species can be represented by figures 6 and 7. Figure 6 has a 7,8,7 chelate ring size sequence and would therefore be less strained than figure 7 which has a 7,5,5 sequence. The distance between the coordinated atoms in figure 6 is large and therefore the formation probability of this complex is lower than that of figure 6 in which the coordinating atoms are closer together. Figure 7 seems to be the best choice of a structure representative of the 110 species.

The 11-1 Species

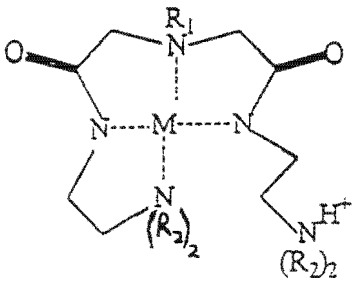

Figure 8

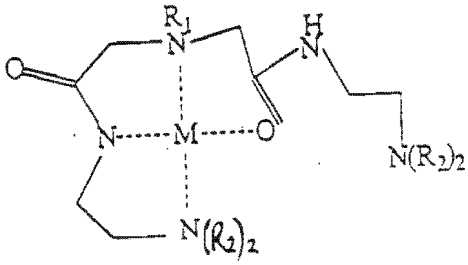

Figure 9

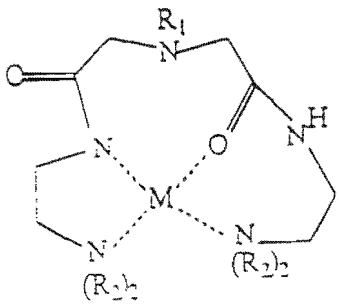

Figure 10

The formation of the hydroxy or deprotonated species results for the loss of a proton from the amide or a coordinated water molecule. This species occurs in the 8 to 9.5 pH range. Figure **8** shows the coordination of both amide nitrogen atoms with the loss of both amide protons. With the protonation of the uncoordinated terminal nitrogen atom the 11-1 designation is satisfied. It is however unlikely that with both amide protons ionised, the terminal amine nitrogen would still be protonated. This structure therefore does not represent this stoichiometry.

Figure **9** shows the coordination of one amide nitrogen atom with the accompanying ionisation of the amide proton, in exchange for the coordination of a carbonyl oxygen in figure **6**. Figure **10** is a represents the coordination of an amide nitrogen in exchange for a carbonyl oxygen in figure **7**. The re-arrangement of coordination to the copper atom from an oxygen atom to the amide nitrogen atom is inevitable with the increase in pH.

The 11-2 Species

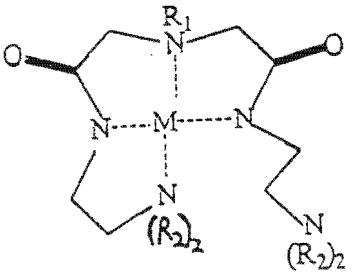

Figure 11

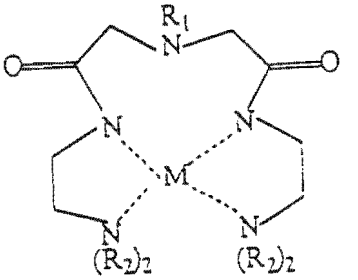

Figure 12

This species occurs from pH 9.5 onwards to the highly alkaline pH at which the deprotonation of both amide nitrogen atoms is possible. The protonation of the terminal amine nitrogen atoms is unlikely in this pH region. Figure **11** represents the formation of this species by the coordination of the second amide nitrogen in figure **10**. This gives a 5.5.5 chelate ring size sequence that is highly strained. Figure **12** represents the formation of this species by the exchange of the coordinated carbonyl oxygen in figure **9** for the coordination of the second amide nitrogen atom. This gives

a 5,8,5 chelate ring sequence that is more stable than the 5,5,5 of figure **11.** The low stability of this species could be a result of the high strain in figure **11** or the low rigidity introduced by the 8-membered ring in figure **12.**

In summary, it is notable that the copper complexing ability of the present ligands falls in between that of Dtda and that of 6UM. They form a sequence of species ranging from the protonated at low pH, the unprotonated in the neutral, the mono-deprotonated in the near alkaline and the doubly deprotonated in the far alkaline regions. However, even though these ligands have copper complexing ability that is slightly higher than that of 6UM they are still too close to 6UM in this respect. Work still needs to be done on the ligand structures to bring the stabilities of their copper complexes closer to those of the Dtda copper complexes. They should not, however, be as high as those of this and the Ttda complexes, as these are excreted unchanged when injected into mice (Kelly, 1991). The copper is not bio-available under these conditions.

b) Zinc

The chemical models of the zinc systems of this study have been shown to be very large and to consist of many hydroxy species. The large number of species can be accounted for by the ability of zinc to easily adopt the four, five and six coordination geometries (Glusker, Katz, Beebe, Bock; 1996). The numerous hydroxy species are a result of the low pKa (~7) of a zinc(II)-bound water molecule (Kimura, 1992).

c) Calcium

The calcium complexation systems showed that there is limited interaction between calcium (II) and the ligands. The observed species could be a result of the coordination of the amide carbonyl oxygen atoms (Cotton, Wilkinson, Gaus; 1987) as calcium prefers to coordinate to oxygen than to nitrogen (Glusker, 1996).

The purpose of including zinc and calcium in this study was for the inclusion of the formation constants of their complexes with the present ligands in the blood model in order to fully evaluate the copper plasma mobilising indices.

3.2 SPECTROPHOTOMETRIC STUDIES

3.2.1 UV-Visible Spectroscopy Theory

In the human body, the labile form of copper is normally found complexed by amino acids and small peptides. It may have an unsaturated coordination environment and hence be in a position to react with additional donor molecules. The nature of the incoming donor molecules which will be preferred depends on the coordination environment already surrounding the metal ion and the donor capacity of these molecules. The final result of full or even partial coordination in the metal-ion sphere determines its bio-availability and dictates the kind of interactions in which it may be involved. An insight into the coordination sphere of the metal-ion at different conditions of pH, as would be provided by spectrophotometry, would help in the understanding of the molecular mechanisms that underlie the anti-inflammatory properties of copper complexes. Many inorganic substances, among which are the copper complexes, absorb in the visible region (400-700nm) (Linder, Torrington; 1982).

The use of spectroscopic analytical methods requires prior knowledge of the prevalent energy states of the "particle" under study as well as the region of the wavelength of electromagnetic radiation that will interact with it to give a detectable signal. At the orbital level, matter has a wave-like nature and radiation in quanta, may, conversely be regarded as particulate. Appropriate interaction of these two entities yields a signal that can be unraveled into a world of information about the ultrastructural intricacies of matter.

The human biological system is endowed with various kinds of ligating atoms among which are the amino, peptide and imidazole nitrogen, and the carboxylate, peptide, water and hydroxide oxygen. The electrons of these different donor-atom types are always in continuous competition for accessible orbitals as dictated by the demands of the physiological processes of the body. The ligand field strength of each of these different types of donor atom depends on the chemical nature of the molecule in which they exist.

the chemical nature of the metal that is being complexed at any particular time and the biochemical dictates of their biological niche.

The different kinds of donor atoms possess different capacities for splitting a set of degenerate orbitals. A method has been proposed (Billo, 1974) for the calculation of total electronic transition energy contribution made by the donor atoms in the coordination sphere of the metal-ion. This is calculated by the formula:

$$\nu_{calc} = \sum \nu_i \qquad ...(4.1)$$

ν_i being the energy contribution of atom *i*. After experimental work (Billo, 1974) on about 34 copper complexes, the following energy contributions were proposed for some of the types of oxygen and nitrogen donor atoms physiologically prevalent in the human body:

$$\nu_{(NH3)} = (4.53 +/- 0.07) \times 10^3 /cm$$
$$\nu_{(H2O\ or\ OH^-)} = (3.01 +/- 0.03) \times 10^3 /cm$$
$$\nu_{(carboxylate)} = (3.42 +/- 0.10) \times 10^3 /cm$$
$$\nu_{(peptide\ N)} = (4.85 +/- 0.04) \times 10^3 /cm$$

The effects of the rest of the atoms of the ligand molecule are assumed to be either negligible or allosterically additive onto the direct effect of the co-ordinating atom. This is, indeed, true because theoretical calculations of the absorption maximum, based on the possible donor atoms present on the ligand framework, yield several possible coordination geometries, out of which only one is applicable.

The several donor atoms of a polydentate ligand are sequentially coordinated to the central atom. In the process the conformation of the ligand molecule changes markedly in an attempt to occupy all the accessible coordination sites. This results in the formation of chelate rings between the central metal-ion and the ligand atoms. Hexagonal chelate rings confer stability to the complex. The formation of rings bigger than this, is in terms

of entropy, not favourable. Like any other heterocyclic ring, the chelate ring assumes a conformation that is determined by the number of member atoms of the ring and by whether or not it is contiguous with other chelate rings (Hancock, Martell; 1989).

In the visible region (400-700nm) the wavelength of maximum absorption (λ_{max}) of the *d-d* electronic transitions of transition metal-ions is normally sought. Electronic transitions are allowed between energy levels of different symmetry (*g* or *u*) and different orbital angular momentum. The visible spectra observed for any metal complex will depend on the initial *d*-orbital electronic occupancy of the metal ion and the amount of energy absorbed. This results in a symmetry of the complex which is predetermined by the ground state electronic configuration of the central metal-ion.

A homogenously aquated copper (II) ion absorbs maximally at 790nm. A progressive blue shift of the absorption maximum is observed as the aqua-ions are sequentially replaced by ammonium ions, the λ_{max} moving to 745, 680, 645 and 590nm as the number of ammonium ions increases from 1, 2, 3 to 4 respectively (Cotton, Wilkinson; 1972). The nature of electronic transitions accompaying a chelating ligand can be concluded from the effect of related monodentate ligands on the degenerate orbital of a metal ion. The effect of the ammonium ions is related to the complexation of copper (II) ions by a nitrogen-containing polydentate ligand. As the speciation of the metal complexes is pH dependent so also, are their absorption spectra. In the present study, the colour of the copper-ligand solutions changes from clear blue, through an intense blue to a purple tinge as pH increases.

When surrounded by an octahedral ligand-field, the copper (II) ion with its unsymmetrically filled *d*-orbitals is distorted. The resultant Jahn-Teller distorted complex formed brings an increase in the number of allowed electronic transitions. The single broad band that is recorded is composed of three electronic state transitions ($^2A_{1g} \Leftarrow {}^2B_{1g}$), ($^2B_{2g} \Leftarrow {}^2B_{1g}$) and ($^2E_{g2} \Leftarrow {}^2B_{1g}$). During copper-ion complexation, as the coordinating ligand field is made stronger, a hypsochromic shift (Gordon, Macrae; 1987) of the absorption maximum of the broad band is observed.

In solution, water molecules normally occupy the axial positions of copper complexes. The co-ordination of other ligands at these sites has an additional influence on the energy of the *d-d* electronic transitions. This "pentaammine effect" (Billo, 1974) brings about bathochromic shifts of 1800 cm^{-1} for two axially co-ordinated carboxyl groups and one of 1000 cm^{-1} for a hydroxyl, a carboxyl or an amine group. The presence of any of these groups in the co-ordination sphere results in the partial loss of the degeneracy of the e_g orbital. This reduces the overall crystal field splitting energy of the metal complex, hence the "red" shift.

Compared to other transition metals, the low-lying *d*-orbitals and the d^9 electronic configuration of copper (II) make it easier to study by spectrophotometry. Electronic absorption spectroscopy may not be the ultimate tool in the elucidation of the structure of our copper complexes but in conjunction with some computer-aided molecular modeling, an insight into the metal-ion coordination sphere may be obtained.

d-d transitions are generally Laporte-forbidden and hence have low intensity. This selection rule may be lifted by distortion of the molecule. The most common source of distortion is vibration but more chemically informative are changes in intensity due to electronic (Jahn-Teller distortion) or geometric effects. Geometric distortion may arise form steric strain imposed by chelate rings or by different coordination donor atoms. Thus the intensity of electronic transitions may be useful in predicting the distortion of a complex.

3.2.1.1 Data Analysis (Voye, 1993)

According to the Beer-Lambert law (Christian, 1986), the absorbance of a sample is directly proportional to the path length and the concentration of the absorbing species, represented as:

$$A = \epsilon c l \qquad ...(4.2)$$

where ϵ is the molar absorptivity, $\mathbf{c}$ is the molar concentration and l is the optical path length. This relationship is straightforward if the sample contains only one absorbing species. Complexometric titration solutions, however, may contain a number of absorbing chemical species, so that the observed total absorbance of a sample of the reaction mixture will be dependent on the summed concentrations of all the component species and their characteristic absorption coefficients. Equation (4.2) will then become:

$$A = l(\epsilon_1 \mathbf{c}_1 + \epsilon_2 \mathbf{c}_2 + \epsilon_3 \mathbf{c}_3 + \ldots \epsilon_n \mathbf{c}_n) \qquad \ldots(4.3)$$
$$= l \sum \epsilon_i \mathbf{c}_i$$

At different values of pH, the concentration of the different species will vary and so will the absorbance. This can be represented as:

$$A_{H1} = l(\epsilon_1 \mathbf{c}_{1H1} + \epsilon_2 \mathbf{c}_{2H1} + \epsilon_3 \mathbf{c}_{3H1} + \ldots \epsilon_n \mathbf{c}_{nH1}) \qquad \ldots(4.4)$$
$$= l \sum \epsilon_i \mathbf{c}_{iH1}$$

$$A_{Hx} = l(\epsilon_1 \mathbf{c}_{1Hx} + \epsilon_2 \mathbf{c}_{2Hx} + \epsilon_3 \mathbf{c}_{3Hx} + \ldots \epsilon_n \mathbf{c}_{nHx}) \qquad \ldots(4.5)$$
$$= l \sum \epsilon_i \mathbf{c}_{iHx}$$

where A_{H1} is the total measured absorbance at the first pH value and $l \epsilon_i \mathbf{c}_{iHx}$ is the absorbance of species i at the first value of pH. The same applies to the subsequent values of pH up to the x*th* value (equation 4.5), for all the species up to the n*th* species. If the concentration of the absorbing species at each pH value is known ($\mathbf{c}_{iHx}$) then the set of simultaneous equations can be solved for ϵ of each species.

If at each pH, the absorbance is measured over a range of wavelengths, the total absorbance of the sample at each wavelength will be:

$$A_{\lambda 1} = l(\epsilon_{1\lambda 1} \mathbf{c}_1 + \epsilon_{2\lambda 1} \mathbf{c}_2 + \epsilon_{3\lambda 1} \mathbf{c}_3 + \ldots \epsilon_{n\lambda 1} \mathbf{c}_n) \qquad \ldots(4.6)$$

$$= l \sum \epsilon_{i\lambda 1} \mathbf{c}_i$$

.

.

.

$$A_{\lambda y} = l\,(\epsilon_{1\lambda y}\mathbf{c}_1 + \epsilon_{2\lambda y}\mathbf{c}_2 + \epsilon_{3\lambda y}\mathbf{c}_3 \ldots \epsilon_{n\lambda y}\mathbf{c}_n) \qquad \ldots(4.7)$$

$$= l \sum \epsilon_{i\lambda y}\mathbf{c}_i$$

where $A_{\lambda 1}$ in equation 4.6 is the total absorbance at the first wavelength and $l\epsilon_i\mathbf{c}_{i\lambda 1}$ is the absorbance of species i at this wavelength. This can be extended to wavelength y (equation 4.7). The range of equations for total absorbance can be solved iteratively for the value of ϵ for each of the component species of the chemical system.

The SPEC2 software program developed in our laboratory, was used to deconvolute the data into the spectra of the individual species. This program was written in Pascal 7.0, uses partial singular value decomposition to solve a set of linear equations (Nash, 1987). The coding has been tested using known systems and proved to be very robust (Jackson, Linder, Voye; 1996).

3.2.2 Experimental

Procedure

For each ligand system a potentiometric titration was set up and operated in the manual mode of the microprocessor system. Absorbance readings at 20nm intervals for the 400 to 800 nm range were taken with the use of a PYE Unicam spectrophotometer. The absorbances of the starting reaction solution were scanned and recorded over the said range, with the electrode slope and the initial emf of the solution being used to calculate the next emf for analysis. The absorbance of the solution was scanned at intervals of half a pH unit from the initial pH to a pH of approximately 11. The pH of the solution was adjusted by the manual addition of sodium hydroxide dispensed from a Dosimat burette. Water was used as a blank.

3.2.3 Results

The absorption maxima and the corresponding molar absorptivities of the copper complexes of the present ligands are presented in table 3.2.3a. These are then illustrated in the spectral curves that follow Figs. 3.2.2a-f.

Table 3.2.3a: Wavelengths (nm) of maximum molar absorptivity for the solution species of present ligands.

Species	ligand	ZDA	BID	EDA	DME
111	ϵ	–	–	–	160
	λ_{max}	–	–	–	630
110					
	ϵ	120	80.5	50	158
	λ_{max}	620	620	610	630
11-1					
	ϵ	70	80.42	71	135
	λ_{max}	600	600	550	580
11-2					
	ϵ	50	61.4	60	162
	λ_{max}	600	580	550	570

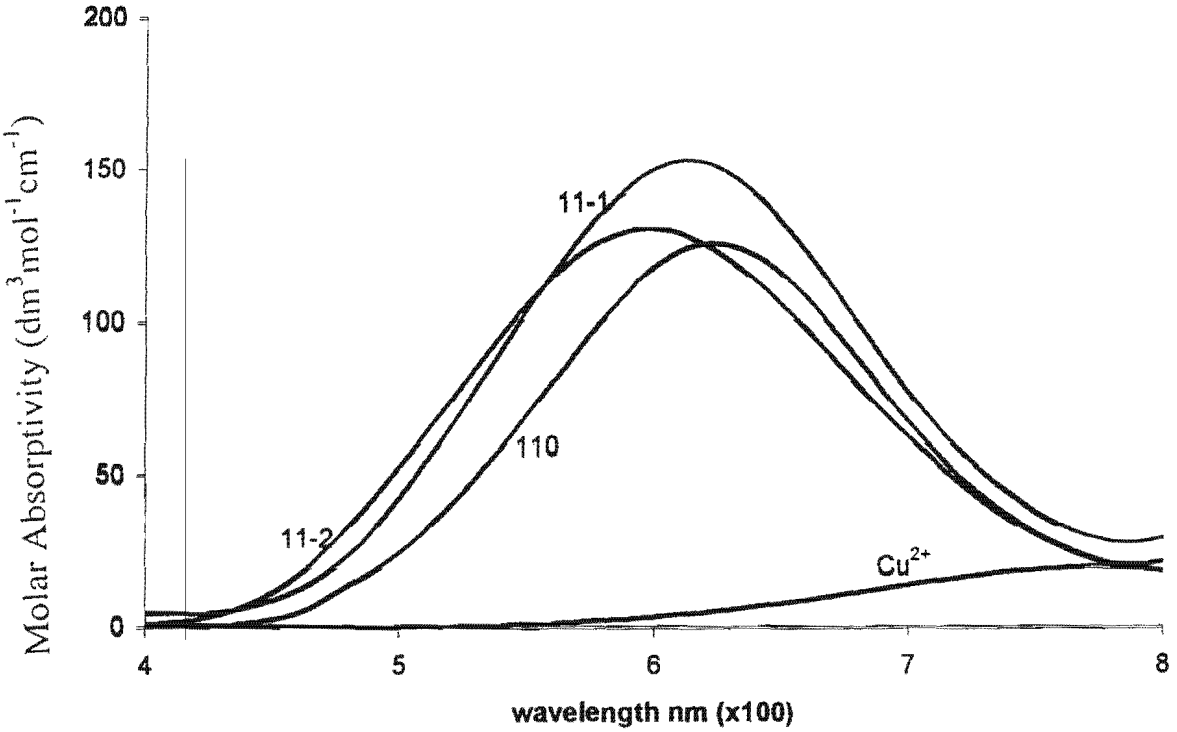

Figure 3.2.2a: Calculated electronic spectra of the copper (II)-ZDA species in aqueous solution. Molar absorptivity is in units of $dm^3\ mol^{-1}cm^{-1}$.

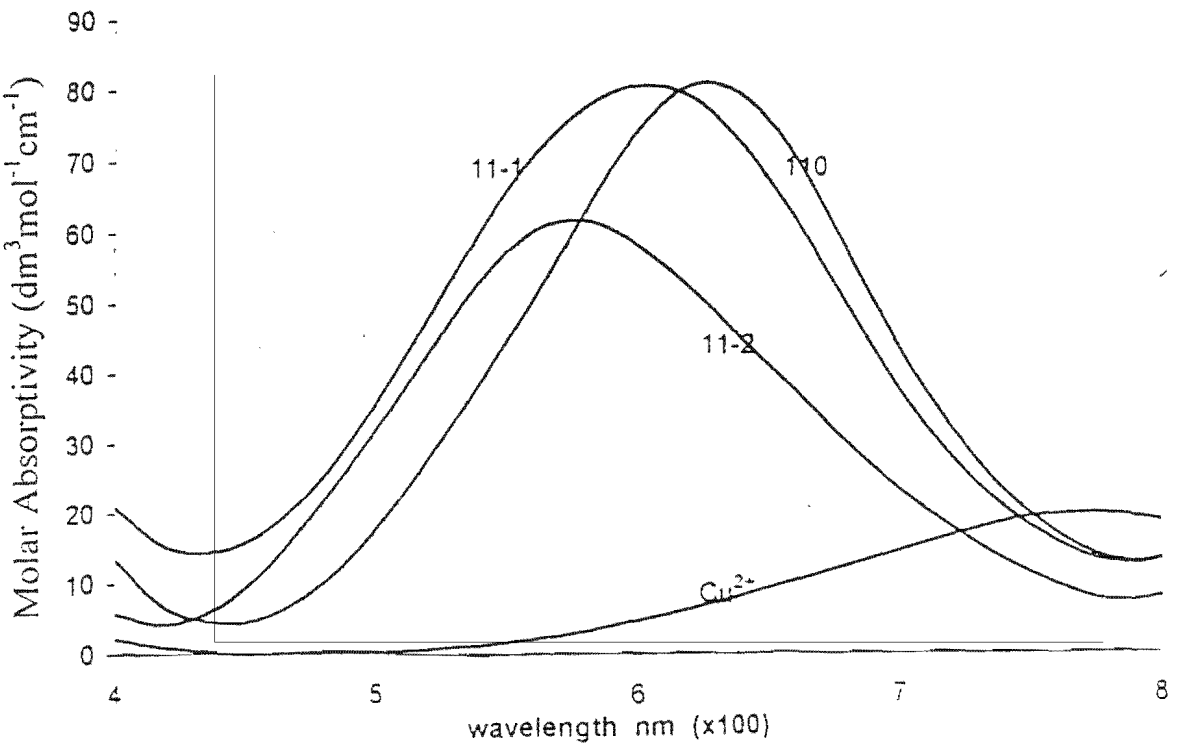

Figure 3.2.2b: Plot of electronic spectra of copper (II)-BID species in solution, with omission of the CuLH species. Molar absorptivity is in units of $dm^3\ mol^{-1}cm^{-1}$.

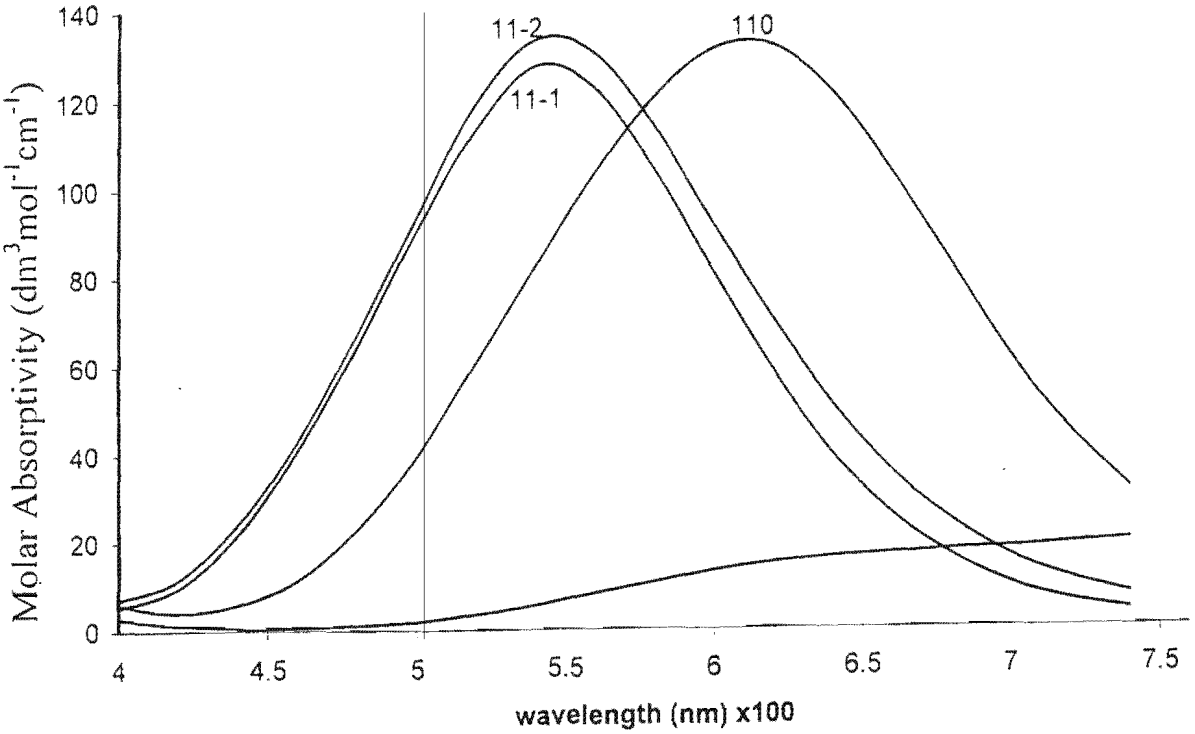

Figure 3.2.2c: Calculated electronic spectra for copper (II)-EDA species in solution. (CuLH species omitted.) Molar absorptivity is in units of $dm^3\ mol^{-1}cm^{-1}$.

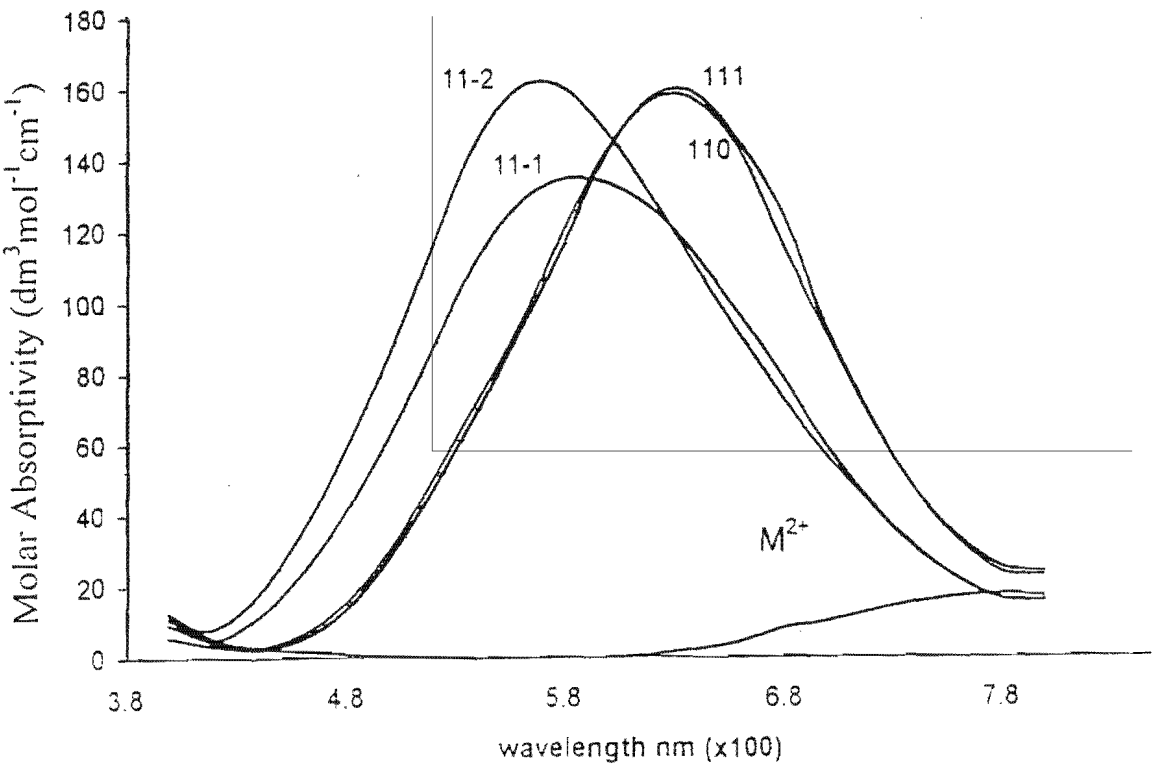

Figure 3.2.2d: Calculated electronic spectra for the copper (II)-DME species in solution. Molar absorptivity is in units of $dm^3\ mol^{-1}cm^{-1}$.

3.2.3 Discussion

In the treatment of the spectroscopic data, each wavelength is analysed independently to yield molar absorptivities. Thus, a final smooth curve of ϵ versus λ is an indication of the correctness of the speciation model used. Also, the extinction coefficient of aquated Cu^{2+} is calculated and can be compared with independent measurements. The absorption band shown by each species corresponds to the three spin allowed transitions $^2A_{1g} \leftarrow {}^2B_{1g}$, $^2B_{2g} \leftarrow {}^2B_{1g}$ and $^2E_g \leftarrow {}^2B_{1g}$, that are characteristic of a d^9 tetragonally distorted copper (II) complex. Due to the unequal *d*-orbital electron occupancy of the d^9 system, the influence of the coordinating environment on the crystal field splitting allows for the prediction of the solution structure of the complex species.

A notable feature of the spectra is the general hypsochromic shift in λ_{max} as the speciation changes from the 111 species, in the acid region, to 11-2 species, in the alkaline region. This is indicative of a progressive increase in the number of nitrogen atoms in the coordination sphere of the metal ion. The number of nitrogen atoms in the coordination sphere of the metal ion is estimated from the copper (II)-ammine coordination measurements of λ_{max} (Cotton, Wilkinson; 1972) with the consideration that, due to the chelate effect, the complexes will absorb at slightly shorter wavelengths.

Under the conditions used to determine the electronic spectra, with the exception of DME, the 111 species was only present at a low concentration. For this reason it was not possible to determine the electronic spectrum of this species with any accuracy. In the case of DME, where the spectrum of the 111 species was determined, it was found to be almost identical to the spectrum of the 110 species. This indicates that, upon deprotonation, there is no change in the coordination sphere of the metal.

For the 110 species, the λ_{max} is in the range of 610 – 630 nm indicating the presence of, at most, two nitrogen atoms in the coordination sphere of the copper (II) ion. Then there is a blue shift to an average value of 600 nm for the λ_{max} value of the 11-1

species. The coordination of three nitrogen atoms is inferred for this species. The average λ_{max} value of 575 nm that is calculated for the 11-2 species of these complex systems points to the coordination of four nitrogen atoms to the copper (II) ion. The λ_{max} order of 111 > 110 > 11-1 > 11-2 shows that the amide protons and not coordinated water protons are being dissociated (Chung, Liu; 1984).

The intensity of d-d electronic transitions is often used as a measure of the distortion of the coordination sphere of the metal ion. The classic example of this is the progressive increase in ϵ_{max} with consecutive replacement of the coordinated water molecules by ammine molecules in the $[Cu(H_2O)_6]^{2+}$ (Cotton and Wilkinson, 1972). This copper hexaaqua complex has an ϵ_{max} of approximately 15 $dm^3mol^{-1}cm^{-1}$. The complexes found in the present study, all have extinction coefficients in the range of 50 to 160 $dm^3mol^{-1}cm^{-1}$. These values are in reasonable agreement with literature values for related ligands (Jackson, Linder, Voye; 1996, Jackson, Nakani; 1996). The relatively high extinction coefficient is indicative of a distorted octahedral arrangement of the coordination atoms around the metal ion.

3.3 MOLECULAR MECHANICS

3.3.1 Introduction

Molecular mechanics (MM) is a popular tool for describing structures and relative energies of many classes of molecules (Bygott, Sargeson; 1998). It has been used extensively in the modeling of molecular structure of organic macromolecules. However it has not been used as extensively in the study of transition metal complexes. The main reason for this is the difficulty in developing force fields for the different metal ions. The question arises from the lack of experimental data that can be used in force field parameterisation, the variability of the coordination number of the metal ion, the effect of the overall charge of the complex molecule and the difficulty in the definition of reference angles around the metal ion (Bygott, Sargeson; 1998). Recently, however, a generic force field, esff, applicable across the periodic table has been developed. This is the force field used in this study.

The aim of performing the MM calculations was two-fold. In the first instance, at a qualitative level, it was necessary to see that the structures proposed for the different species were feasible. It is a simple matter to postulate different structures on paper but these often turn out to be impossible as three-dimensional structures when all the bond angles and lengths are taken into account. Secondly, at a quantitative level, it was hoped that calculation of the strain introduced into the ligand by virtue of the conformation adopted during coordination to the metal ion may throw some light onto the true solution structure.

3.3.2 Theory (Leach, 1996)

Force Fields

For each kind of molecule, there are ideal bond lengths and angles; and ideal in-space orientations of non-bonded atoms with optimum in-space interactions. The specification of these functions with the appropriate constants in an energy equation constitutes the force field that can be applied in the modeling of the molecule. Molecular modeling force fields are made up of terms that describe four kinds of inter- and intramolecular forces that are at play inside the molecule. These include bond

stretching, angle bending, bond rotation and non-bonded interactions. As each of these aspects of the molecule deviates from a set reference value, the energy of the molecule is increased.

Force fields may be differentiated by either their functional form or their parameters. There are different kinds of force fields designed to handle different kinds of molecules. The main difference in force fields is in the parameters and not in the functional form. This implies that a functional form that is used in one force field may well be adopted in another force field, but this does not extend to the interchange of parameters. Even though some parameters are fairly constant and may safely be interchanged between force fields, it is always advisable to specify unique parameters for each particular force field.

Force fields are empirical and there is no "correct" form. Functional forms that have proved more successful than others become popular and are therefore more commonly used. Better functional forms may still be developed for novel molecules. In the selection of a functional form of a force field, a balance between accuracy and computational efficiency is always sought. The more accurate functional form may not be easy to solve and therefore one that is less accurate but more tractable may be chosen for use. With the advancement in MM programs, reliable models are becoming more achievable. Improved computers are an advantage in the first and second derivations of these bulky energy equations in the calculation of energy minima and in determining the dynamics of a molecule.

The most important concept in the preparation of the input for a molecular mechanics calculation is the accurate definition of the atom type. The aspects of the atom type that have to be considered are the atomic number, the geometry, the overall charge and the spin multiplicity of the atom. The latter two are not absolutely necessary for the force field. The geometry, in the form of the hybridisation state of the atom, is the most important as it describes its local environment.

Bond Lengths

There are several potential energy equations that may be used to describe the energy associated with bond stretching. The Hooke's law formula however, normally suffices in this regard. This is because it is very rare to find that a bond significantly deviates from the reference bond length (RBL). The RBL is the length of the bond when all other terms of the energy equation are set equal to zero. It is different from the equilibrium bond length (EBL), which is the length of the bond when the energy of the molecule is at a minimum.

It has to be stated that even the bond length of a molecule at the hypothetical motionless absolute zero state deviates from the EBL due to vibration of the molecule. The EBL may vary with experimental technique because different techniques have different optimal working temperatures. The force constants for bond stretching increase with bond strength due to the amount of energy that is required to deform the bond.

Even though it may be computationally efficient to use the Hooke's law formula, it becomes less applicable outside the "true" potential well. This necessitates the application of an equation that can be expanded even up to the quartic level. Such high level expansion of the equation is important because, if expansion is only up to the cubic level, a problem of observing overstretched bonds prevails. This apparent overstretching of bonds comes from the fact that the cubic function, at some point, goes through a maximum. In any case, however, all these functional forms of the bond stretching term are more applicable close to the equilibrium geometry of the molecule and inside the "true" potential well.

The energy associated with angle bending is generally lower than that associated with bond stretching. Therefore since distortion arises primarily from angle bending, the angle bending term can be expanded to higher orders. It is a fact, however, that most structural variation arises from torsional and non-bonded interactions. The energy barriers to free rotation limit the number of conformations that a molecule may

assume. The staggered and eclipsed conformations of ethane are examples representing the change in the energy of a molecule from just the rotation of a bond. The energy profiles associated with the different conformations must be clearly specified in the definition of the force field.

The torsional term has a component that specifies the height of the rotational energy barrier, the number of minima and maxima; and the angles at which these are achieved during rotation. The torsional term can also be extended to cater for the dipolarity of the rotating bond, effects of (hyper-)conjugation and steric interactions between non-bonded 1,4 atoms. A force field containing an expanded torsional term needs careful parametrisation for successful application.

The esff Force Field

Some force fields, like the AMBER (see glossary) force field, are more detailed in the definition of the local environments of atoms in a molecule. These are designed for modeling specific classes of molecules. The AMBER force field is specific to the modeling of proteins and amino acids. In this study, the extensible systematic force field (esff) has been used to model the copper complexes, its advantage being its capability to model most of the elements of the periodic table. Even though it cannot accurately represent high vibrational frequencies and conformational changes, it is hoped that in future it will provide a basis for the development of force fields accurately usable on a wide variety of organic and organo-metallic compounds.

From the force field point of view, coordination complexes are not very different from organic systems (Leach, 1996). The major difference lies only with the modeling of the metal ion because of its ability to assume different geometries. The symmetrical octahedral and square planar geometries are easier to model than distorted geometries. In the latter case the problem can be overcome by disregarding angle bending at the metal ion and calculating van der Waals interaction only between the atoms bonded to the metal ion.

The parameters used in the esff force field are derived from atomic parameters using a certain set of rules to give precise parameter values. These parameters are either obtained from experimental data or calculated. The esff force field potential energy function contains energy terms for bond stretching, angle bending, torsional strain and non-bonded interactions. Each term has special features that describe the specific situation in the molecule.

The bond energy term, which is in the Morse functional form, requires that parameters for bond dissociation energy, the reference bond length and anharmonicity be specified. To arrive at these parameters, the force field relies on the type of the atoms, the bond orders and whether the bond is exo or endo to 3-, 4- or 5-membered rings. Electronegativity, hardness and the ionisation of the atoms are calculated and they are used as guidelines in the construction of parameters. Fit parameters such as atomic anharmonicities, covalent radii and well depths also guide the parametrisation process.

The angle bending term can be made up of several functional forms that depend on the type of angles that are present in the molecule being modelled. The angles can be categorised as normal, linear, perpendicular or equatorial. The parameters that define the angles are functions of the atomic radii and the well depths of the central and end atoms. The rules that apply in the selection of the functional form of the angle bending term depend mainly on the ionisation potential. For equatorial angles, periodicity is the determining factor and for planar angles it is the two overlap quantities and the 1 to 3 equilibrium distances.

The torsional term of the potential energy function normally contains only a cosine function. But since torsion can go as far as approaching the 0 and 180 degree angles, the esff force field introduces the sine function in this term. This ensures that the function is not discontinuous but smoothly approaches and reaches zero, which is what really happens.

The non-bonded interaction energy term can specify either interaction between partially charged atoms or van der Waals interactions. Partial charges on all the atoms are treated as resulting in the overall charge of the molecule. The esff force field considers the electronegativities and the hardness of the atoms that constitute the molecule. The density of the atoms is determined by their hybridisation states which determine the charges of the atoms of a molecule relative to each other. Calculations based on density functional theory result in the electronegativity and hardness of each constituent atom.

In the esff force field the van der Waals interactions are based on rules that are consistent with the charges of the atoms. The polarisability and the ionisation potential of each of the interacting atoms determine the energy associated with each interaction. The ionisation potential is inversely proportional to the number of electrons and this proportionality directly relates to the polarisability of the atom. In the esff force field, the ionisation potential of metal atoms has been modified with respect to their formal charge and hardness and for non-metals, the partial charges have been accounted for in terms of the effective number of electrons.

Incorporating The Metal Ion

The esff force field works with all the atoms of the periodic table up to radon. Each atom can occur in several different types depending on the combination of hybridisation, formal charge and symmetry. Metal atom types are named based on the oxidation state and coordination number of the metal in the metal complex. The oxidation number of the metal ion is determined by the total charge of the complex and the difference between the summation of the charges of the atoms not bonded and those bonded to the metal. This is represented in equation 3.3.1 (Discover, 1995):

$$N_{ox} = Q_t - 1/N_m \Sigma Fq_i - \Sigma Fq_j/N_b \qquad \ldots(3.3.1)$$

where Q_t is the total charge on the complex, and the sums over Fqi and Fqj are of formal charges on atoms not bonded to metal and bonded to metal, respectively. N_m is

the number of metal atoms in the complex and Nb is the number of metal atoms bonded to the *jth* ligand atom.

3.3.3 Molecular Mechanics Calculations

This work was done on a Silicon Graphics Indigo computer. The copper complexes were constructed from fragments using the BUILDER module of Biosym/MSI's *Insight II* package. The problem was formulated according to the dictates of the esff force field. To eliminate the effect of the +2 charge of the metal on the partial charges of the atoms of the organic ligand, the overall charge of the molecule was set equal to zero. Molecular mechanics calculations were performed using the *Discover_3* program which was run as an application in the *Insight II* package.

The models developed were asssumed to be the same irrespective of which of the ligands studied was coordinated to the metal ion.

3.3.4 Results

- The structures did not show Jahn-Teller distortion. This is clearly a limitation of the force field. However, as axial coordination was by water in most cases, this limitation was not important.
- The structures presented here are not compared in terms of total potential energy but in terms of their internal energies. This was done so as to exclude the effect of the contribution of the non-bonded electrostatic interactions, which are greatly influenced by the charge of the copper ion. Also excluded are the entropy that is associated with the chelate effect and the contribution of the crystal field stabilisation energy to the overall stability of the complex. The internal energy, on the other hand, only indicates the strain energy around the central metal ion regardless of the strengths of the different dative bonds to the metal ion. This is the criterion that will be used to compare the stabilities of the different complex structures.

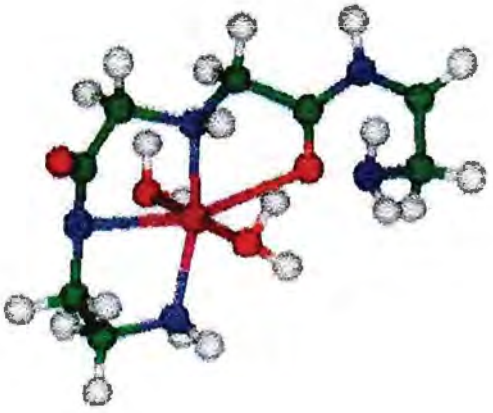

Figure a (87.27 kcal/mol).Coordinated to the copper (II) ion in the equatorial plane are one carbonyl oxygen, the central amine nitrogen, one amide nitrogen and one terminal nitrogen atoms, giving a 5,5,5 chelate ring size sequence. Both axial coordination positions are aquated.

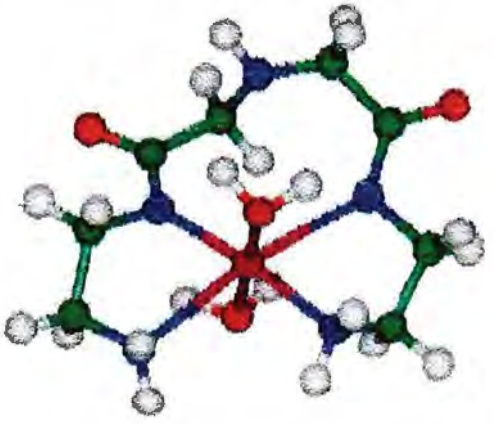

Figure b :(44.67 kcal/mol). Coordinated to the copper (II) ion in the equatorial plane are the two amide nitrogen and the two terminal amine nitrogen atoms giving a 5,8,5 chelate ring size sequence. Both axial coordination positions are aquated

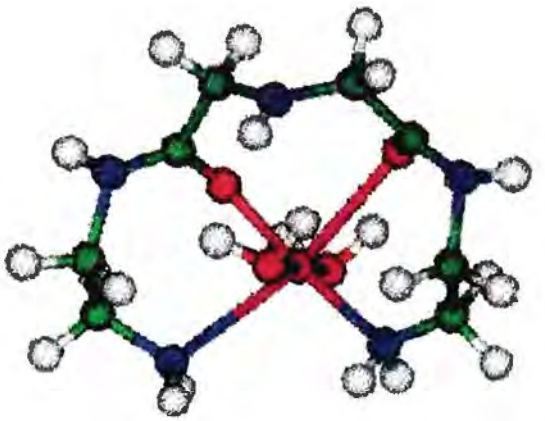

Figure c: (72.98 kcal/mol). Coordinated to the copper (II) ion in the equatorial plane are both carbonyl oxygen and both terminal amine nitrogen atoms, resulting in a 7,8,7 chelate ring size sequence. Both axial coordination positions are aquated.

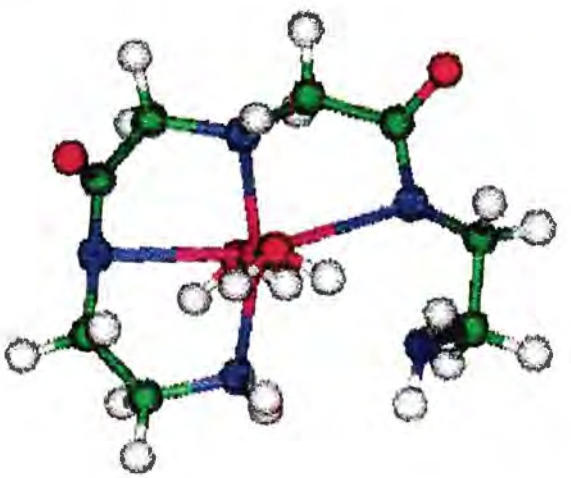

Figure d: (74.47 kcal/mol). Coordinated to the copper (II) ion in the equatorial plane are the central amine nitrogen, both amide nitrogen and one terminal amine nitrogen atoms, resulting in a 5,5,5 chelate ring size sequence. Both axial coordination positions are aquated.

Figure e: (52.83 kcal/mol). Coordinated to the copper (II) ion in the equatorial plane are both terminal amine nitrogen, one carbonyl oxygen and one amide nitrogen atoms, resulting in a 7,8,5 chelate ring size sequence. Both axial coordination positions are aquated.

Figure f: (85.84 kcal/mol). Coordinated to the copper (II) ion in the equatorial plane are the central amine nitrogen, both amide nitrogen and one terminal amine nitrogen atoms. The other terminal amine nitrogen is coordinated in one of the axial positions leaving the other to be aquated. This results in a highly strained 5,5,5,5 chelate ring size sequence.

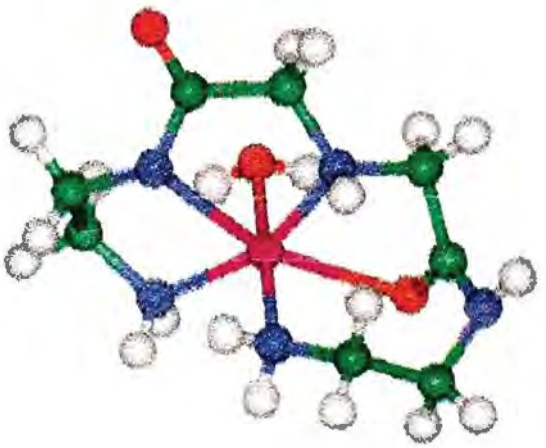

Figure g: (88.47 kcal/mol). Coordinated to the copper (II) ion in the equatorial plane are the central amine nitrogen, one amide nitrogen, one terminal nitrogen and one carbonyl oxgen atoms. In one axial position is coordinated the other terminal nitrogen atom leaving the other axial position aquated. This results in a 5,5,5,6 chelate ring size sequence.

Details about the minimised energy structures are presented in Tables 3.3.4a-c.

Table 3.3.4a: Internal (E_{int}), bond, angle bending (Angle), bond twisting (Torsion) and out-of-plane (Oop) distortion energies (kcal mol^{-1}). The headings of columns 2-8 indicate the figure and the chelate ring size sequence associated with each structure.

	a555	**b585**	**c787**	**d555**	**e785**	**f5555**	**g5556**
E_{int}	87.27	44.67	72.98	74.47	52.83	85.84	88.47
Bond	14.96	6.16	8.47	13.21	7.41	13.72	10.11
Angle	49.95	31.32	21.2	50.6	20.83	54.01	54.03
Torsion	20.91	6.7	42.7	9.73	24.45	15.45	20.27
Oop	1.43	0.51	0.65	0.912	0.14	2.65	4.06

Table 3.3.4b: Metal-to-donor atom bond lengths (*r*) in Angstroms. Designations; mo = metal-to-carbonyl oxygen, mn = metal-to-amine nitrogen, mna = metal-to-amide nitrogen bonds. Bonds *r*1 to *r*4 are in the equatorial plane and *r*5 is in the axial orientation.

Fig	*r*1	*r*2	*r*3	*r*4	*r*5
a	2.60 mo	1.99 mn	2.54 mna	2.01 mn	
b	2.01 mn	2.59 mna	1.92 mna	2.68 mn	
c	2.69 mn	1.89 mo	2.58 mo	2.01 mn	
d	2.69 mna	1.99 mn	2.65 mna	2.02 mn	
e	2.00 mn	2.69 mna	1.89 mo	2.70 mn	
f	2.55 mn	2.00 mn	2.54 mna	2.03 mn	2.04 mn
g	2.57 mo	2.01 mn	2.54 mna	2.02 mn	2.05 mn

Figure T.

D = donor atom.

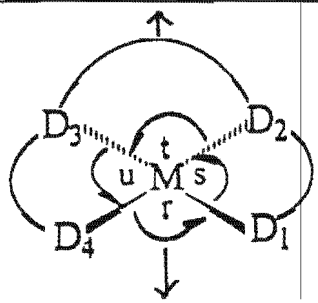

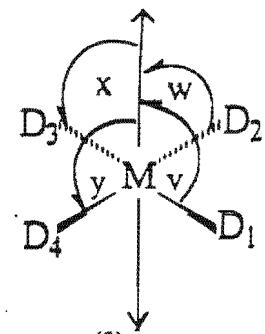

Table 3.3.4c: Angles between equatorial donor atoms (θe) and angles of equatorial donor atoms from one axial ligand (θa) in degrees (°).

The angles r-y are illustrated in figure T.

	a	b	c	d	e	f	g
θ_e° r	119.1	97.76	101.99	117.72	101.00	121.05	120.75
s	78.24	73.41	82.89	79.02	77.06	77.93	82.37
t	82.24	112.44	85.63	83.08	97.23	80.26	78.45
u	80.20	76.40	89.08	80.68	84.74	78.67	78.03
θ_a° v	89.4	89.84	85.84	91.09	88.49	77.93	91.10
w	94.1	91.67	89.16	85.61	88.74	95.21	93.27
x	88.22	88.76	90.10	93.21	92.02	99.95	92.54
y	92.90	88.22	85.71	88.71	87.17	92.84	93.17

3.3.5 Discussion

According to the internal energy of each structure, their stability is in the order: **b> e > c > d > f > a > g**. This corresponds to the chelate ring size sequence order of 5,8,5 > 7,8,5 > 7,8,7 > 5,5,5 > 5,5,5,5 > 5,5,5 > 5,5,5,6. The strain in these structures arises from the sequence of the sizes of the chelate rings formed around the metal ion upon donor atom coordination. The first three structures (**b, c, e**) of the stability series have alternating chelate ring size sequences and are stable compared to those that have contiguous five-membered chelate rings (**d, g, f, a**). The other source of strain contributing to difference in stability is energy associated with torsion of bonds as the different donor atoms are oriented for coordination to the metal ion. This is observed in the exchange of the amide nitrogen atoms for coordination of both oxygen atoms occurring between figures **b** and **c**.

A general search in the Cambridge Crystallographic Database revealed the following typical bond length ranges of atoms to a copper (II) atom:

- Carbonyl oxygen – 1.90 – 2.50 A, including long bonds that are Jahn-Teller distorted.
- Amide nitrogen – 1.87-2.1 A
- Amine nitrogen – 1.9-2.13 A

These values were used as a reference in order to get an idea of how stretched the bonds in structures **a** to **g** were. It appears that all the copper-to-amide nitrogen bonds are stretched beyond their possible upper limit. Consequently, the bond to the metal ion that is diagonally opposite the amide nitrogen in the equatorial plane is also over-stretched. This results in the relaxation of the other two bonds in the plane, which are observed to be within their normal bond length range. The axially coordinated amine nitrogen atoms are at the normal bond length, and this, as explained earlier, is due to the non-recognition of Jahn-Teller distortions by this software. It seems though, that bond stretching has no significant contribution to the differences in the strain energies of these molecules. Most differences in internal energy contribution appears to come from the twisting of bonds and bending of angles as the coordinating atoms are accommodated around the central metal ion. This effect is to be expected because of

the planarity of the amide group. As coordination changes from a carbonyl oxygen to the amide nitrogen with increase in pH, major bond twisting occurs and this is accompanied by angle bending.

3.4 Overall Conclusion

The stability of each complex species is determined by several factors among which are bond strength, entropy and strain. The strength of the bond is determined by the basicity of the donor atoms that are in the coordination sphere of the metal ion. It must be appreciated that the ability of the donor atom to bond to the metal ion will be in competition with the protonation of the donor atom. If the coordinating ability of the donor atom is weak, weak bonds will result and the complex will easily break down in the presence of better coordinating atoms. Entropy is an indication of the disorder that is introduced by the coordination of the donor atoms on a chelating ligand as opposed to monodentate ligand coordination. The large size (seven members or more) of a chelate ring is an indication of the low probability of the coodination of the second donor atom that closes the ring after the coordination of the first. In such cases it is possible that by the time the second donor atom attempts to close the ring, the first donor atom is about to de-coordinate. If the coordinating donor atoms are separated by two or three non-coordinating atoms (to form 5- or 6-membered chelate rings), closure of the chelate ring is more probable because of the close proximity of the second coordinating atom in the coordination sphere. There is therefore very little change in the entropy of the system when a large than when a small chelate ring is formed.

The strain of a complex molecule is a result of the attempt by each donor atom to approach the metal ion at the best bonding orientation. Due to lack of ideal separation between the donor atoms on the ligand, such ideal bonding orientation may be achieved with difficulty resulting in strain in the complex molecule. Such strain can elevate the internal energy contribution to the overall potential energy of the molecule resulting in low complex stability. In this study, strain energy was one of the aspects with regard to which complex stability was investigated.

Based on the molecular mechanics calculations, it was easier to begin with the structural determination of the 11-2 and the 11-1 species. This is because, in the pH region in which they occur, it is more definite that ligand donor atoms occupy all equatorial coordination positions. Sequence **S** below shows the order of increase in the internal energy of the tetracoordinate species.

Sequence **S.**

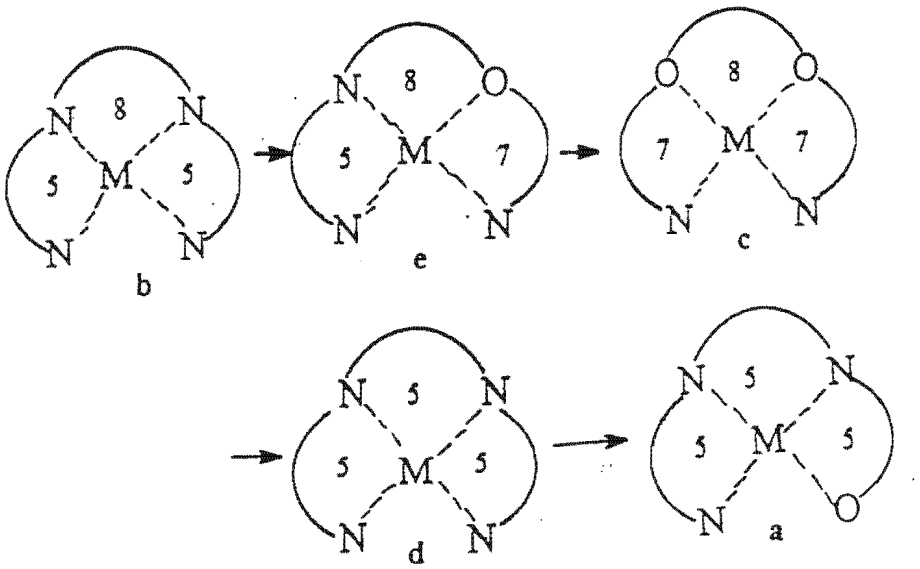

In this energy sequence only the tetracoordinate species are considered.

- For the 11-2 species, the two 4-nitrogen coordinated structures were considered. Of the two structures that have four nitrogen atoms, figure **b** has lower internal energy than figure **d.** The latter is more strained as it posseses three contiguous 5-membered chelate rings. Even though this structure is more strained, the shorter distance between the coordinating atoms means that it would be more readily formed and could well represent this stoichiometry. However since strain seems to be the major factor determining complex stability, figure **b** would be more likely to be the structure of the 11-2 species.
- The 11-1 species could be represented by structures **a** and **e.** Considering strain in the complex molecule, structure **e** apppears to be more likely to represent this stoichoimetry. However, the entropy factor disfavours this structure and therefore **a** would be the best option.

- For the 110 species, it can be concluded that as pH is decreased and owing to the unlikelihood of the coordination of the amide nitrogen, the coordination sphere is left with two amine nitrogen atoms, giving the observed λ_{max} of this species. Structure **c** has two amine nitrogen atoms in the coordination sphere and has higher internal energy than the 11-2 species. This is a result of the simultaneous coordination of the carbonyl oxygen atoms which compromises the planarity of both amide systems. In terms of the entropy of the system, this structure is disfavoured.
- At a pH lower than that of the 110 species, the other amine nitrogen that is not included in the coordination sphere is protonated to give the 111 species.

The above discussion can be summarised in two possible speciation schemes as outlined in **I** and **II** below. In **I**, the central nitrogen atom is not at all coordinated to the copper (II) ion and in **II** it is.

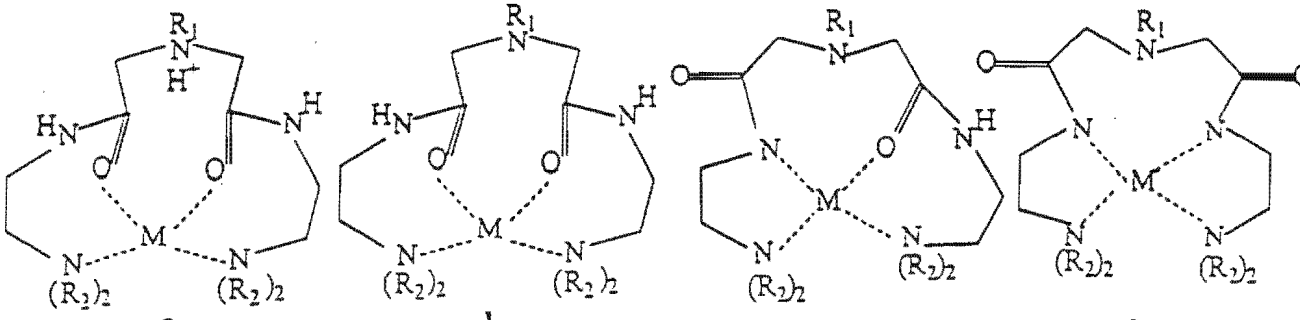

Scheme **I**

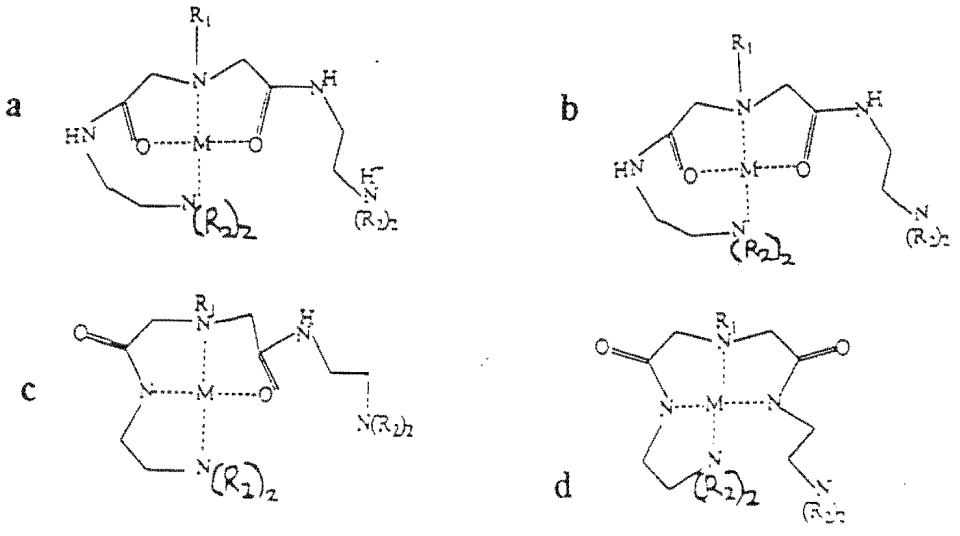

Scheme II

For these two schemes it is apparent that the structures that have an eight-membered ring (scheme **I**) have less internal energy than those of scheme **II.** Considering the entropy of the system, the formation of the large-ringed structures is less probable than the formation of structures such as those of scheme **II**. However, it is possible that the speciation sequence alternates between the two schemes. For that reason the different coordination geometries of each complex species will be discussed in turn.

For the 111 species it appears that figure **IIa** is more likely to represent the coordination arrangement for this species. This is because the protonation of the terminal amine nitrogen atom is more probable at low pH than that of the central amine nitrogen atom. For large chelate rings like those that are formed in figure **Ia** the chelate effect is negligible and therefore the structure is highly unlikely.

For the 110 species figure **IIb** best represents this stoichiometry. For the same reason of the large chelate ring, figure **Ib** is less likely to be representative of this stoichiometry. The basicity of the terminal amine nitrogen atom, especially in the presence of the divalent copper atom in the complex, supports its deprotonation in the neutral pH region.

In table 3.3.4a, figures **Ic** and **IIc** are named **a** and **e**. Figure **Ic** best represents the 11-1 stoichiometry. At the pH in which this species occurs, the terminal amine nitrogen atom is more favourably coordinated than the central amine nitrogen atom. Figure **IIc** shows an uncoordinated terminal nitrogen atom and this is unlikely in the alkaline pH region. The affinity of the copper atom for oxygen has decreased in favour of the nitrogen atom and therefore one amide nitrogen atom is coordinated in place of one oxygen atom. The large sizes of the chelate rings of figure **Ic** compared with those of figure **IIc** are the reason for the observed lower internal energy. The main difference in energy between these two structures comes from the angle bending contribution, which is higher in the strained figure **IIc.** The equatorial angle **r** is more obtuse in structure **a** than in structure **e** implying the strain in the molecule when the molecule is chelated in five-membered rings with the metal ion.

The 11-2 species occurs at high pH at which the coordination of both amide nitrogen is possible. In table 3.3.4a, figures **Id** and **IId** are named **b** and **d**. Figure **Id** best represents this stoichiometry. Figure **IId** is disfavoured because the terminal amine nitrogen atom will, at pH above 9, be coordinated . Also the three contiguous five-membered rings of figure **IId** mean that the molecule is highly strained and this implies complex instability. This is also shown by the large difference in angle bending energy between these two structures. Table 3.3.4c shows that the angle **r** is more obtuse in structure **d** than in structure **b**. This indicates that the three contiguous five-membered rings are strained.

The angles v, w, x and y indicate the planarity of the equatorial plane. The strained structures of each stoichiometry (**a** and **d**) are less planar than the structures that are less strained (**b** and **e**). In the strained structures, these angles do not approach 90° as closely as in the less strained structure. Ideally, these angles must be 90°.

CHAPTER FOUR

4. OTHER STUDIES

4.1 INTRODUCTION

In this chapter are three experiments that were performed to supplement and support the observations that were made in the potentiometric experiments. Firstly there is the investigation of the sequence of protonation of the three amine groups of the ligands by NMR. For this purpose only ligand ZDA was used as representative of all the four ligands. Secondly, there is the investigation and results of the superoxide dismutase-like activity of the copper complexes of the four ligands. Lastly, is a presentation of an investigation into the lipophilicity of the species of each of the chemical models of each copper-ligand system.

4.2 NMR STUDIES

4.2.1 Materials

15 five-millilitre glass vials

pH meter

20 mL Ligand solution (in D_2O)

Conc. NaOH (in D_2O)

4.2.2 Procedure

In fifteen 5-mL glass vials, one millilitre portions of 0.007 M stock D_2O solution of ligand ZDA were adjusted for pH using concentrated NaOH. The pH ranged from 2.89 to 11.76 as will be shown in table 4.1. The proton magnetic resonance spectra of the D_2O solution were plotted. Acetone was used as the reference. As the pH of each solution differed, the protonation of the ligand donor atoms also changed. This affected the chemical shift of the α-protons. The pH of the solutions were calculated from the relationship:

$$pD = pH + 0.4$$

4.2.3 Results

Ligand structural formula of ZDA showing different proton types *(a)* - *(d)*:

$(CH_3)_2$*(a)* NCH_2*(b)* CH_2*(c)* $NHCOCH_2$*(d)* $NHCH_2CONHCH_2CH_2N(CH_3)_2$

Table 4.1 The protonation positions of 0.007 M ZDA versus Acetone Recorded at 400MHz and 25°C.

Type of protons				
PH	*(a)*	*(b)*	*(c)*	*(d)*
2.89	589.07	671.7	737.48	809.4
4.09	588.27	671.43	736.41	805.4
4.48	588.54	671.17	735.68	801.4
5.54	588.27	670.63	734.81	768.5
5.96	588.26	670.36	732.66	732.66
5.72	588.53	670.09	732.66	722.77
6.64	587.47	669.49	730.78	685.34
7.04	587.46	668.75	731.06	688.27
7.50	586.66	667.15	729.72	681.29
8.06	580.77	660.46	726.78	676.77
8.33	559.92	636.40	718.76	674.1
8.72	542.27	616.07	711.54	671.96
9.86	481.04	543.61	688.55	667.91
10.65	453.06	510.82	676.35	664.58
11.76	449.48	506.17	677.58	667.42

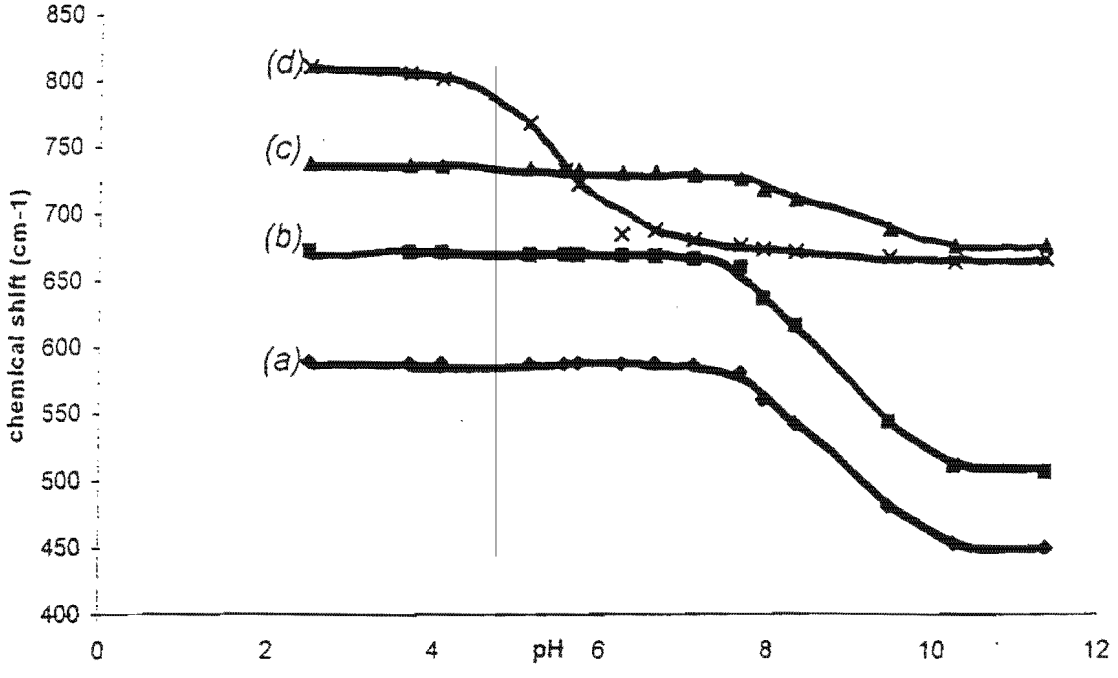

Figure 4.1: Change in Proton Chemical Shift with pH.

4.2.4 Discussion

Figure 4.1 shows that as pH increases, the central nitrogen atom is deprotonated first. This occurs in the 4 to 6 pH range. The upfield movement of the d proton chemical-shift, at lower pH affords evidence for this. In the 8 to 10 pH range, the chemical shifts of protons **a** and **b** are shifted upfield, indicating de-protonation of the terminal nitrogen atoms. In terms of protonation, this indicates that the terminal nitrogen atoms are protonated first and the third nitrogen atom last. This protonation sequence is unlike the one observed for diethylenetriamine pentaacetic acid (DTPA) whereby the central nitrogen atom is protonated first, then deprotonated in favour of one of the other nitrogen atoms before being protonated again with all the others at low pH (Letkeman, 1979).

4.3 SUPEROXIDE DISMUTASE (SOD)

4.3.1 RA and Free Radicals

It has been shown (Roberts, Robinson; 1985) that rheumatoid arthritis is a result of chronic inflammation in which white blood cells degrade connective tissue by the production of free radicals such as superoxide and peroxynitrite. A multicomponent enzyme NADPH oxidase located in the plasma membrane of the white cell is designed to produce superoxide (McCord, 1994). This finding indicates the importance of agents that combat oxy free radicals in the management of the disease. It has been realized that treatments of superoxide-mediated diseases such as RA must include SOD/catalase mimetic pharmaceutical compounds (Riley, Weiss; 1994, Riley, Weiss, Henke, Lennon, Neuman, Rivers, Aston, Sample, Rahman, Ling, Shieh, Busch, Szulbinski 1996; Sorenson, Zhou; 1998). The drug Orgotein is one commercially available variant of the naturally occurring enzyme (Kiely, 1988). Lipophilic, low molecular weight copper complexes and substituted metal-based porphyrins (Karpishin, Vannelli, Glover; 1997; Mattson, 1998) make a good starting point for drug development. The SOD mimetic compounds may be bound to certain organelle proteins so as to enhance their access to specific target areas.

It is reported that one of the target tissues of free radicals is hyaluronic acid (HA) (Greenwald, 1986). This material is responsible more for the viscosity of joint tissue than it is for joint lubrication. A joint affected by rheumatoid arthritis is less viscous than a normal joint because of the depolymerisation of HA. The absence of hyaluronidase from inflamed joint tissue at the height of the disease shows that the depolymerisation process is not enzyme-mediated (Greenwald, 1986). However the presence of polymorphonuclear leucocytes and copper ions shows that depolymerisation is by some free radical mechanism that may be metal ion-mediated.

Collagen is also a target for free radicals. Normally, it can only be degraded by collagenases but since it is found in the extra-cellular matrix where no SOD occurs, it is exposed to the action of superoxide radicals. Greenwald (1986) showed that the double

helical conformation of collagen is completely lost after exposure to the superoxide radical. This is further evidence that diseases like RA are free radical-mediated.

Biological processes that produce the superoxide anion include active phagocytosis, oxygen transport by haemoglobin and galactose oxidation. Neutrophils and macrophages (Maeda *et al*, 1989) are known to undergo a respiratory burst (Weissman, 1986) during phagocytosis. This entails a high consumption of oxygen, a high production of hydrogen peroxide and a depletion of glucose *via* the hexose monophosphate shunt. The superoxide anion and hydrogen peroxide are produced as part of the antimicrobial armamentarium of these cells. At low levels, hydrogen peroxide is disposed of by the action of glutathione peroxidase (Fridovich, 1979), a selenium-based enzyme that also plays a major role in the defence against oxygen toxicity (Emsley, 1984).

4.3.2 The Superoxide Dismutase Enzyme

Superoxide dismutase (SOD) is a metalloenzyme that acts as a defence mechanism against oxygen toxicity (Michelson, McCord, Fridovich, 1977; Baum, 1992). It may be manganese, iron or copper-zinc based. The Mn and Fe-based forms are structurally related (Vance, 1998) and are different from the Cu-Zn form. In the human body copper-zinc and manganese SODs occur. The manganese containing SOD is found as a dimer in the mitochondria, the oxidation centre of the cell. The copper-zinc form is found as a dimer in the cytosol (Pierre, Chautemps, Refaif, Beguin, Marzouki, Serratrice, Saint-Aman, Rey; 1995) and as a tetramer in the extracellular space. The zinc atom in this enzyme is only structural since its replacement with a copper atom does not augment the SOD activity of the enzyme (Pierre, Chautemps, Refaif, Beguin, Marzouki, Serratrice, Saint-Aman, Rey; 1995). The function of these enzymes is to keep the steady state concentration of the superoxide anion diminishingly low. The SOD enzymes have an electrostatic surface potential that guides the negatively charged substrate to the active site.

The monomer of copper-zinc SOD has a molecular weight of 32kDa (Mattson,1998). The copper and the zinc atoms in this enzyme share a common ligand, a bridging histidine. In this way, both the copper and the zinc centres are bound through an imidazolate side chain (Valentine, Lu, Roe, Bender, Peisach, Banci, Bertini, Gralla; 1996). This SOD enzyme seems to be too elaborate a molecule for such a substrate as small as the superoxide radical, especially since the substrate can also be metabolised by other compounds (Fridovich, 1979). The active site covers less than 1% of the total surface area of the enzyme, which itself has a net charge of –4 at pH 7 (Sharp, Fine, Hong; 1987). In view of the detrimental effect of the action of the superoxide anion, nature has not left its removal to chance, hence the justification of a specially designed molecule for that function. The specificity of the enzyme is witnessed by its generation at the slightest detection of the presence of the superoxide anion and the build up of the substrate in the absence of the enzyme.

SOD catalyses the reaction of two superoxide radicals in acidic medium to form hydrogen peroxide and dioxygen. The rate-limiting step of this reaction is almost entirely diffusion controlled, with a second order rate constant of $10^9 M^{-1}$ sec^{-1} (Sharp, Fine, Hong, 1987; Ellerby, Valentine, Cabelli, Graden; 1996). In this reaction, the reactive centre metal cycles between its oxidised and reduced forms. In both oxidation states, the substrate is involved.

4.3.3 Superoxide Dismutase Determination

There is a "standard assay" for superoxide dismutase-like activity (Fridovich, Michelson, McCord, 1977) which involves the inhibition of the reduction of cytochrome *c* by xanthine oxidase (XO). XO is one of the most convenient (Hill, 1979) enzymatic sources of the superoxide radical. It is commercially available and has been well studied and characterised. If this enzyme is allowed to work on hypoxanthine and purine, generation of the radical becomes continuous. Hypoxanthine is more water-soluble and gives twice the amount of the radical per molecule than xanthine whilst purine gives out thrice as much per molecule. For the effective application of this reaction as a detector of SOD activity, the enzymatic radical generator has to be

coupled with such detectors as cytochrome *c* and nitroblue tetrazolium (NBT) (Fridovich, McCord, Michelson; 1977).

The superoxide anion may also be generated photochemically, electrochemically, or by target-oriented chemical reactions. Respectively, these other methods operate by the spontaneous re-oxidation of photochemically reduced flavin, by univalent reduction of dioxygen at the surface of a platinum electrode immersed in an aqueous solution and by pH-controlled auto-oxidation chemical reactions (Fridovich, McCord; Michelson; 1977). In all these methods the radical detection methods remain the same with slight modifications to suit the experimental conditions. Since the scope of the present work focuses on the enzymatic method, the details of the other methods will not be given here.

The ability of low molecular weight copper complexes to dismute the superoxide anion is normally assessed with the nitroblue tetrazolium test. This test has the advantage of high sensitivity to the superoxide anion. Nitroblue tetrazolium is a freely soluble yellow compound, which is converted to formazan by a reduction reaction. Formazan is an intense blue, water-insoluble compound that has a tendency to precipitate quickly out of solution. This makes it difficult to use the solution for spectrophotometric measurements. It is normally recommended that such precipitation be reduced by the addition of 0.33mg/mL gelatin to the test solution. The rate constant of nitroblue tetrazolium reduction by the superoxide anion is said to be 50 000 /Msec at pH 7.8, decreasing to 10 000 /Msec at pH 10.2. The superoxide anion is susceptible to direct reduction by other reductants present in test solution. It is also metabolised by dehydrogenases but this process cannot be detected as SOD activity (Fridovich, McCord, Michelson; 1977).

The NBT test may be modified to suit prevalent conditions as sometimes there are competing metal ions in the reaction medium. Ethylenediaminetetraacetic acid (EDTA) or diethylenetriaminepentaacetic acid (DTPA) may be added to remove possible interfering metal ions such as iron. It is however important to ensure that the

resultant complex does not exhibit SOD activity otherwise it will give misleading results. Catalase is normally added to remove any hydrogen peroxide formed in order to keep the reaction proceeding forward (Oberly, Spitz; 1985).

The principle of the NBT assay can be represented (Zhu, Zheng, Fu, Huang, Tang; 1998) as:

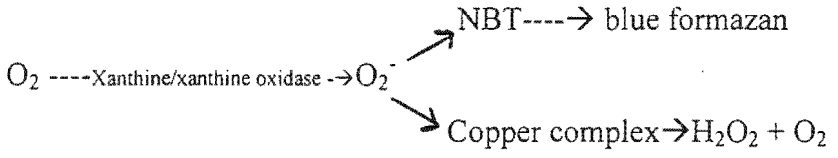

4.4 EXPERIMENTAL

The procedure used in the present study for the determination of SOD activity is described below. It is a modification of a method used to assay cell tissue homogenates (Greenwald, 1986). Superoxide radical anions generated by the xanthine/xanthine oxidase enzymatic system at pH 7.8 (phosphate buffer, 25°C) were analysed spectrophotometrically by the reduction of NBT to blue formazan.

4.4.1 Reagents

1. 0.05M Potassium phosphate buffer pH 7.8
2. 1.8mM Xanthine prepared in phosphate buffer weekly.
3. 2.27mM Nitroblue tetrazolium in buffer
4. 40 units/m*l* Catalase in buffer
5. 10^{-2} units/ml Xanthine oxidase in buffer.
6. 0.001M SOD solution in buffer.

4.4.2 Procedure

For a seven-tube assay, 1.2m*l* xanthine, 0.5m*l* NBT and 1m*l* catalase were mixed in a total volume of 21m*l* with buffer solution. Three millilitre portions of this homogenous solution were dispensed into each of seven test tubes. To one test tube that was to act as a blank (without SOD activity) was added 1m*l* buffer solution. One-millilitre portions of SOD solution at different concentrations were then added to the rest of the tubes. The concentrations of SOD ranged from 2.27×10^{-4} M to 1.14×10^{-5}M. From this point on, one tube was fully assayed before proceeding to the next.

To each tube 0.4m*l* xanthine oxidase was added and the tube was shaken for about 15 seconds after which the contents were transferred to a cuvette so that the first reading could be taken at 30seconds. Absorbance (ABS) at 560nm was read at 30s intervals for a period of 10minutes. For each test-tube, absorbance was then plotted against time and the slope of each plot was determined.

The extent to which each concentration of SOD inhibited NBT reduction was calculated using the formula:

$$\% \text{ Inhibition} = (S_0 - S_i) / S_0 \times 100$$

where S_0 is the slope of the calibration curve, S_i is the slope of the plot at concentration *i*. A plot of % inhibition against concentration was drawn (Figure 4.5.1) for each metal-ligand system, and the concentration of complex required to yield 50% inhibition for each SOD system read off. This value is referred to as the 50 percent inhibition concentration (IC_{50}) and the higher the concentration of complex at IC_{50}, the lower the SOD-like activity of the complex.

It is noteworthy that the SOD-like activity experiments were performed at pH 7.8. This was the pH stipulated in the original SOD detection method (Greenwald, 1986). This pH was not changed as it was deemed close enough to the plasma pH range of 7.2 to 7.6. At pH 7.8, the present copper complex systems show a mixture of the 110 and the 11-1 species, both in equal proportions. The amount of free metal ion is nil. It suffices then to assume that any SOD activity observed here is due to the copper complex.

4.5 RESULTS

The values of IC50 found for the various copper complexes investigated are presented in Table 4.5.1.

Table 4.5.1 IC_{50} of Copper (II)-Ligand Systems

CuL system	IC_{50}
CuDME	131μM
CuBID	165μM
CuZDA	167μM
CuEDA	195μM

Figure 4.5.1 Plots of %Inhibition of NBT-reduction versus Concentration of copper (II) complex

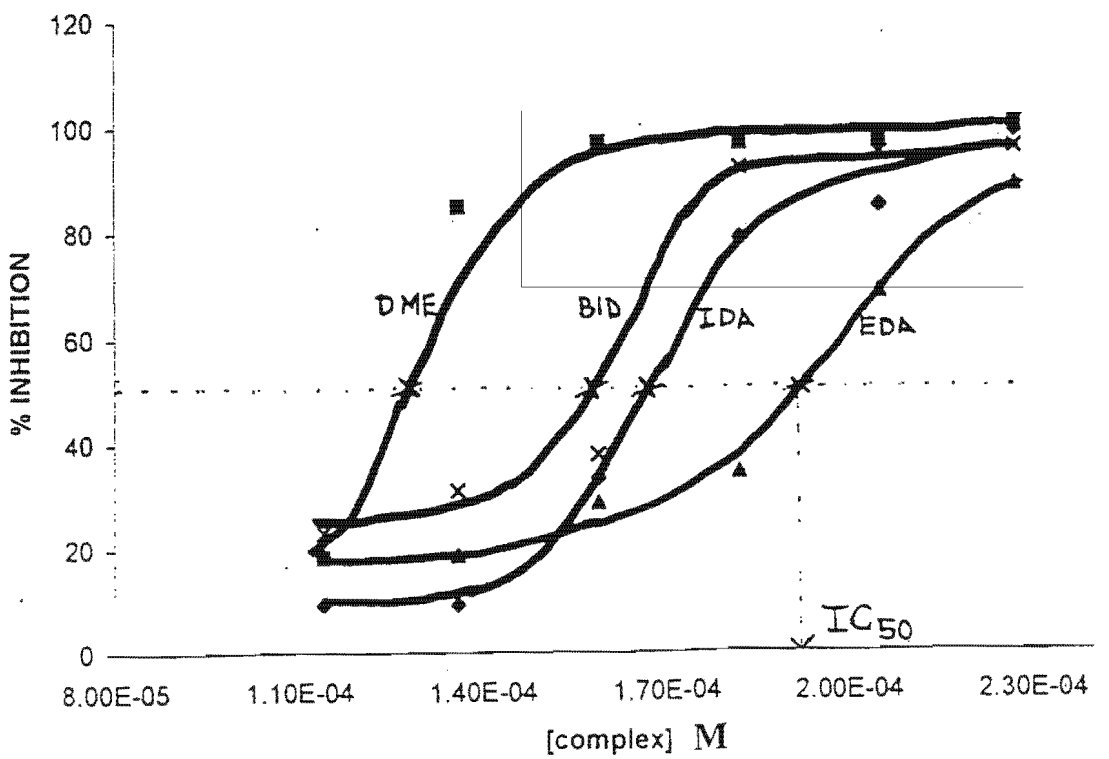

4.6 DISCUSSION

From the results in Table 4.5.1 it appears that the lower the stability of the complex, the higher the SOD-like activity, as evident from the fact that the IC50 of the CuDME complex is the lowest of those investigated. The highly substituted DME ligand has the lowest complex stability. This means that the coordination strength is lower than that of the other complex systems. The SOD activity is related to the ability of the copper ion to interact with the superoxide anion. If the metal ion is strongly ligated, its geometry is more fixed and the metal centre is less labile. The superoxide must be able to interact with the copper ion for it to be dismuted.

The complexes of ligands ZDA and BID can be concluded, within experimental error, to have similar SOD-like activity. In their ability to coordinate to the copper ion, they are not different at all. Both these ligands are methyl substituted at the terminal nitrogen atoms. These are the principal atoms that are involved in the coordination sphere of the metal atom. The only difference in the structure of these two ligands is at the central nitrogen atom, which carries a benzyl group in one case and not in the other. In the stability studies, this substitution was shown to introduce a certain degree of instability which seems not to have a marked affect to the SOD-like activity of the two CuL systems.

The complexes of the EDA ligand have the lowest SOD activity. This ligand is not alkyl substituted at the terminal nitrogen atoms which greatly reduces the steric effects that are otherwise observed with the other ligands and thereby lends greater coordination opportunity to the donor atoms.

All the present complexes have three to four orders of magnitude less SOD-like activity than those found in literature. One copper-imidazolato-copper complex has been reported to have an IC_{50} = 0.225μM (Tabbi, 1997). Another related compound displayed SOD-like activity with an IC_{50} value of 0.35μM (Zhu, Zheng, Fu, Huang, Tang; 1998). In another study, a dicopper and a copper-zinc cryptand complexes both showed SOD-like activity of IC_{50} = 0.5μM (Pierre, Chautemps, Refaif, Beguin,

Marzouki, Serratrice, Saint-Aman, Rey; 1995). This was in the presence of bovine serum albumin indicating that the complexes would have a reasonable half-life *in vivo*. In terms of SOD activity, native bovine erythrocyte preparations have an IC_{50} of only 4 x 10^{-8}M. The amino acids that occur naturally in human blood plasma show IC_{50} values ranging from 4.5μM for histidine to17-20μM for tryptophan, arginine and tyrosine. Common anti-inflammatory drugs like aspirin, indomethacin and chloroquine also fall in this region, just like the different structural isomers of 1,3-diaminopropane (Roberts and Robinson, 1985).

It is clear that the present complex systems cannot be of much use in the dismutation of the superoxide radical, since their IC_{50} values are much lower than those of other copper complexes, though they compare quite closely with those of antiinflammatory drugs such as aspirin.

It is worth mentioning that the phosphate-copper (II) interactions are not negligible in the copper speciation. This then alters the concentration of the effective complex that inhibits the reduction of NBT to formazan i.e. the value of the IC_{50} of the complex under investigation becomes higher than it really is. However, in the literature the possibility of phosphate coordination is always ignored. Hence, in order to compare our results with literature results we have done the same. In some instances, EDTA is added to the solution in order to mimic the effect of endogenous ligands.

4.7 LIPOPHILICITY OF COMPLEXES

One aspect upon which biological activity depends is the ability of the drug to reach the target area of action. In the human body, drugs have to traverse a number of body tissues before they can impart their therapeutic effect. The pharmacological effect of a copper complex is evidence that it is not completely dissociated *in vivo*. This effect is due to the lipophilic nature of the complex (Greenwald, 1978).

Exogenous ligands may form ternary and quaternary complexes with the endogenous proteins and peptides. These new higher order complexes enhance the stability of the lmw complexes and increase their half-life in plasma. They are also better able to dissolve into tissue and deliver trace elements where necessary. It is believed that the higher the organic proportion of the complex is, the more lipophilic it is. This is the basis upon which most topically administered drugs are designed. It was of interest therefore in this study to observe the effect of the different alkyl substituents present on the ligands, on their feasibility as topically administered drugs. For this reason, the lipophilicity of the present ligand complexes were investigated.

4.7.1 Topical Drug Administration

Drugs are normally administered *via* the skin masked in an agent called a vehicle or ointment base (Polano, 1984). A vehicle may be monophasic (powder, grease or liquid), biphasic (liquid/powder, powder/ grease, oil in water or water in oil) or triphasic (liquid/powder/grease). Out of this wide variety of vehicles, the final choice depends on its compatibility with the drug and its effectiveness in drug delivery. Drugs can also be percutaneously administered by the use of liposomes which have the ability to permeate the horny outer layer of the skin (Lasic, 1992) and get into the lower layers epidermis.

The latest in transdermal drug delivery is the use of the patch. This is a flat (5mm) circular object of diameter up to three centimetres. It consists of an outer aluminised plastic layer and a drug resevoir covered by a semipermeable membrane. Around this is an adhesive layer that is used to attach the patch to the skin (Wick, 1995). It can be

worn on any suitable part of the body where it will effect a slow and long-term delivery of the drug to the blood stream. More advanced drug delivery patches are rigged with electronic gadgets that stimulate the skin to increase drug absorption (Stix, 1994).

The ointment base effects contact between the drug and the skin to initiate drug penetration. This necessitates that the base must possess emollient, astringent and protective properties. The vehicle must not in any way inhibit the progress of the drug into the circulatory system. Unsuitable vehicles tend to bind the active drug and prevent delivery or cause local irritation at the site of administration. In order for a pharmaceutical company to decide on with a vehicle suitable for whatever drug it is intended for, the properties of the drug must be well known so that a choice is made out of the three possible forms of vehicle.

4.7.2 Partition Coefficient

The partition coefficient P is a physical property defined as the logarithm of the quotient of the concentration of the solute in the organic and in the aqueous phase (Mailhot, Peters; 1988). It is normally expressed as follows:

$$P = \log (C_i^{o} / C_i^{a}) \qquad \ldots(4.7.1)$$

where C_i^{o} is the concentration of solute I in the organic phase and C_i^{a} is the concentration of i in the aqueous phase.

The partition coefficient is as important a parameter as the pK_a parameter (Avdeef, Comer, Thomson; 1993) encountered in acid-base investigations. Partition coefficients (Mailhot, Peters, 1988; Richards, Essex, Reynolds; 1992) are usually employed as criteria in quantitative structure-activity relationship (QSAR) studies in biomedical chemistry. The approach may be used also for the investigation of the bioaccumulation (Connell, Coates, Barron; 1985) of pollution in the bodies of aquatic animals. Even though the partition coefficient may not be a true indicator of events in a system that

does not reach true equilibrium, as it often is the case with the human body, its value shows the way in which the drugs begin the process that finally ends up in substrate-receptor recognition.

Partition coefficients may be studied using different biphasic solvent systems. Water is normally used as the aqueous phase. Organic phases that may be used include chloroform, carbon tetrachloride and 1,2-dichloroethane (Fresco, 1964). The most commonly used biphasic system is that of octanol and water (Mailhot, Peters, 1988; Westall, Johnson, Zhang, 1990; Politzer, Brink, Murray; 1993) which has been widely accepted as most representative of biological tissue membranes.

An investigation of a biphasic system at varying pH values interestingly shows the role that speciation plays in the determination of the partition coefficients. The change in charge in successive complex formation is accompanied by a change in the solubility of the solutes in the two phases, (Beck, Nagypal 1990). This then necessitates the knowledge of the aqueous speciation trend of the complex system before any plausible interpretation is possible of observed partitioning behaviour of the solutes, (Schwarzenbach, Arnold, Weidenhaupt, David, Muller, Hardelein, 1997).

4.7.3 The Two Phases

After partitioning equilibrium has been reached, the same species will be observed on either side of the interface but in different concentrations. Mutual solubility of the two phases is inevitable and the extent to which this occurs depends on the difference in their physicochemical properties (Politzer, Brink, Murray; 1993). Electrolytes transferring from the aqueous phase "drag" (Testa, Tsai, Fan, Tayar, Carrupt, Kier; 1993) water into the organic phase and this tendency will vary with their electronic and steric properties.

Even though it is understood that the water-solute interactions at the interface between two immiscible electrolyte solutions (ITIES) (Girault, Testa, Carrupt, Steyaert, Reymond; 1996), are more complex than is apparent, the amount of water carried into

the organic phase has been linked to the H-bond donor acidity (Girault, Testa, Carrupt, Steyaert, Reymond; 1996) of the solute. The specific nature of each biphasic system supports either solute-water or solute-solute association equilibrium at some specific concentration of solute. If there are too many different stoichiometries of hydrated species, it becomes very difficult to compare the hydration capacities of different solutes for one and the same biphasic system. In the case of weak acids and weak bases, association of ionic components is quite predominant and therefore analysis of equilibria is more involved.

The mechanisms of transfer of these species from one phase to another differ for different regions on the pH scale. In some regions whole species can be transferred across the interface and in some dissociation occurs before transfer followed by association in the new phase. Speciation occurs both within and between the phases. Quantification of all the equilibrium constants that describe a biphasic system requires the collaborative use of several analytical tools. The least that can be done is a thorough study of the aqueous phase by such tools as glass electrode potentiometry.

The organic phase of the octanol/water biphasic system is highly structured (Testa, Tsai, Fan, Tayar, Carrupt, Kier; 1993). The saturation water molecules are tightly bound to the organic molecules to form an extensive network of the phase. The octanol OH has two H-bond acceptor sites and one H-bond donor site whilst the water molecule has two acceptor sites and two donor sites (Westall, Johnson, Zhang, 1990). High H-bond-donor acidity of the solute assists its hydration in the organic phase. The hydration of aprotic solutes also makes some contribution to the introduction of water into the organic phase. There are certain features of the solute compounds that favour this hydration. These include the orientation of the H-bond acceptor, the manifestation of the inductive effects of functional groups on the molecular framework and the length of the chain.

It must be appreciated that the octanol/water partition experiments performed in this study were not of just the organic ligand but of their copper complexes. Several factors

come into play here. Firstly there is hydration of the axial positions of the metal ion which might lower the lipophilicity. Then there is the degree of coordination of the organic ligand to the metal ion as opposed to its solubility in the organic phase. There is also the effect of the charge of the complex on its retention in the aqueous phase. Whatever the case may be, it is more informative to perform the experiment in such a way that the results may be related to those of the chemical speciation of the system under investigation.

4.8 EXPERIMENTAL

The method used for the measurement of the partition coefficients in this study is described below. Octanol being the organic phase represents the skin and water, the topically applied aqueous cream.

4.8.1 Equipment and Reagents

1-Octanol

De-ionised water

25m*l* 1:1 Copper-Ligand solution

1m*l* Saturated sodium hydroxide solution

Pasteur pipette

pH Meter

4.8.2 Procedure

A 25ml, 0.007 M copper/ligand solution was prepared and 1.0 m*l* of this solution was pipetted into each of 18 five-millilitre glass vials. Leaving one of the vials at the original pH noted, the pH in the rest of the vials was adjusted to read approximately 0.5 pH units apart using a saturated sodium hydroxide solution. This was so as not to considerably alter the volume of the ligand-metal solution in each vial. Into each vial was then pipetted 1.0 m*l* portions of 1-octanol pre-saturated with water. Each vial was stoppered and shaken by hand for about a minute, swirled gently to collect droplets from the sides of the vial and set aside to allow the two phases to separate and reach

equilibrium. The organic phase was carefully extracted with a Pasteur pipette and added to a bigger glass vial containing 10m*l*, 0.1 M HCl solution. The bigger vial was then shaken to extract all the contents of the organic phase into the acidic solution which was then analyzed for copper (II) ion content by ICP spectrometry.

Considering all dilution, the partition coefficient of each species at the pH domains in which they are at their maximum, was calculated using equation 4.7.1.

4.9 RESULTS

Figure 4.9.1 is a plot of the concentration of copper (II) in the organic phase against pH. Noted from the species distribution diagrams obtained in the potentiometric investigation, was the pH at which each species of the chemical model was in the highest concentration. At each pH of interest, the predominant species existed with another species, either preceding or succeeding or both, that was in a lower concentration. Taking that into consideration, the partition coefficient of the species predominant at that particular pH was calculated. This was done twice iteratively in order to arrive as close to the exact partition coefficient as was possible. The values of the partition coefficients are shown in Table 4.9.1

Table 4.9.1. Log Partition Coefficients of Species of Different $Cu^{2+}L$ Systems

Species	L = ZDA	BID	EDA	DME
111	-6.3	-5.6	-4.5	-4.3
110	-5.6	-4.4	-4.3	-3.8
11-1	-5.3	-3.7	-4.7	-3.5
11-2	-5.2	-4.1	-4.4	-4.4

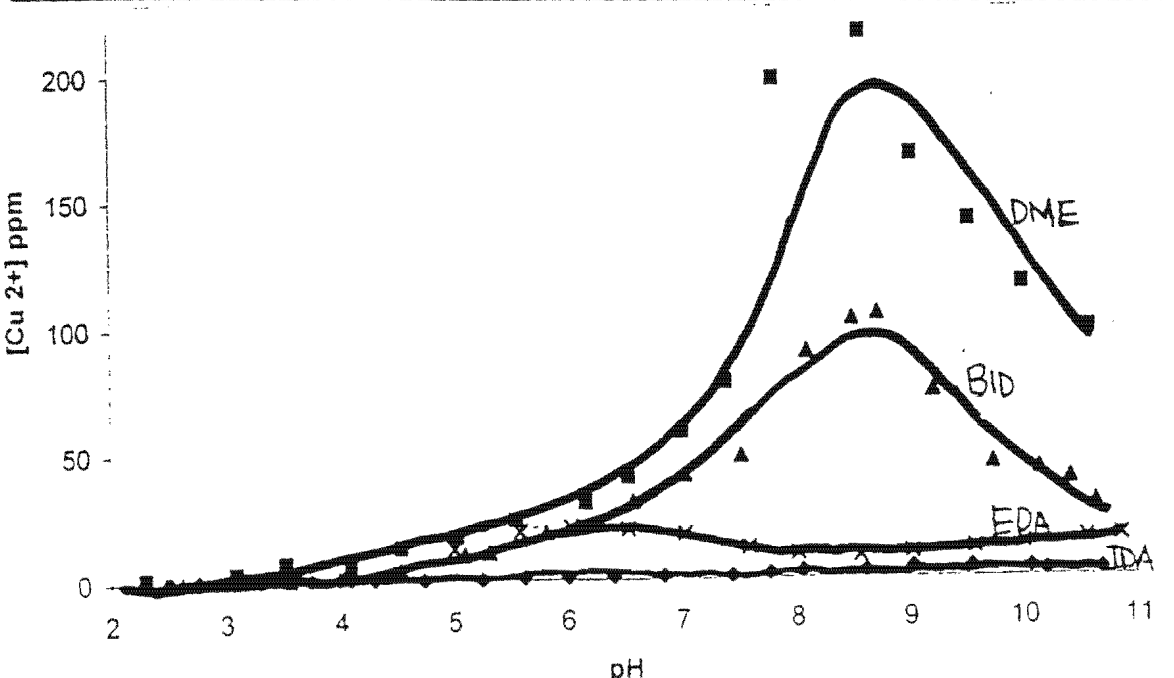

Figure 4.9.1. Concentration (ppm) of metal-ion in the Organic Phase versus pH.

4.10 DISCUSSION

The first trend observed in the results for complex systems ZDA, BID and DME is an initial increase of the concentration of copper (II) in the organic phase with increase in pH up to about pH 9, after which the concentration decreases. The maximum lipophilicity of the EDA ligand system is at pH 6, in which respect it differs from all the other ligand systems. The reason for the increase in lipophilicity with pH is that as deprotonation occurs on the ligand, the complex loses its hydrophilicity and hence its affinity for the organic phase increases. The overall charge of the complex plays a major role in its hydration such that as a neutral molecule is formed, transference into the organic phase increases but then decreases as a charged molecule is formed in the alkaline pH region. The stereochemistry of the chemical species of the present copper-ligand complexes is comparable and therefore is not expected to be the major contributing factor to the partitioning of the different species. The stability of the ML-H species of the copper (II)-EDA system is higher than that of the same species of the other ligands, which accounts for the observed achievement of species neutrality at a lower pH.

From figure 4.9.1, it is observed that an increase in the number of alkyl groups attached to the ligand is accompanied by an increase in the partitioning ability of the system into the organic phase. It is also apparent that the increase in the bulk of the alkyl group has further increased the general lipophilicity. As long as the organic ligand contains no charged functional groups, an increase in the percentage of the organic portion of the complex will favour partitioning into the organic phase. If the ligand contains pH dissociable functional groups, like the carboxyl group, then much more bulkier alkyl substitution has to be employed to increase lipophilicity. This may even necessitate the alkylation of too many points on the ligand, which is likely to decrease complex stability due to increased steric hindrance.

It is interesting to note that the formally charged 11-1 species has a higher partition coefficient than the neutral 11-2 species. This illustrates the difficulty in predicting partition coefficients.

CHAPTER FIVE

5. OVERALL DISCUSSION

The aim of the present work was to find a ligand to form copper complexes that would be effective in the alleviation of the symptoms of RA. Several ligand or copper complex characteristics were therefore sought. The ligand was to be of high copper binding specificity and could form a complex that is stable enough to be absorbed into the blood stream yet at the same time not so stable that it would be excreted from the body unchanged. The copper complex formed would have to be that of appreciable lipophilicity so that it could be transdermally administered into the body. A copper complex exhibiting biologically effective suoperoxide dismutase activity would also be advantageous with regard to free radical mediated inflammation.

In investigating the copper specificity of the ligands of the present study, the stability constants for their copper (II), zinc (II) and calcium (II) complexes were put into the ECCLES model of blood plasma so as to calculate the copper plasma mobilising indices. The logarithms of the plasma mobilising indices are shown in figure 5.1.

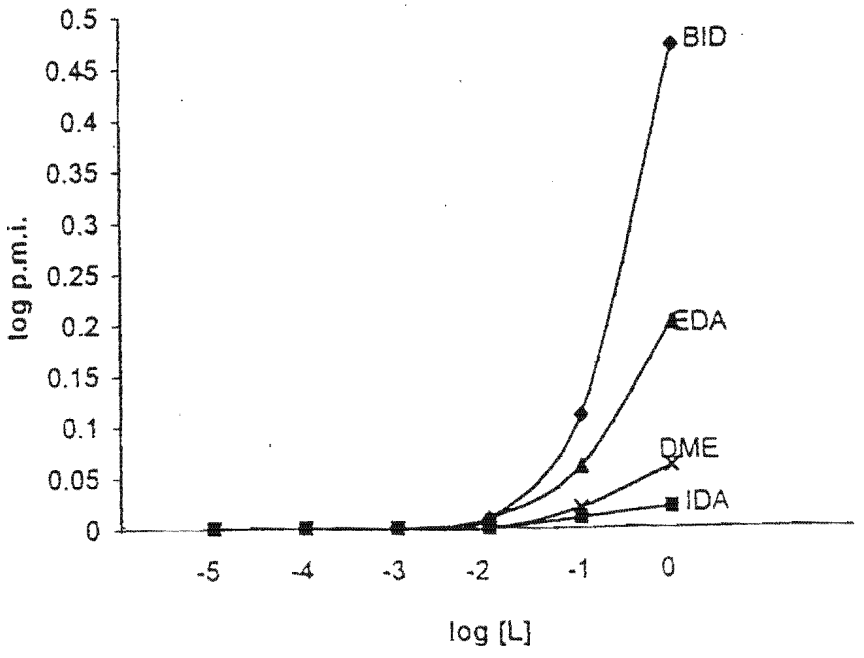

Figure 5.1: Logarithms of the copper (II) plasma mobilising index for ligands of the present study, plotted as a function of the logarithms of the ligand concentrations.

In comparing the copper plasma mobilising capabilities of the present ligands it was observed that this decreased in the order BID > EDA > DME > ZDA. However, to fully appreciate the plasma mobilising capabilities of these ligands, the logarithms of their p.m. i. were plotted together with those of ligands of previous studies (Kelly, 1989 and Voye, 1993). This is shown in figure 5.2.

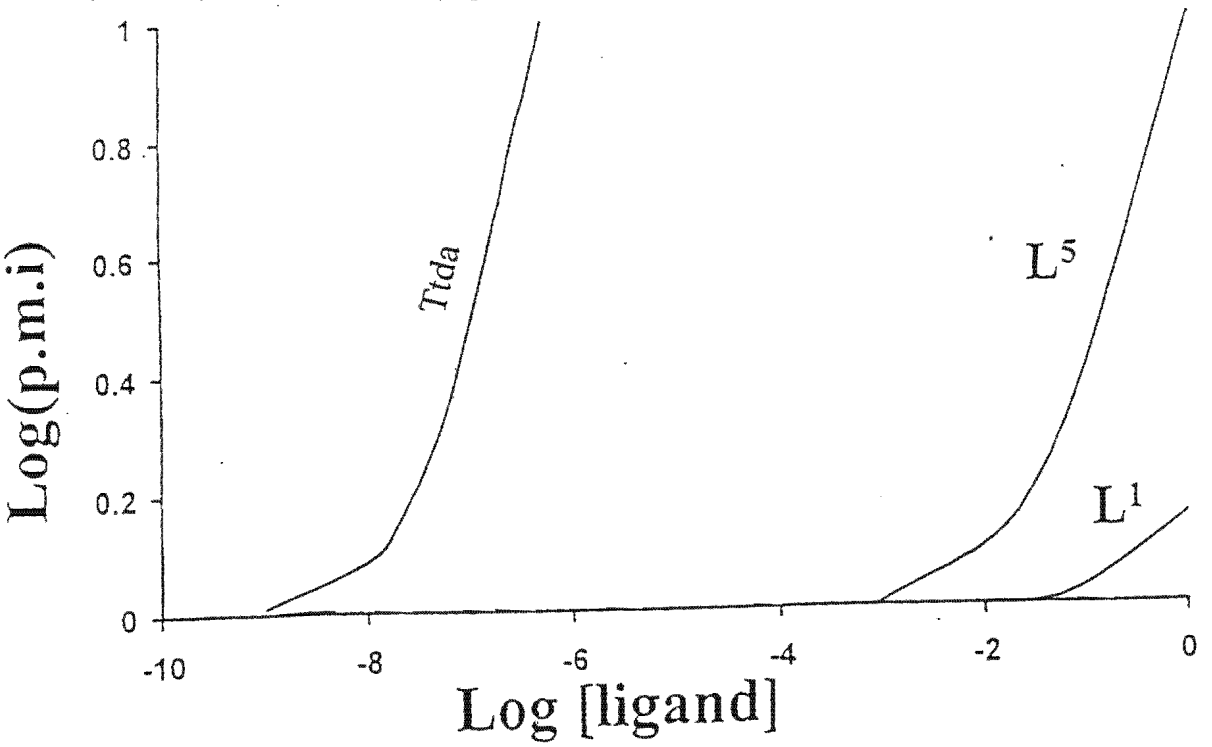

Figure 5.2: Logarithms of the copper (II) plasma mobilising index for ligands of the present study (L^5) Voye ligands (L^1) and Kelly ligand (Ttda).

Figure 5.2 shows that the ligands of the present study are on the lower end of the copper plasma mobilising ability scale. On this plot, the direction of ligand design can be inferred. It was realised that Ttda formed complexes that were too stable to deliver the copper in the body and that the Voye ligand-complexes were too weak to withstand the coordination competion present in blood plasma. The ligands of the present study feature between these two extremes but regrettably too close to the weaker-complex ligands. The fact that the present ligands are better able to mobilise copper than the Voye ligands implies that the structural modifications that were made on the Voye ligands were in the correct direction. Since chelate ring strain was found to be the major cause of

complex instability, it would be interesting therefore to see if relief of such strain could improve the p.m.i. of the ligands.

With the ligands of the present study having been found to have low copper mobilising ability, it was found that their calcium and zinc mobilising ability was higher. This is illustrated in figure 5.3:

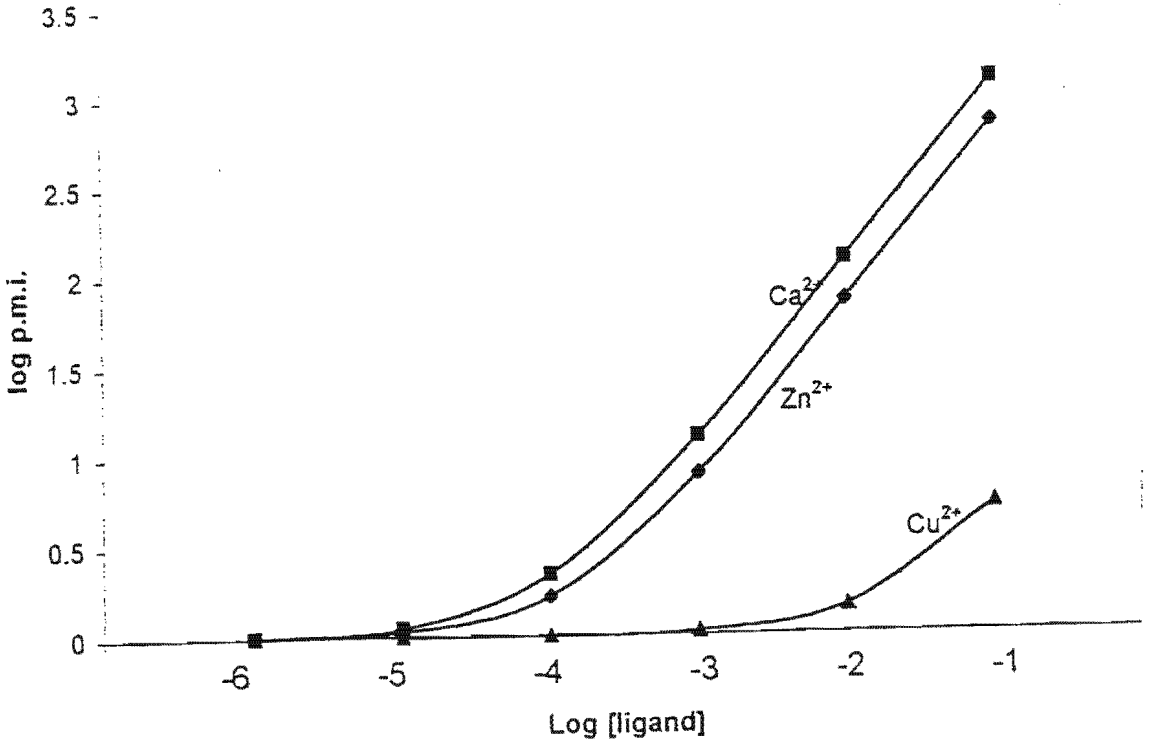

Figure 5.3: Average P.M.I. curves of divalent copper, zinc and calcium for the ligands of the present study

The fact that these ligands have a greater effect to the metabolism of zinc and calcium than to that of copper could mean interference in other biological processes of the body which may be deleterious. This point serves to emphasize the necessity of the specificity of the ligand for copper (II).

The lipophilicity of the ligand is necessary for the topical administration of the anti-inflammatory copper complexes. High alkyl substitution of the ligand was found to favour lipophilicity. Since the pH of the skin is in the 4.2 to 5.2 range and normal blood plasma is at a pH of 7.4, it would be advantageous that the most lipophilic complex

species occur in the 4.2 to 7.4 pH range. The formulation of a vehicle for use in the administration of the complex would have to be such that the speciation occurring in this pH range is chemically supported so that delivery of the copper ions at the target sites is ensured. In this study it was found that the species of maximum lipophilicity occurred at approximately pH 8.5 which showed that this lipophilicity was not applicable to the present biological system of interest i.e. the human body. This opens an avenue for further investigation in this regard.

The investigation of the SOD-like activity of the complexes was not in the original list of ligand design criteria. It was performed, as it could not be overlooked as a possible functional property of these complexes. It would be advantageous if the present ligand complexes exhibited some biologically effective SOD-like activity. As it was found that the SOD-like activity of the present ligands was negligible, it became apparent that for a compound to appreciably possess this property, the ligand would have to be specially designed. The ligand would have to be of high molecular weight and properly pre-organised for the copper ion. Low molecular weight ligands like those of the present study, seem to be sufficient only to increase the pool of plasma exchangeable copper.

The delivery of copper and its effect at the site of inflammation is best investigated with animal studies. As the plasma mobilising ability of the ligands of the present study showed that the copper complexes were not stable in blood plasma, no animal tests were performed. The study of dermal absorption using skin would have been more informative if the species of maximum lipophilicity occurred at the relevant physiological pH, otherwise the quantification of the permeation rate of the administered species would be difficult. Besides, such a study requires the clear definition of criteria of the type of material used to model skin. This is another avenue for further work.

The results of the present study have been able to set a stage for further investigation. In light of the present study Figure 5.4 shows a pair of ligands that are proposed for further work.

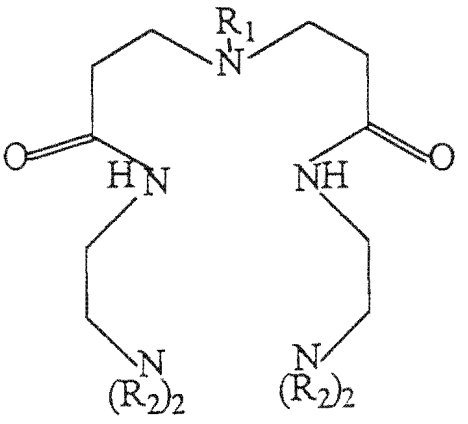

Ligand K

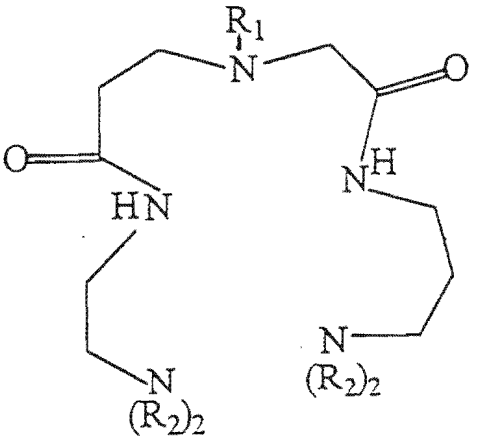

Ligand L

Figure 5.4: Ligands that are proposed as improved modifications of the ligands of the present study.

Upon complexation to the copper (II) ion Ligand K would form a 5,6,6 chelate ring sequence in the equatorial plane. Ligand L would, depending on the terminal amine nitrogen atom coordinated, either form a 5,6,5 or a 6,5,6 chelate ring sequence in the equatorial plane. Synthetically, Ligand K would be more straightforward to produce but is not expected to to give the kind of thermodynamic results desired for the next study. On the other hand, the more synthtically challenging Ligand L would be more likely to give better plasma-copper mobilising efficiency than the present ligands and is earmarked for further studies.

In the ligands proposed in figure 5.4: -

- The phenethyl substitution at the central nitrogen atom must be maintained in order to have high complex lipophilicity.
- The amide groups must be moved to β-positions form the central nitrogen atom in order to reduce their base weakening effect of the central amine nitrogen, at the same time increasing the chelate rings formed with the copper ion by one member. To relieve contiguous chelate ring strain.

- The terminal amine groups must not be alkyl-substituted so as to eliminate steric hindrance to their complexation to the metal ion, increase donor atom basicity and therefore achieve stronger bonding.

With the above modifications of the ligands of the present study, it is hoped that better plasma mobilising capability will be obtained and therefore topical administration is beneficial.

CHAPTER SIX

6. CONCLUSION

The treatment of diseases with drugs is inevitably accompanied by toxic side effects. This is even more so with the least understood diseases like RA. The aim of the present study was to widen the scope of the possible copper-based drugs that have already been investigated in past studies, which have fewer side effects than NSAID. The vast amount of literature on the topic is evidence of the implication of copper metal in the therapeutic course of RA, which warrants an in-depth investigation into the use of this metal in the development of RA drugs.

On the whole, this thesis has contributed to the understanding of the procedures involved in the application of trace metal-based drugs in the treatment of inflammation. In undertaking this project it was appreciated that previous related studies would play a major role in the selection of ligands to be investigated. This entailed an extensive review of literature in search of pertinent findings and conclusions. Strategic planning of the way in which the project was to be carried out in the light of available time, space and analytical tools followed. All the steps of the plan were successfully carried through; ligand synthesis and characterisation, solution chemistry and computer-aided chemical speciation of the ligands, structural determination of the complexes and finally, the investigation possible superoxide dismutase-like activity and lipophilicity determination. The results of these studies have been reported and discussed in this thesis.

Potentiometric studies of the present drugs showed them to be similar in terms of their ability to bind and mobilise copper in blood plasma. This meant that any single one of them was representative of all. They all had the same chemical speciation model on the pH scale and it can be assumed that the coordination geometries of the different chemical species are the same in all four copper-ligand systems. The main reason of selecting ligands of the general structural formula chosen for this research was the hope of finding a pentadentate ligand, which would ensure coordination at one of the axial positions of the aquated metal-ion. Such a structure as represented by figures **f** and **g** (section 3.3.4) of the molecular mechanics calculations is however highly strained and not likely to be stable in blood plasma. Therefore it would appear that these ligands

acted only as quadridentates, as the quadridentately-coordinated structures were found to have the lower strain energy.

In the confirmation of the chemical models found by potentiometry, UV/VIS spectrometry was used as a complementary analytical tool. The smooth plots of absorptivity versus wavelength (deconvoluted spectra) of the individual chemical species showed that the models were essentially correct. The variation in the absorption maxima of the individual chemical species showed that consecutive coordination of the ligand donor atoms occurred as the pH of the reaction solution progressively increased. When these results were related to the results of the molecular mechanics calculations, it was found that indeed, the internal strain energy of the complex was related to the coordination arrangement around the central metal ion.

Even though these complexes were found to have little plasma-copper mobilising utility, their potential as topical anti-inflammatory agents deserves comment. In this regard, the gradual change in pH in traversing from the surface of the skin across the different dermal layers to blood plasma needs to be considered. For this reason the chemical speciation events of the copper complex system in the 4.2 to 7.4 pH range have to be observed closely. From the species distribution diagrams of the four ligand systems studied it appears that the 111 and the 110 species dominate this pH region, with the protonated species at the lower pH and the unprotonated species at the higher pH. The octanol-water partition coefficient studies however indicated that the most lipophilic species was the 11-1 species, which occurs at around pH 8. Therefore it may be concluded that the complexes would have to be administered as a pH 8-aqueous cream which would allow the active compound to partition into the skin. It appears though that the 11-1 species would revert into a 110 species upon reaching blood plasma, which is at a lower pH. Since the 110 species has a lower lipophilicity it may be trapped in the circulatory system and not access inflammed tissue. The fact that higher alkyl substitution of the ligand and lack of charge of the complex favours lipophilicity was clearly demonstrated.

It was also demonstrated that the present ligands have limited superoxide dismutase-like activity. The fact that they are copper-containing, like the native superoxide dismutase enzymes, did not qualify them for the role hence it was appreciated that there is more to this phenomenon than just the involvement of the copper-containing active site. It can then be concluded that if the present complexes were to be stable in blood plasma, their only contribution to the alleviation of the symptoms of RA would be their existence as low-molecular weight transport forms of copper. As it is, they can only deliver the metal ion to endogenous plasma-copper chemical carriers.

Kelly and Jackson (1990) developed complexes which, in laboratory-rat experiments, were excreted as unchanged copper complexes. As the present ligands do not form complexes with copper ion that are nearly as stable as the Kelly complexes, it is suggested that the ligand drawing board be re-visited. As suggested in the preceding chapter, instead of seeking higher denticity, the number of carbon atoms separating the donor atoms have to be increased by one so as to slightly decrease the strain in the chelate rings. On the present ligands, an extra carbon atom may have to be added on either side of the central nitrogen donor atom in order to enlarge the two chelate rings which the amide nitrogen atoms form with this nitrogen atom. It may even be sufficient to add this extra carbon atom on only one side of the central nitrogen donor atom. This would be so as to produce an alternating 5,6,5 chelate ring sequence upon coordination of one terminal nitrogen atom, both amide nitrogen atoms and the central nitrogen donor atoms. Introduction of an extra carbon atom will result in less strain around the metal ion and hence greater stability. These two hypothetically "improved" model structures of the present ligand complexes were constructed and minimised. The two complexes had a 6,5,6 and a 5,6,5 chelate ring sequence. Their internal energies were calculated and found to be 33 and 47 kcal/mol respectively. Even though the 6,5,6 structure showed less strain, its 5,6,5 counterpart, having a greater number of smaller chelate rings, would be the one more attractive to study. With regard to the terminal amine nitrogen atoms, they are better not alkyl-substituted as this only introduces steric instability. This, however, is an avenue that may be explored in another study.

As a closing word, it must be stressed that the search for new ligands must continue. This has the objective of finding those that will, in complexation with ecologically important metal ions, structurally and functionally assist in the definition of the most relevant states of the metal ions in biological and environmental systems.

REFERENCES

REFERENCES

Aeschlimann A., Simmen B. R., Michel B. A., in: Baumgartner H., Dvorak J., Grob D., Munzinger U., Simmen B. R. (Eds), *Rheumatoid Arthritis,* Thieme Medical Publishers, Inc., New York, 1995.

Ahrland S., *Helv. Chim. Acta.,* 1967, **50,** 306.

Avdeef A., Comer J. E., Thomson S. J., *Anal. Chem.*, 1993, **65**, 42-49.

Baes C. F. Jr, Mesmer R. E., *Hydrolysis of Cations,* John Wiley and Sons, New York, 1976.

Baum R., *Chemical and Engineering News*, 1992, October 26, **70**, 19 –20.

Beck M. J., Nagypal I., *Chemistry of Complex Equilibria,* 1990.

Billo E. J., *Inorg. Nucl. Chem.,* 1974, **10,** no.8, 613-613.

Bremner I. in: Ciba Foundation Symposium 79 (Ed.), *Biological Roles of Copper,* Excerpta Medica, 1980.

Brewer G. J. in: K. D. Rainsford, K. Brune, M. W. Whitehouse (Eds.), *Trace Elements in the Pathogenesis and Treatment of Inflammation,* Birkhauser Verlag, Basel, 1980.

Cambridge Structural Database and Cambridge Structural Database System, Version 5.17, April 1999, Cambridge Crystallographic Data Centre, University Chemical Laboratory, Cambridge, England.

Bygott A. M. T., Sargeson A. M., *Inorganic Chemistry,* 1998, **37,** no. 19, 4795 – 4806.

Choppin G. R., Yuan-Xian X., Jiang-Fen C., *Anal. Chem.*, 1996, **68**, 3973-8397.

Connell D, Coates M., Barron D., *Environ. Scie. Technol.*, 1985, **19**, 628 –632.

Cotton F. A., Wilkinson G., *Advanced Inorganic Chemistry,* 1972, Wiley and Sons, New York.

Cotton F. A., Wilkinson G., Gaus P. L., *Basic Inorganic Chemistry,* 1987, Wiley and Sons, New York.

Christian D. G., *Analytical Chemistry,* 1986, Wiley and Sons, New York.

Chung C-S, Liu S-H, *Polyhedron,* 1984, **3,** 559 –566.

Davison W., Woof C., *Anal. Chem.,* 1985, **57,** 2567 – 2570.

Delves H. T., in: *Biological Roles of Copper.* Ciba Foundation Symposium 79, Excerpta Medica. Amsterdam, 1980.

Discover 95.0/3.00, *Forcefield Simulations User Guide, Part 1,* 1995, October, BIOSYM/MSI, San Diego.

Ellerby L. M., Valentine J. S, Cabelli D. E., Graden J. A., *J. Am. Chem. Soc.*, 1996, **118**, 6556 –6561.

Elsworth F. J., Msimang L. N., Jackson G. E, *S. Afr. J. Chem.,* 1996, **49** (1/2).

Emsley J., *New Scientist,* 1984, August 9.

Fresco J., Freiser H., *Anal Chem*, 1964, **36**, no. 3.

Fridovich I, in: *Advances in Inorganic Biochemistry,* Eichhorn/Marzilli, (Eds.), Elsevier North Holland, Inc, 1979.

Fridovich I., Michelson A. M., McCord J. M., *Superoxide and Superoxide Dismutases,* 1977, London/ New York Academic Press.

Frieden E. in: Ciba Symposium 79, *Biological Roles of Copper,* 1980.

Girault H. H., Testa B., Carrupt P.-A., Steyaert G. and Reymond F., *Helvetica Chimica Acta,* 1996, **79,** 101- 117.

Glusker J. P., Katz A. K., Beebe A.S., Bock C. W., *J. Am. Chem. Soc.,* 1996, **118,** 5752-5763.

Gordon M. H., Macrae R., *Instrumental Analysis in the Biological Sciences,* 1987, Blackie, London.

Greenwald R. A., *CRC Handbook of Molecular and Oxygen Radical Research*, 1986, CRC Press.

Hancock R. D., Martell A. E., *Chemical Reviews,* 1989, **89,** 1875-1914.

Hill O. A., in: Ciba Symposium 65, *Oxygen Free Radicals and Tissue Damage,* 1979, Excepta Medica, Heerhugowaard, Netherlands.

Horvai G., Pungor E., *Anal. Chem.*, 1983, **55**, 1988-1990.

Jackson G. E., Kelly M. J., *Inorganica Chimica Acta,* 1988, **152,** 215-217.

Jackson G. E., Kelly M. J., *J. Chem. Soc. Dalton Trans.*, (1990), 1889.

Jackson G. E., Linder P. W., Voye A., *J. Chem. Soc. Dalton Trans.*, (1996), 4606.

Jackson G. E., Kelly M. J., *Polyhedron*, 1991, **10**, no. 8, 883 –884.

Karpishin T. B.. Vannelli T. A., Glover K. J., *J Am. Chem. Soc.*. 1997, **119**. 9063 – 9064.

Kiely T., *Technology Review,* 1988, **91,** 15-16.

Kimura E., *Tetrahedron,* 1992, **48,** no.30, 6175-6217.

Kolling O., *Analytical Chemistry,* 1985, **57,** no.6.

Lasic D, *American Scientist,* 1992, Jan- Feb., **80,** 20 –31.

Leach A., *Molecular Modelling Principles and Applications,* 1996, Addison Wesley Longman Limited, New York.

Letkeman P., *Journal of Chemical Education,* 1979, **56,** 5, 348 –351.

Linder P.W., Torrington R. G., *S. Afr. J. Chem.,* 1982, **32,** 2.

Linder P. W., Torrington R. G., Williams D. R., *Analysis Using Glass Electrodes,* 1984, Open University Press, Belfast.

Maeda H., *Science,* 1989, **244,** 974-976.

Mailhot H., Peters R. H., *Environ. Scie. Technol.* 1988, **22,** 1479-1488.

Martell A. E., Smith R. M., *Critical Stability Constants. Volume 2: Amines,* 1975, Plenum Press, London/New York.

Martell A. E., Motekaitis R. J., *Determination and Use of Stability Constants,* 1988, VCH, New York.

Mattson M. P., *Chemistry and Industry,* 1998 October 19, no. 20, 843-8.

May P., Linder P., *J. Chem. Soc. Dalton Trans.,* 1977, Part 1, 588-595.

May P., Williams D. R., Linder P. W., Torrington R. G., *Talanta,* 1982, **29,** 249-256.

May P., Murray K., Williams D. R., *Talanta,* 1985, **32,** 6, 483-489.

May P., Murray K., *Talanta,* 1988, **35,** 11, 825-830.

May P., Murray K., *Talanta,* 1988, **35,** 12, 927-932.

May P., Murray K., *Talanta,* 1988, **35,** 12, 933-941.

McCord J. M., *Food Technology,* May 1994, 106- 110.

Meier P. C., *Anal. Chem.,* 1985, **57,** 373- 375.

Meloun M., Havel J., Hogfeldt E., *Computation of Solution Equilibria,* 1988, Ellis Horwood, Chichester.

Michelson A. M., McCord J. M., Fridovich I., *Superoxide and Superoxide Dismutases,* 1977, Academic press, New York.

Miller A.-F. and Vance C. K., *J. Am. Chem. Soc.,* 1998. **120,** no. 3, 461-467.

Murray K., May P., *ESTA Manual,* ver1.1, 1984, UWIST, Wales.

Nancollas G. H., *Interactions in Electrolyte Solutions,* 1966, Elsevier Publishing Co., New York.

Older S. A., in Fischbach M (Ed), *Rheumatoid Arthritis,* 1991, Churchill Livingstone, New York.

Perrin D. D., Dempsey B., E. P. Sarjeant, *pK_a Prediction for Organic Acids and Bases,* 1981, Chapman and Hall, London.

Perrin D. D., Clark J., *Chem. Soc. Quart. Reviews,* 1964, **18,** 295- 320.

Pier D.G., Zerbinati O., Aruga R., Ostacolli G., *J. Chem. Soc., Dalton Trans.,* 1988, no. 5, p 1115-20.

Pier D.G., Zerbinati O., *J. Chem. Soc., Dalton Trans.,* 1989, no. 9. P1745-9.

Pierre J.-L, Chautemps P., Refaif s., Beguin C., Marzouki A., Serratrice G., Saint-Aman E. and Rey P., *J. Am. Chem. Soc.,* 1995,**117**, no. 7, 1965 –1975.

Polano M. K., *Topical Skin Therapeutics*, Churchill Livingstone, New York, 1984.

Politzer P., Brink T., Murray J., *J. Org. Chem.* 1993, **58**, 7070 –7073.

Reedijk J., Bonomo R., Driessen W., Tabbi G., Veldman N. and Spek A., *Inorg. Chem.,* 1997, **36,** 1168 –1175.

Richards W. G., Essex J. W., Reynolds C. A., *J. Am. Chem. Soc.*, 1992, **114**, 3634–639.

Riley D. P and Weiss R. H., *J. Am. Chem. Soc.,* 1994, **116,** 387 –388.

Riley D. P., Henke S., Lennon P., Weiss R., Neumann W., Rivers W.,Aston K., Sample K., Rahman H., Ling C-S., Shieh J-J., Busch D., and Szulbinski W., *Inorg. Chem.*, 1996, **35**, 5213 –5231.

Roberts N. A., Robinson P. A., *British Journal of Rheumatology*, 1985, **24**, 128–36.

Rossotti J. C., Rossotti H., *Journal of Chemical Education,* 1965, **42,** 7.

Sanz I., Alboukrek D. in: M. Fischbach (Ed), *Rheumatoid Arthritis*, 1991, Churchill Livingstone, New York.

Schwarzenbach R. P., Arnold C. G., Weidenhaupt A., David M., Muller S. and Haderlein S. B., *Environ. Scie. Technol.*, 1997, **31**, 2596 –2602.

Sharp K., Fine R., Hong B., *Science*, 1987 June 12, **236**, 1460-1463.

Sigel H., *Metal ions in Biological Systems, volume 13*, 1981, Marcel-Dekker Inc.

Sorenson J. R. J., *J. Med. Chem.,* 1976, **19,** 135.

Sorenson J. R. J., Zhou L., *J. Inorg. Biochem.*, 1998, **72,** 217.

Stix G., *Scientific American*, 1994, September, **271**, 87.

Tabbi G., *Inorg. Chem.*, 1997, **36**, 1168 –1175.

Testa B., Tsai R.-S., Fan W., Tayar N., Carrupt P.-A. and Kier B., *J. Am. Chem. Soc.*, 1993, **115**, 9623 –9639.

Tuck D. G., *Pure and Appl. Chem.*, 1989, **61,** 6.

Valentine J. S., Lu Y., Roe J., Bender C., Peisach J., Banci L., Bertini I. and Gralla E., *Inorg. Chem.*, 1996, **35,** 1692-1700.

Vogel A. I., *Vogel's Texbook of Quantitative Inorganic Analysis,* Bassett J. (Ed), Longman, London, 1978.

Voye A., *PhD Thesis*, UCT, 1993.

Weissmann G., *Advances in Inflammation Research*, 1982, vol.3, Raven Press, New York.

Westall J., Johnson C., Zhang W., *Environ. Scie. Technol.*, 1990, **24**, 1803 –1810.

Williams D. R., *The Metals of Life,* 1971, Norstrand/ Reinhold, London.

Wick S. M., *Adhesives Age,* 1995, September, 18- 24.

Woodward C., Redman H. N., *High Precision Titrimetry,* 1973, Society for Analytical Chemistry, London.

Zhu H.-L., Zheng L.-M., Fu D.-G., Huang X.-Y. and Tang W.-X., *Journal of Inorganic Biochemistry*, 1998, 70, 211 –218.

APPENDIX A

Protonation Function Curve (Ligand ZDA) at 25 °C at 0.15 mol dm^{-3} (Na)[Cl].

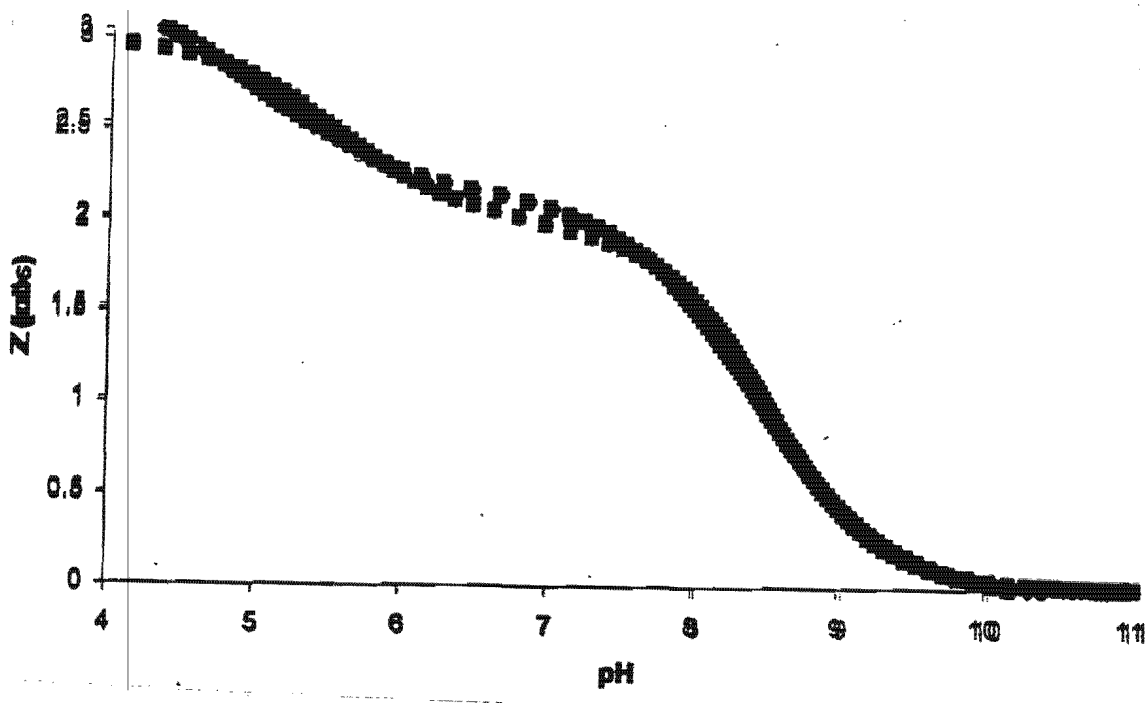

Protonation Function Curve (Ligand BID) at 25 °C at 0.15 mol dm^{-3} (Na)[Cl].

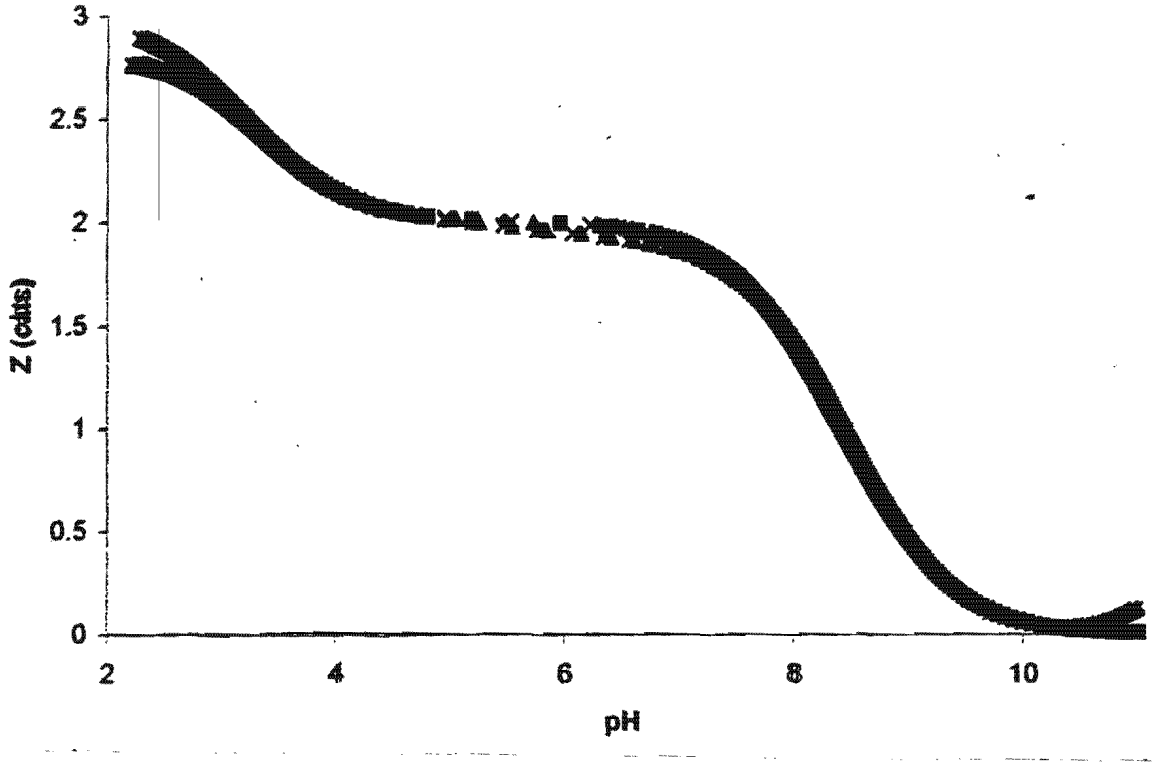

Protonation Function Curve (Ligand DME) at 25 °C at 0.15 mol dm^{-3} (Na)[Cl].

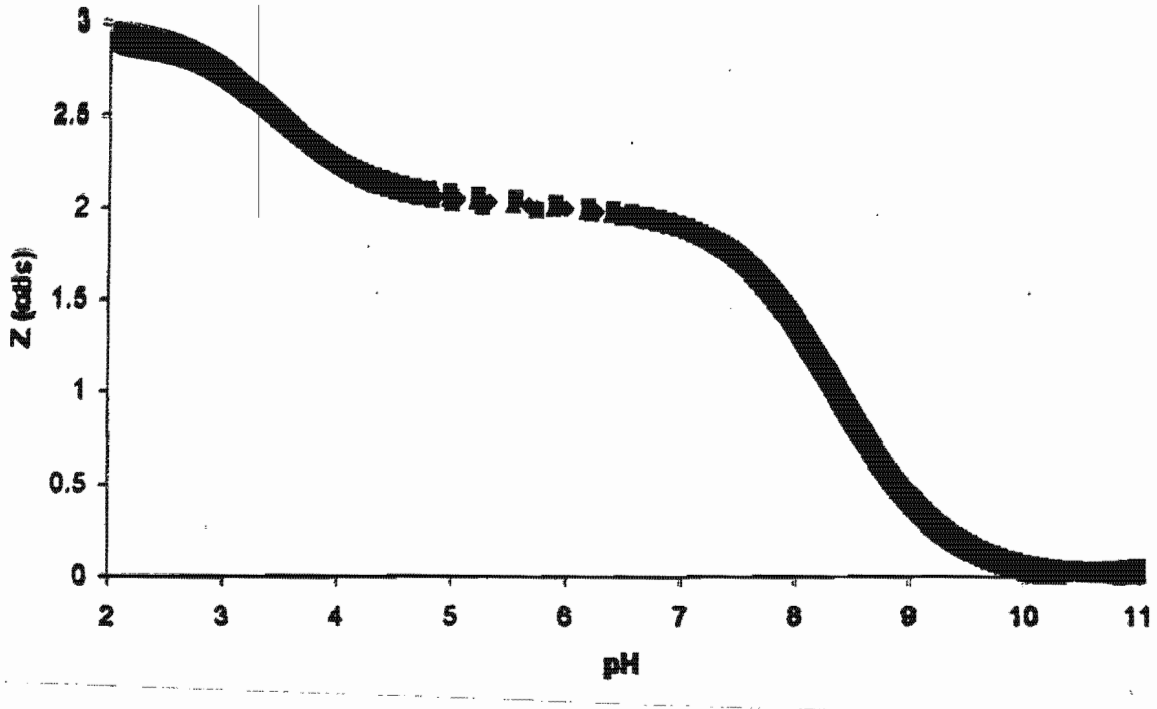

Protonated Species Distribution Diagram for ligand ZDA

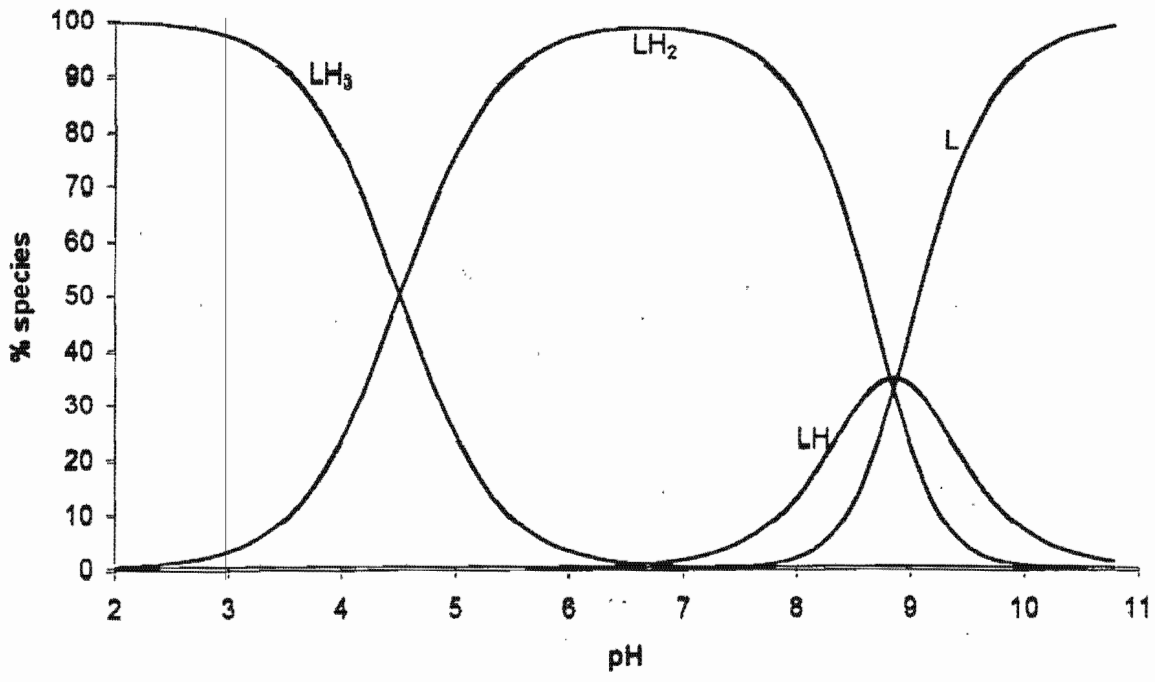

Protonated Species Distribution Diagram for ligand BID.

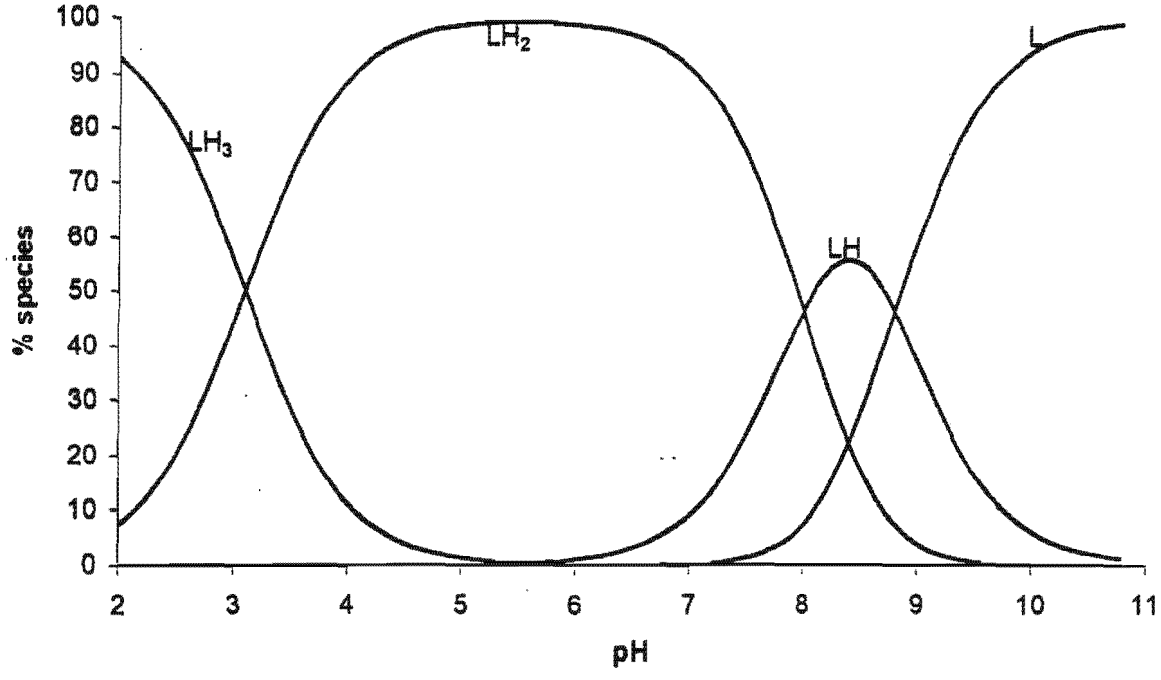

Protonated Species Distribution Diagram for ligand DME.

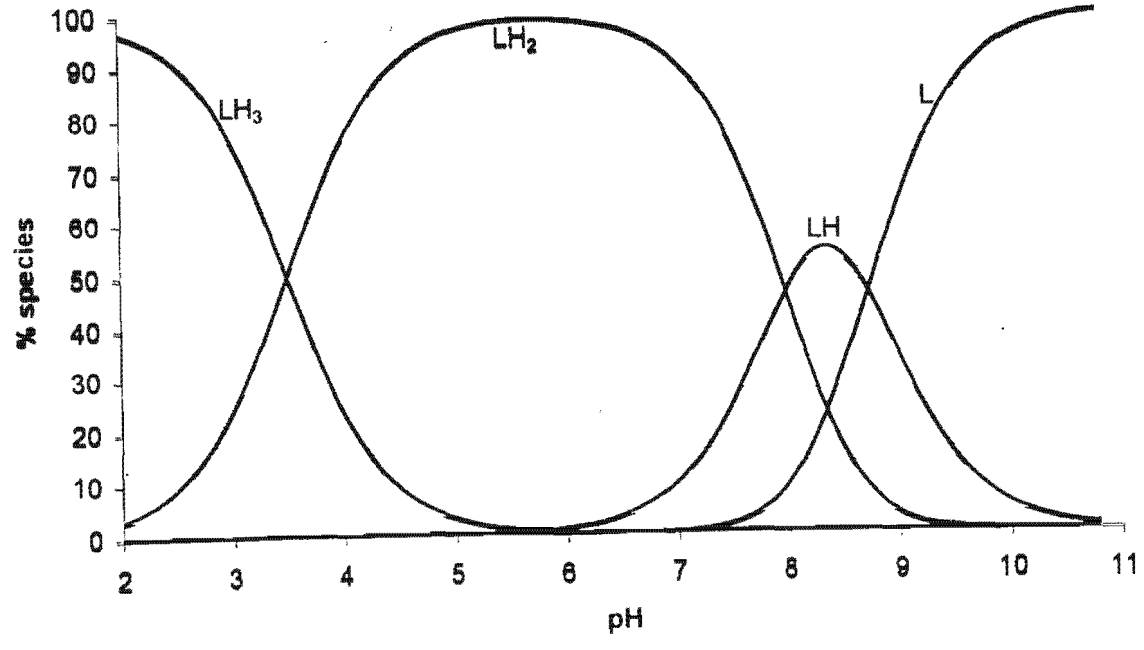

Formation Function Curve ($Z_M$obs) Cu^{2+}-ZDA

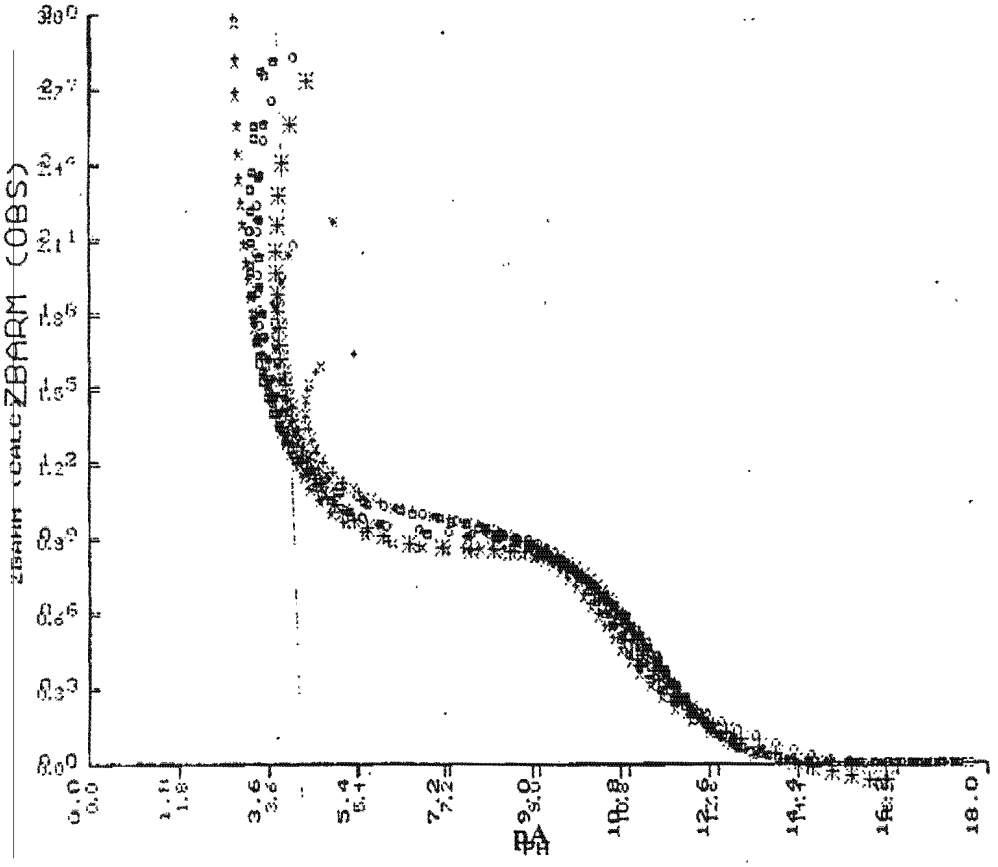

Deprotonation Function Curve ($Q_M$obs) Cu^{2+}-IDA

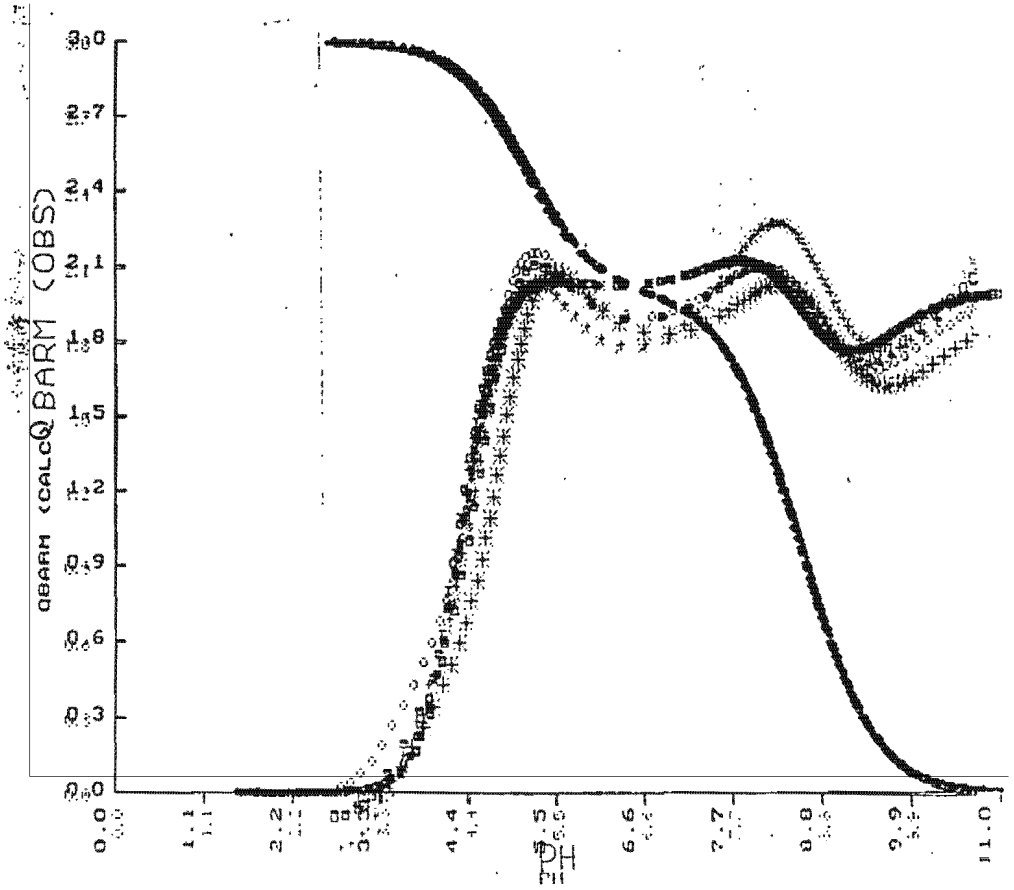

Species Distribution Diagram Cu^{2+}-ZDA

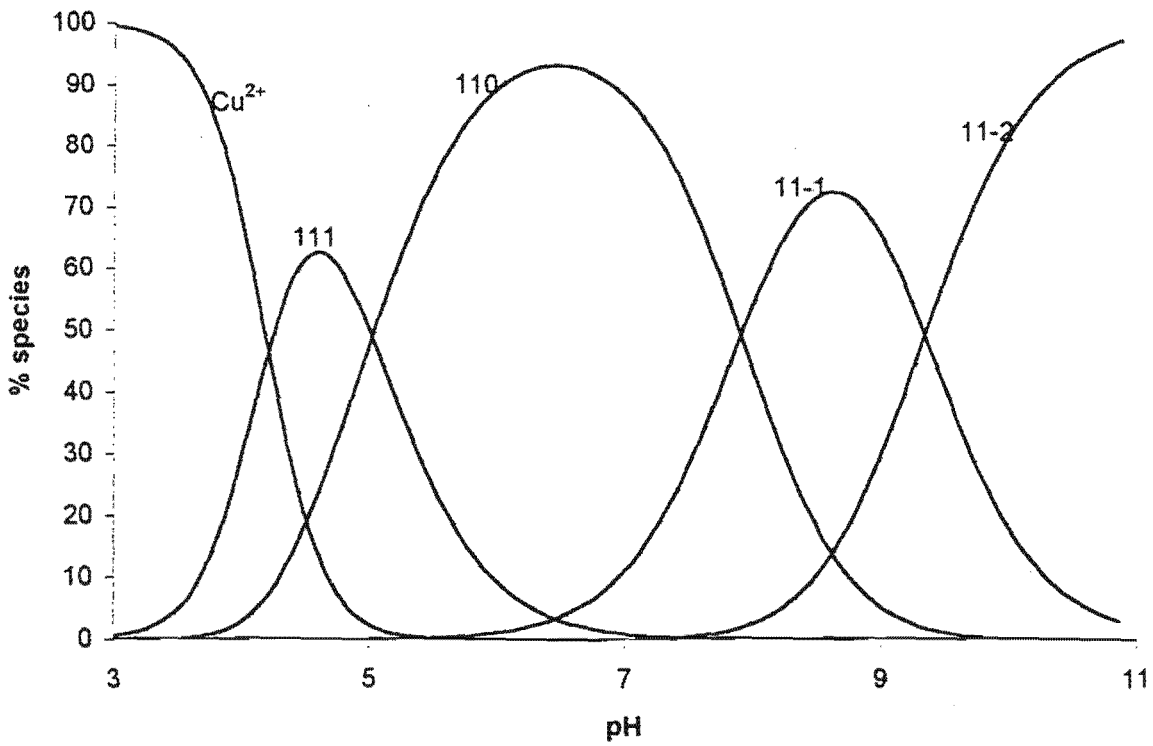

Formation Function Curve ($Z_M$obs) Cu^{2+}-BID

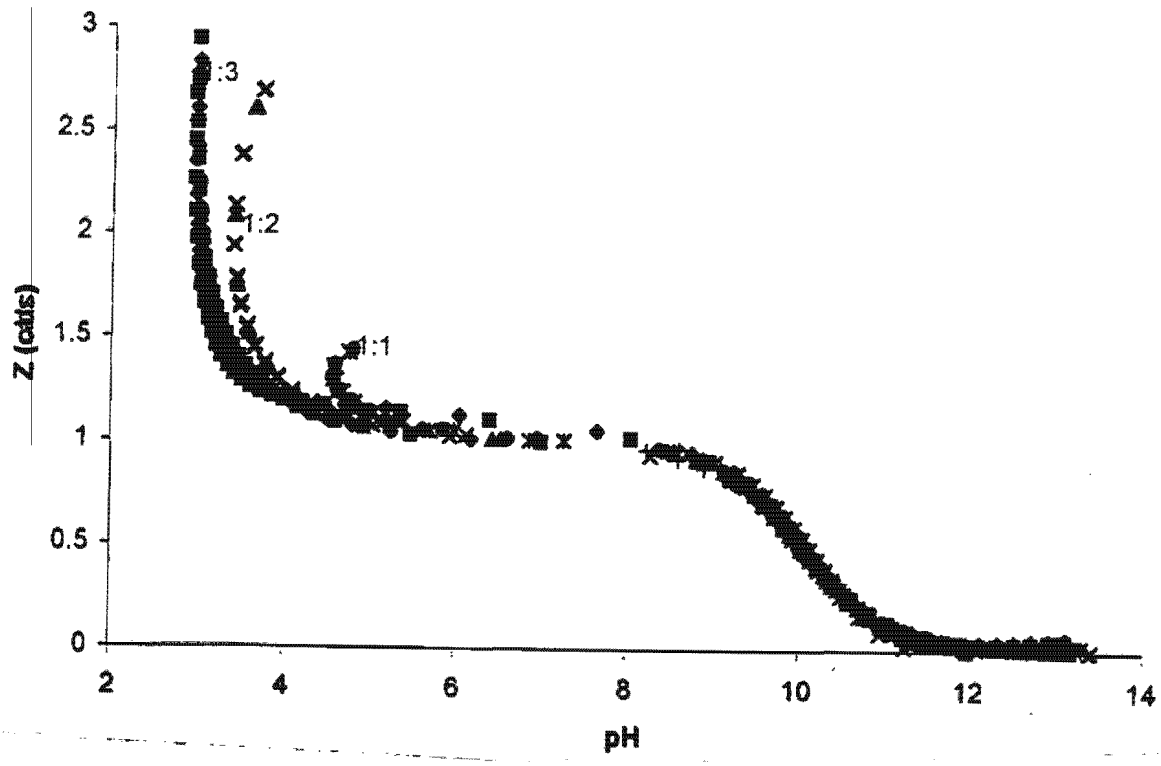

Deprotonation Function Curve ($Q_M$obs) Cu^{2+}-BID

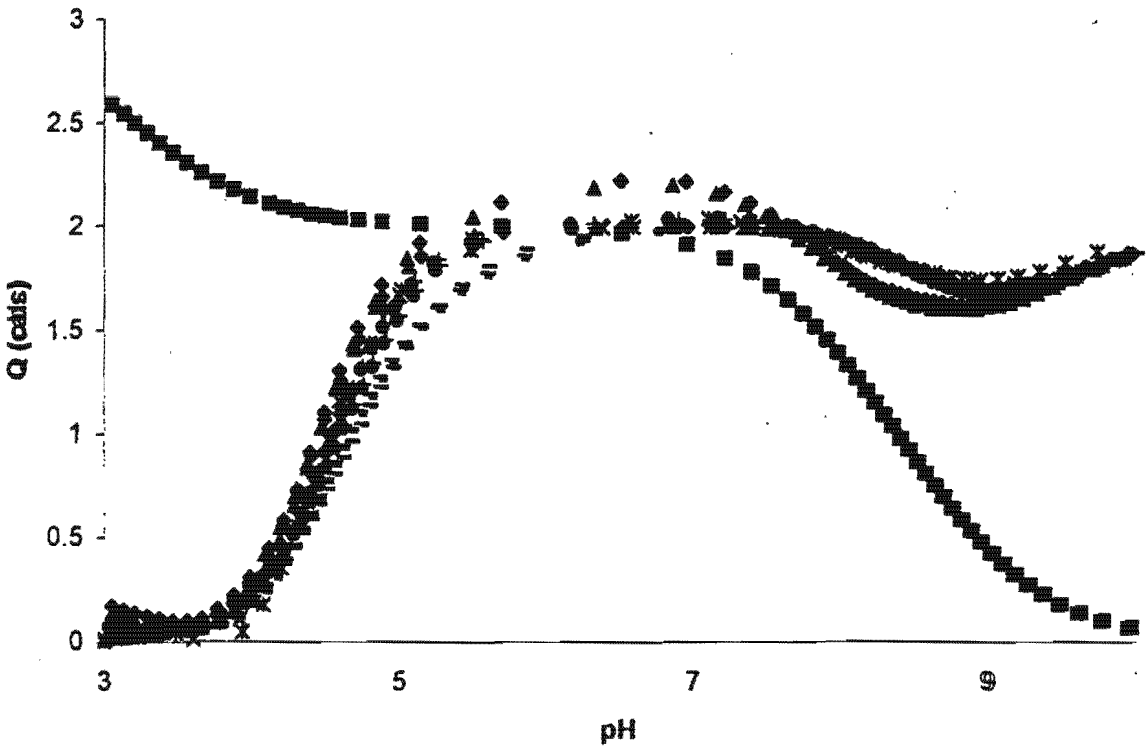

Species Distribution Diagram Cu^{2+}-BID

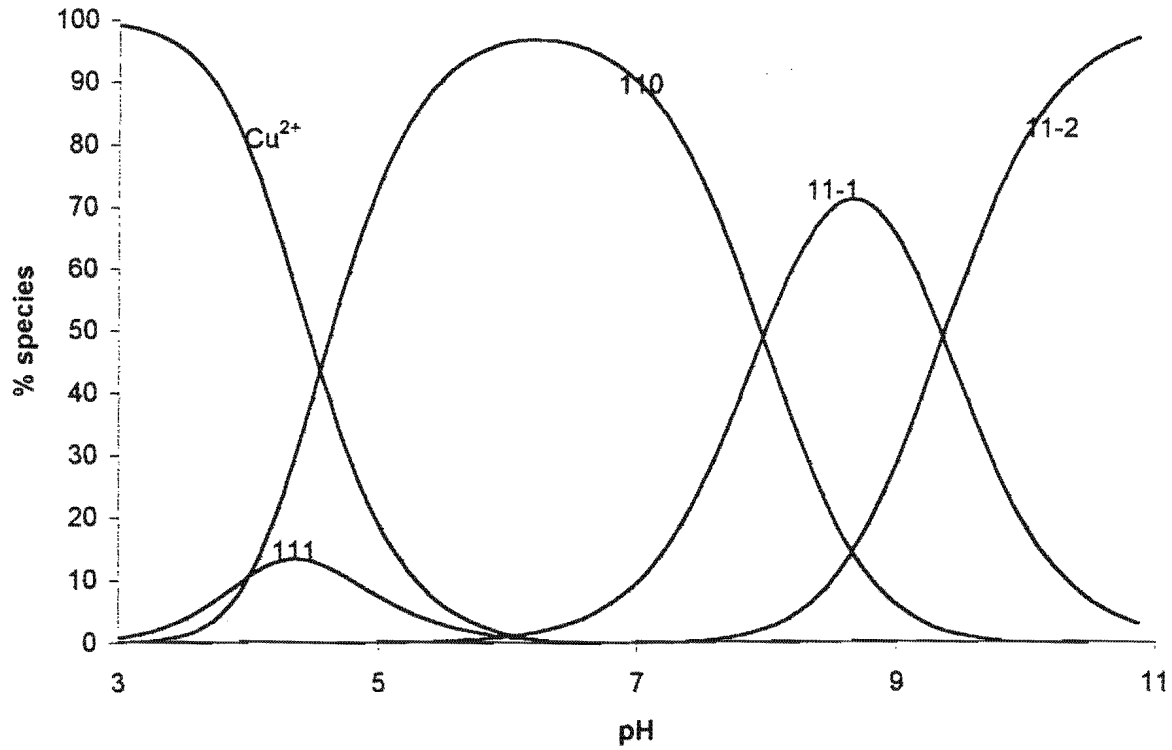

Species Distribution Diagram Cu^{2+}-DME

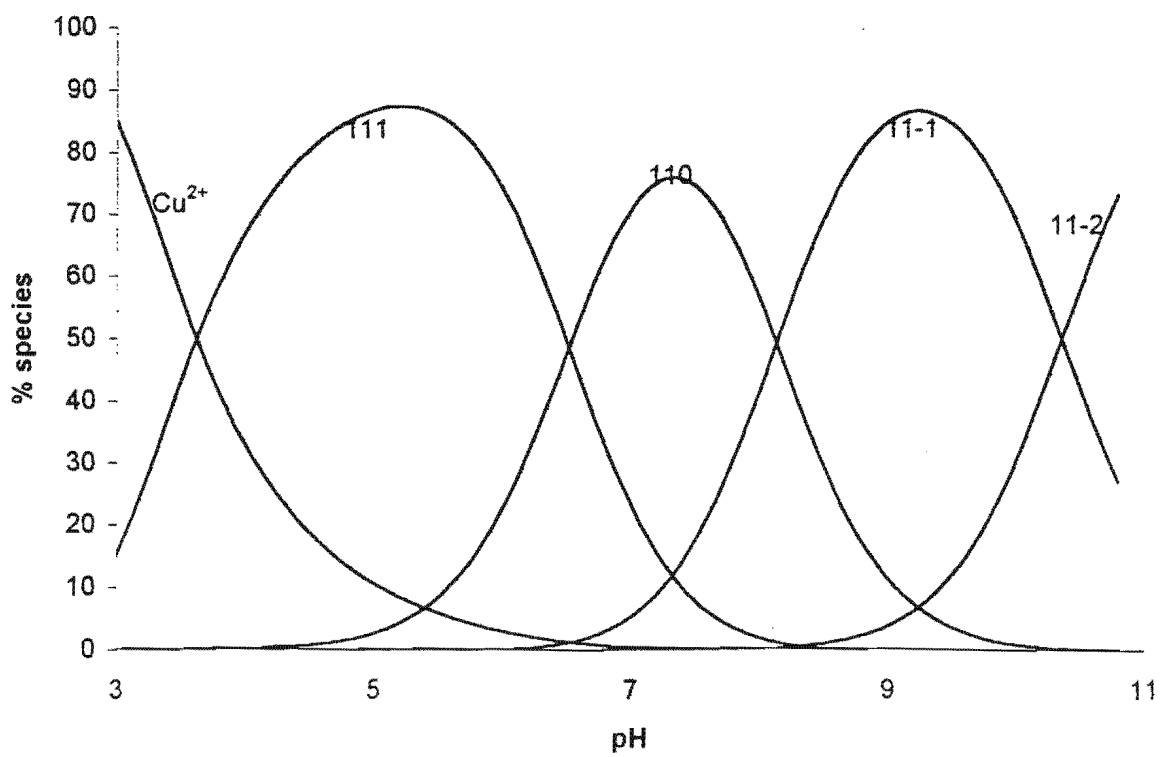

Formation Function Curve ($Z_M$obs) Cu^{2+}-DME

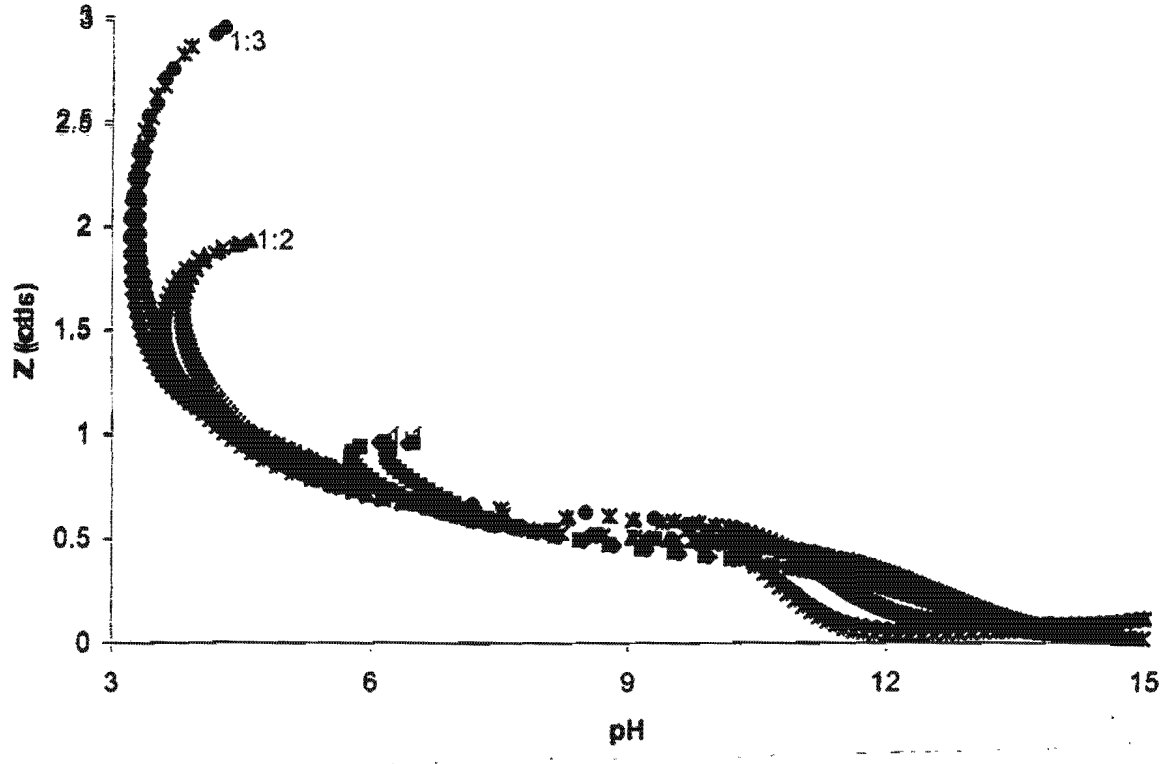

Deprotonation Function Curve ($Q_M$obs) Cu^{2+}-DME

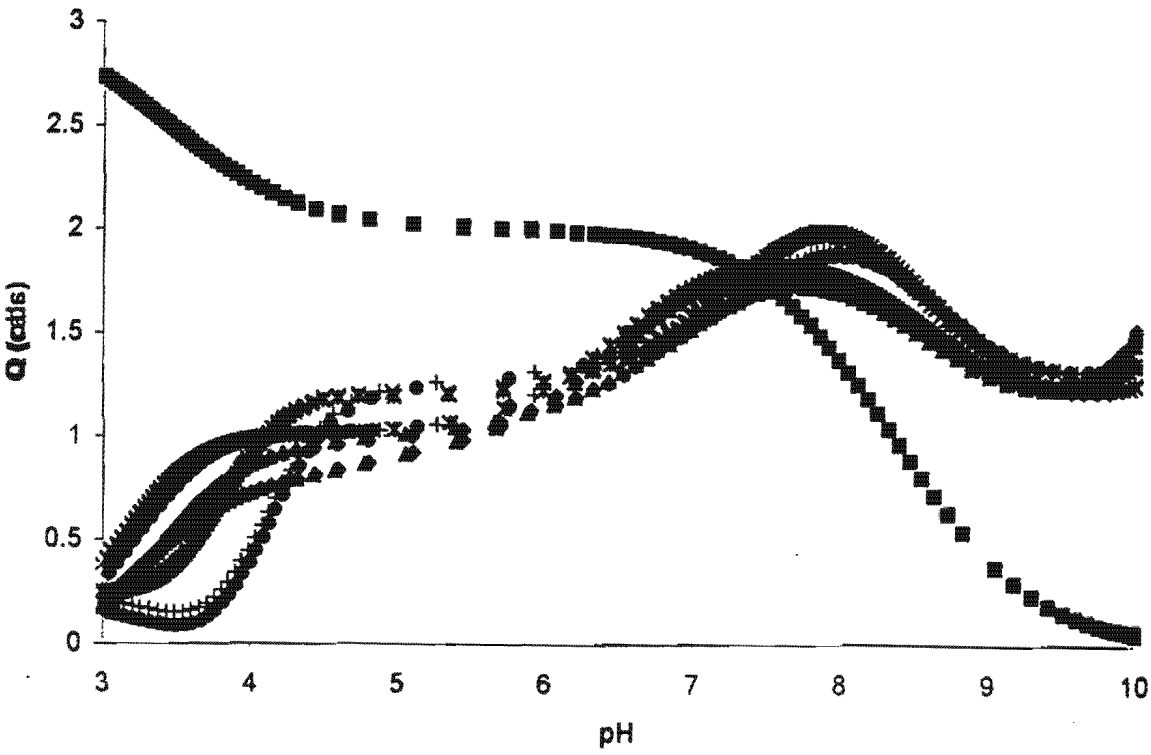

Formation Function Curve ($Z_M$obs) Zn^{2+}-ZDA

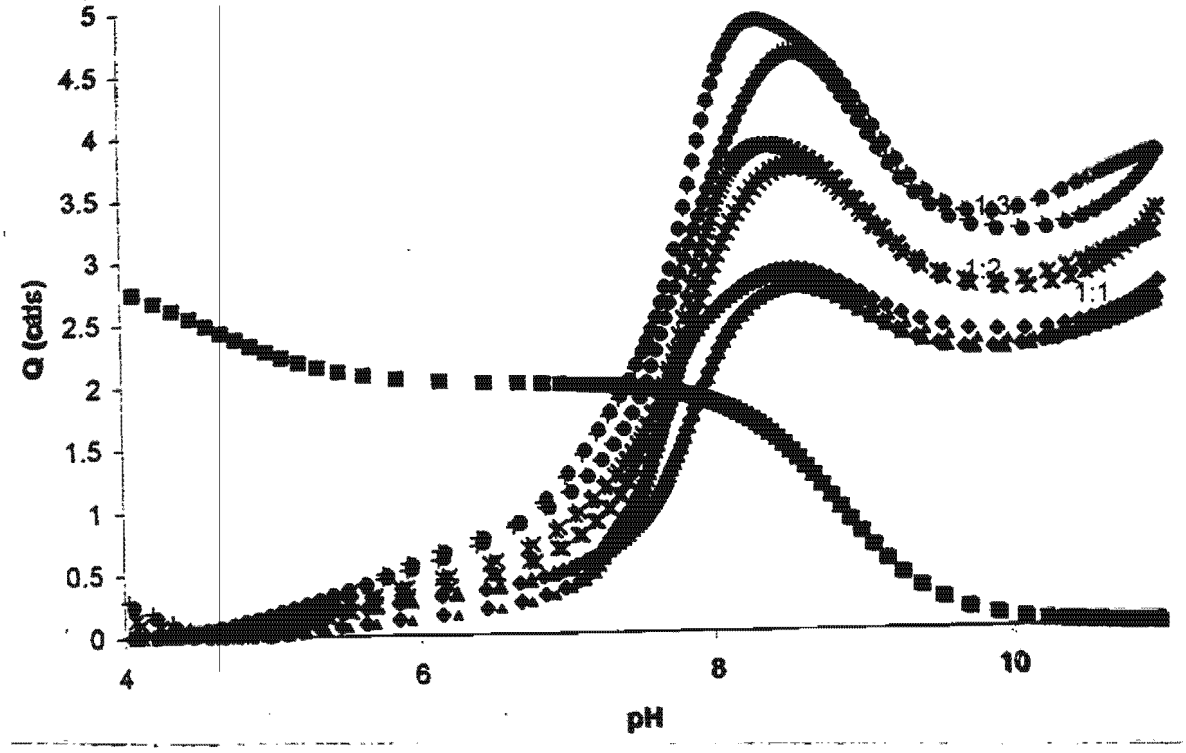

Deprotonation Function Curve ($Q_M$obs) Zn^{2+}-ZDA

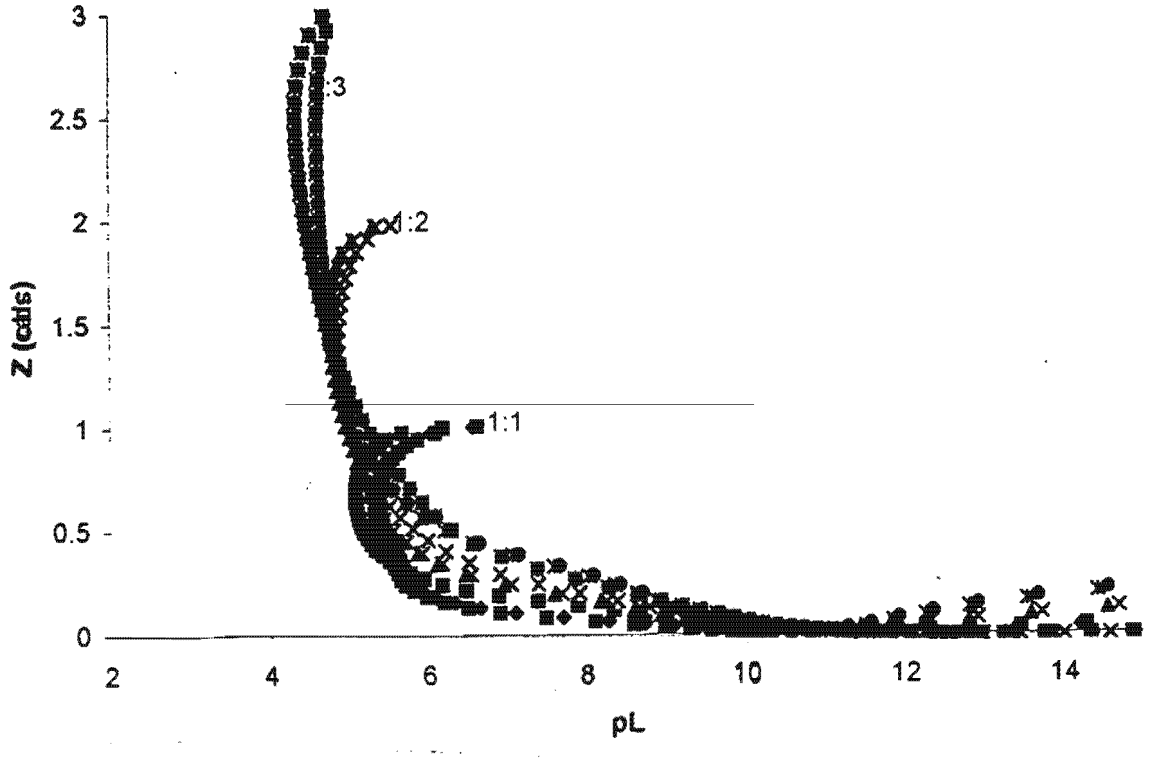

Species Distribution Diagram Zn^{2+}- ZDA

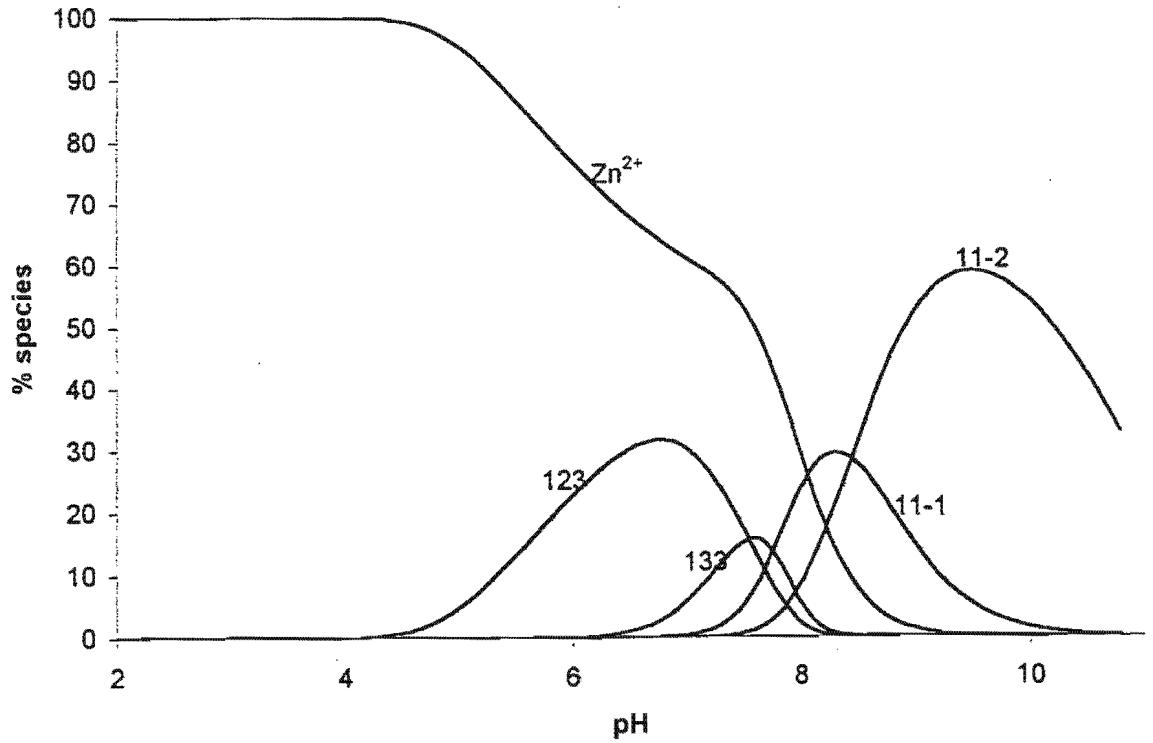

Species Distribution Diagram Zn^{2+}-EDA

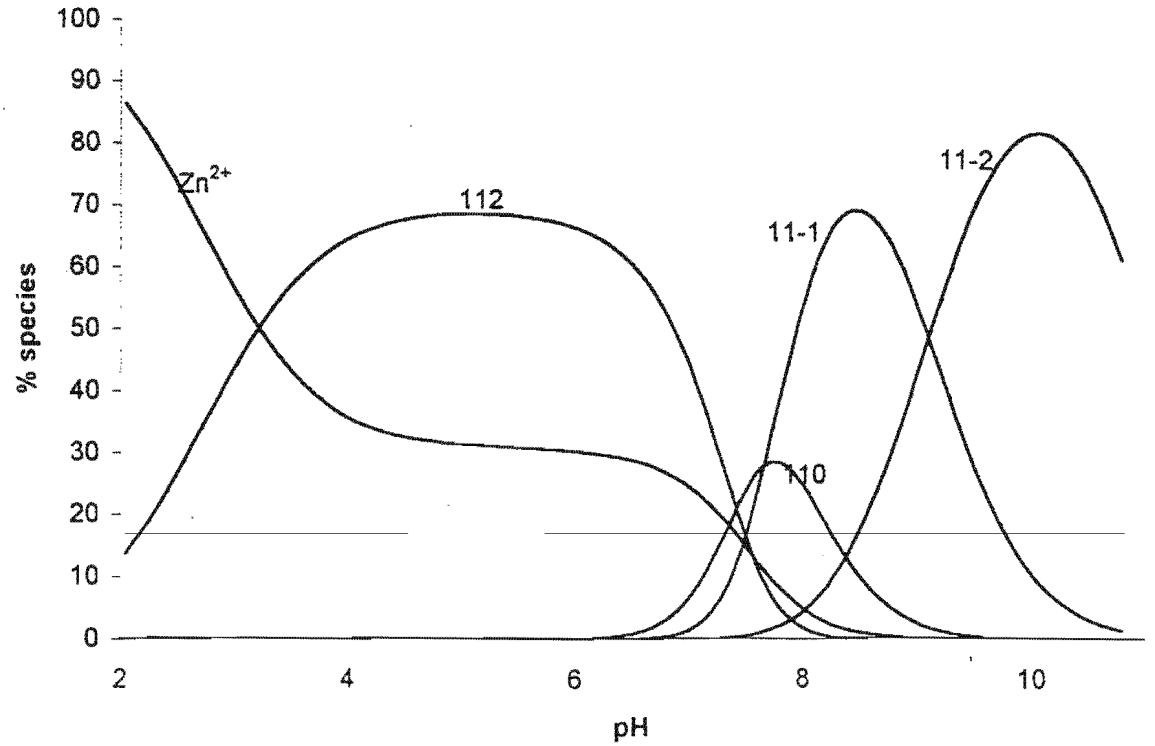

Formation Function Curve ($Z_M$obs) Zn^{2+}-EDA

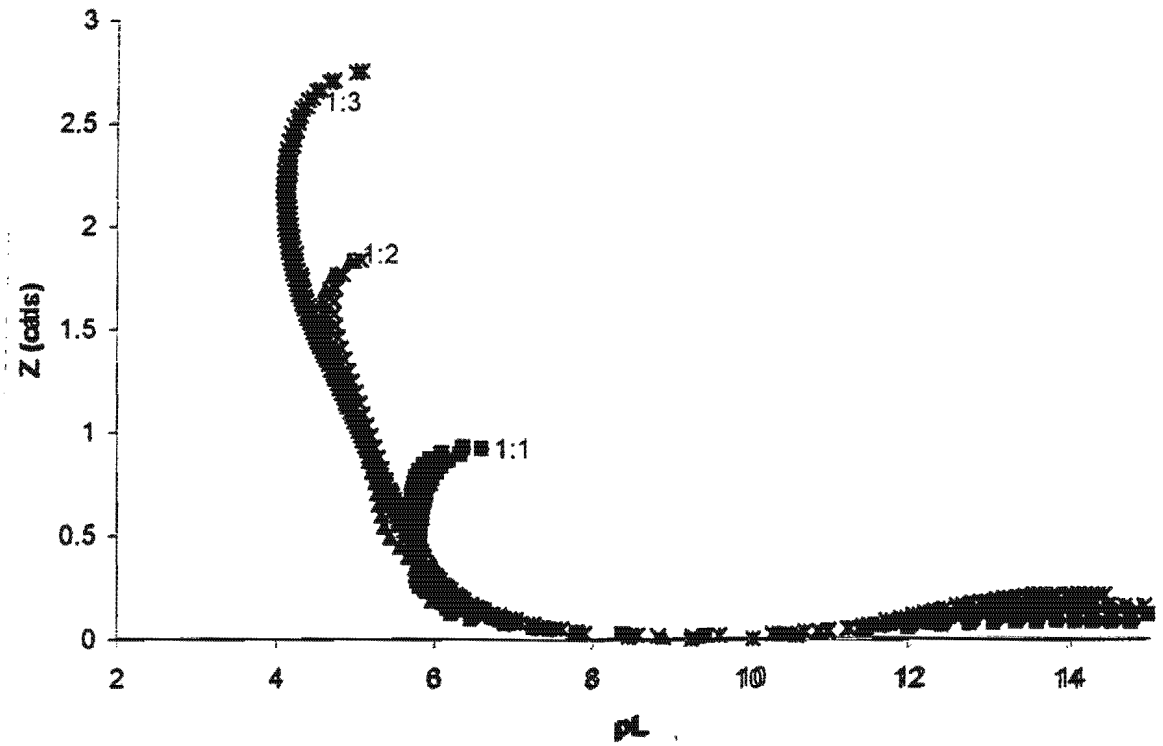

Deprotonation Function Curve ($Q_M$obs) Zn^{2+}-EDA

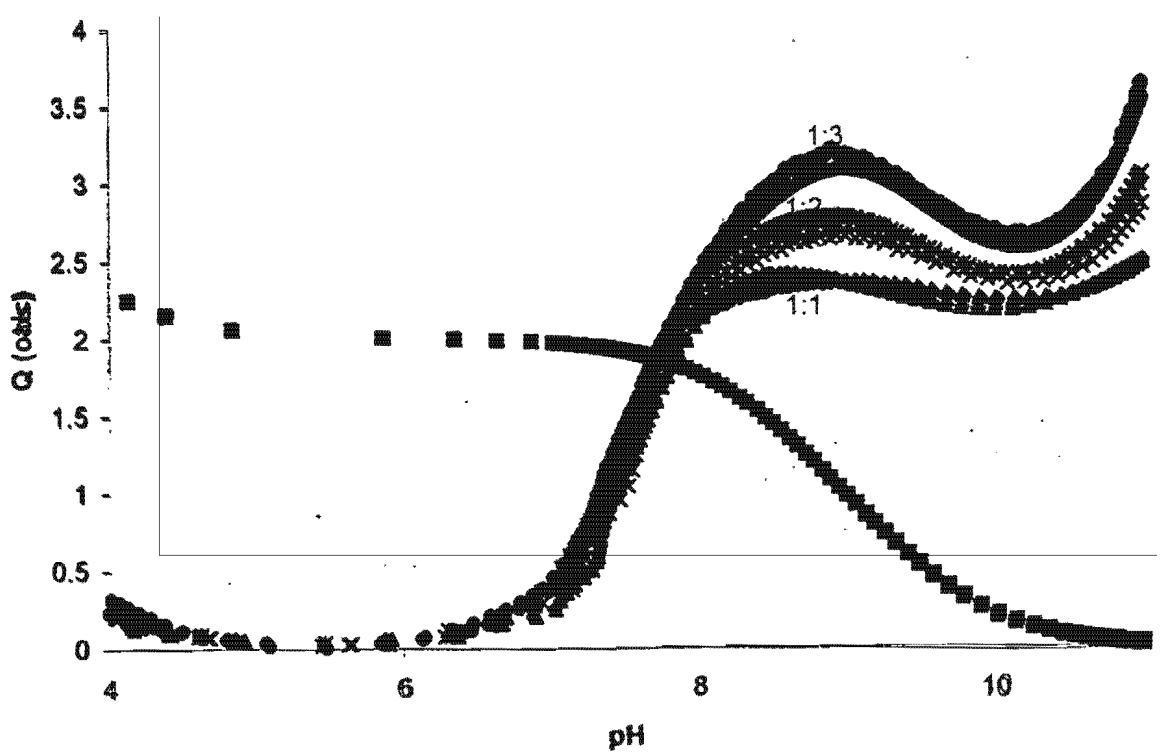

Formation Function Curve ($Z_M$obs) Zn^{2+}-DME

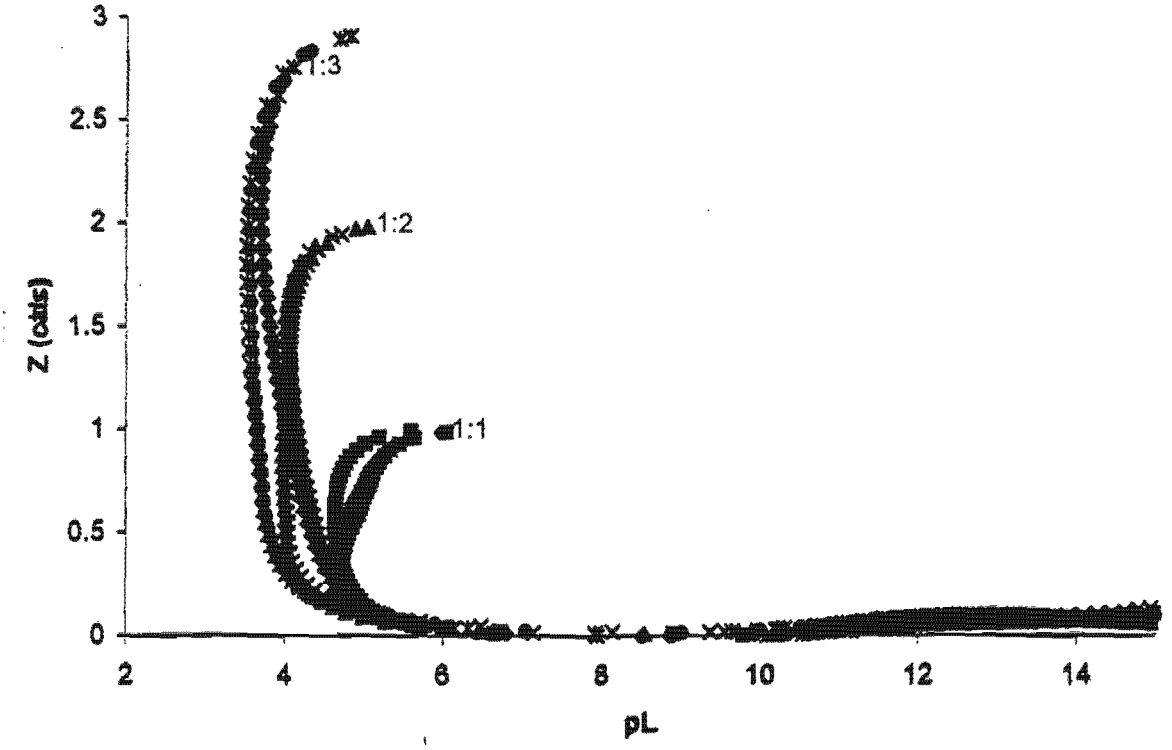

Deprotonation Function Curve ($Q_M$obs) Zn^{2+}-DME

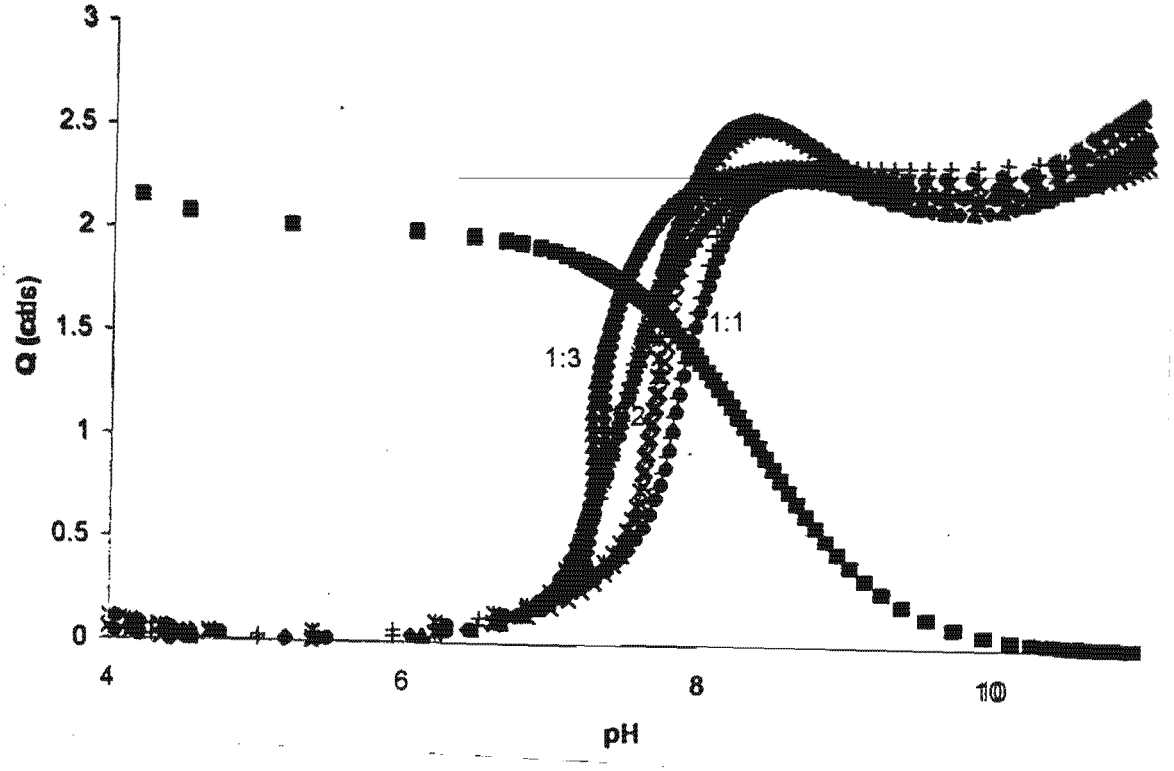

Species Distribution Diagram Zn^{2+}-DME

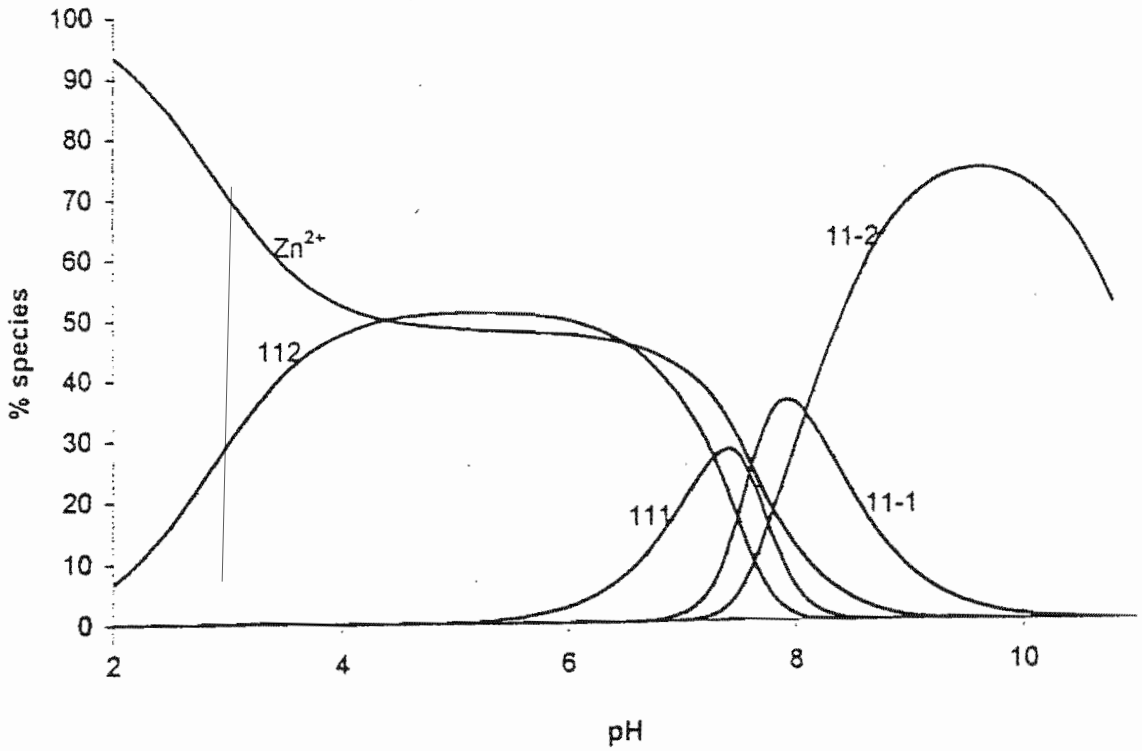

Species Distribution Diagram Ca^{2+}-BID

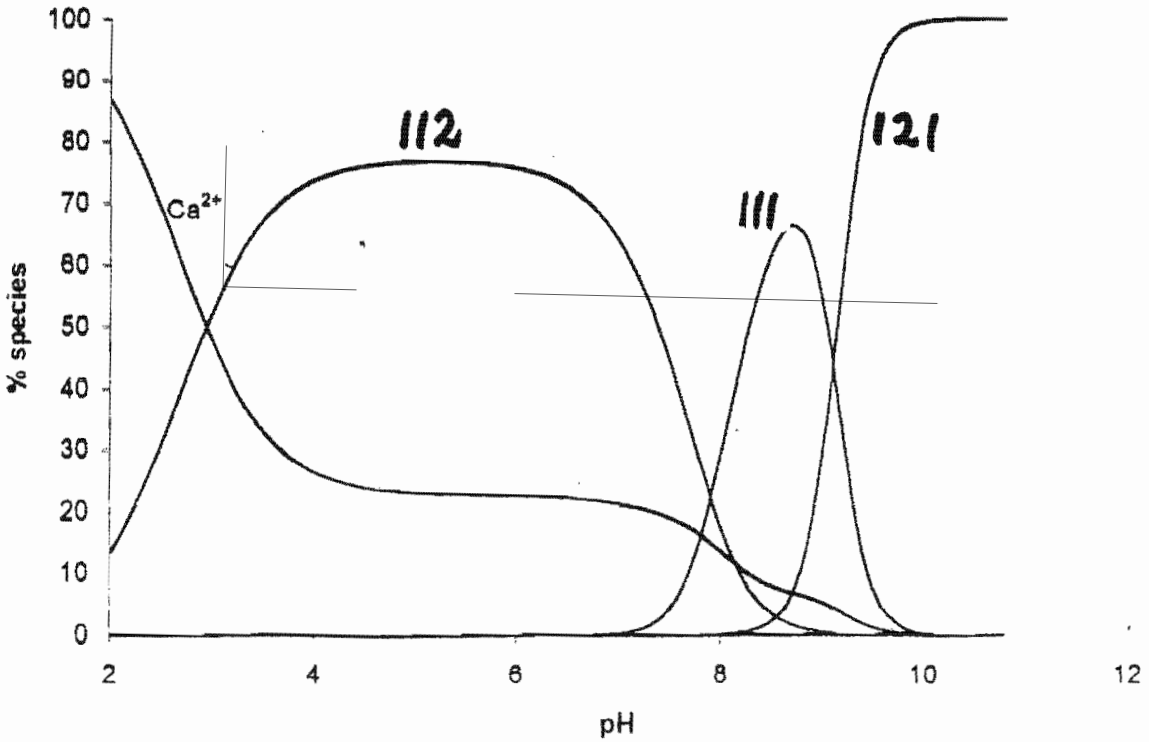

Formation Function Curve ($Z_M$obs) Ca^{2+}-BID

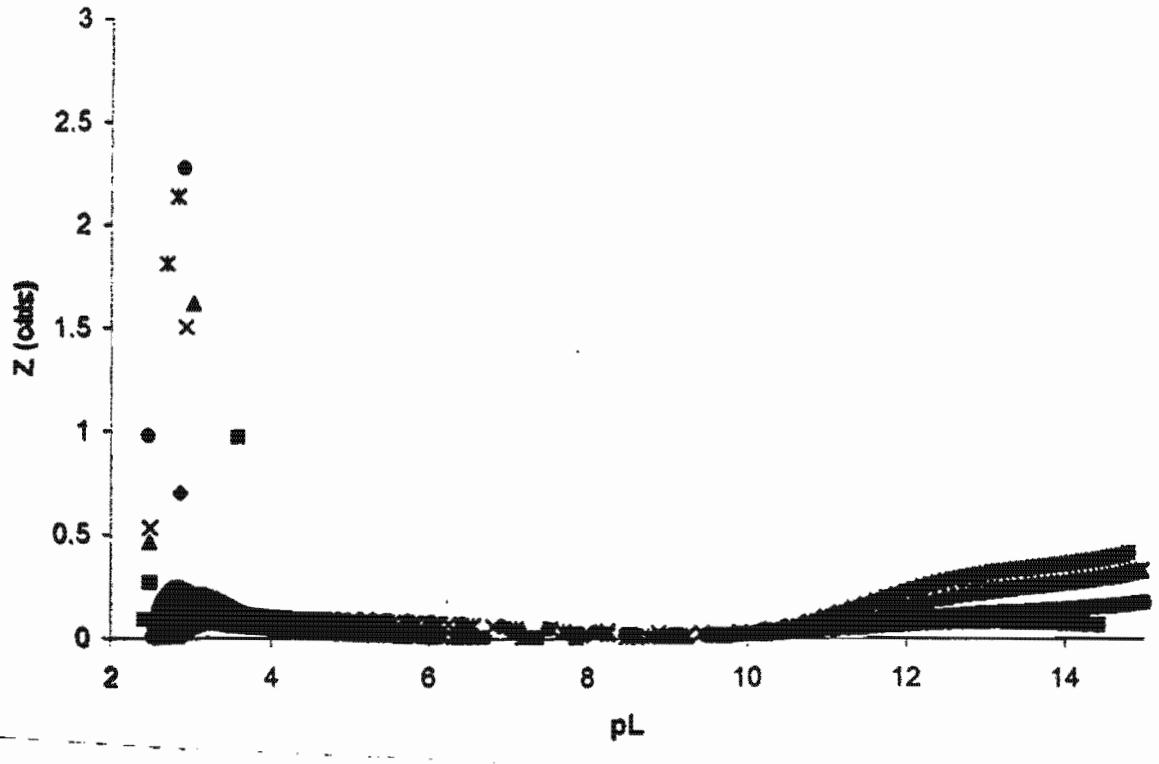

Deprotonation Function Curve ($Q_M$obs) Ca^{2+}-BID

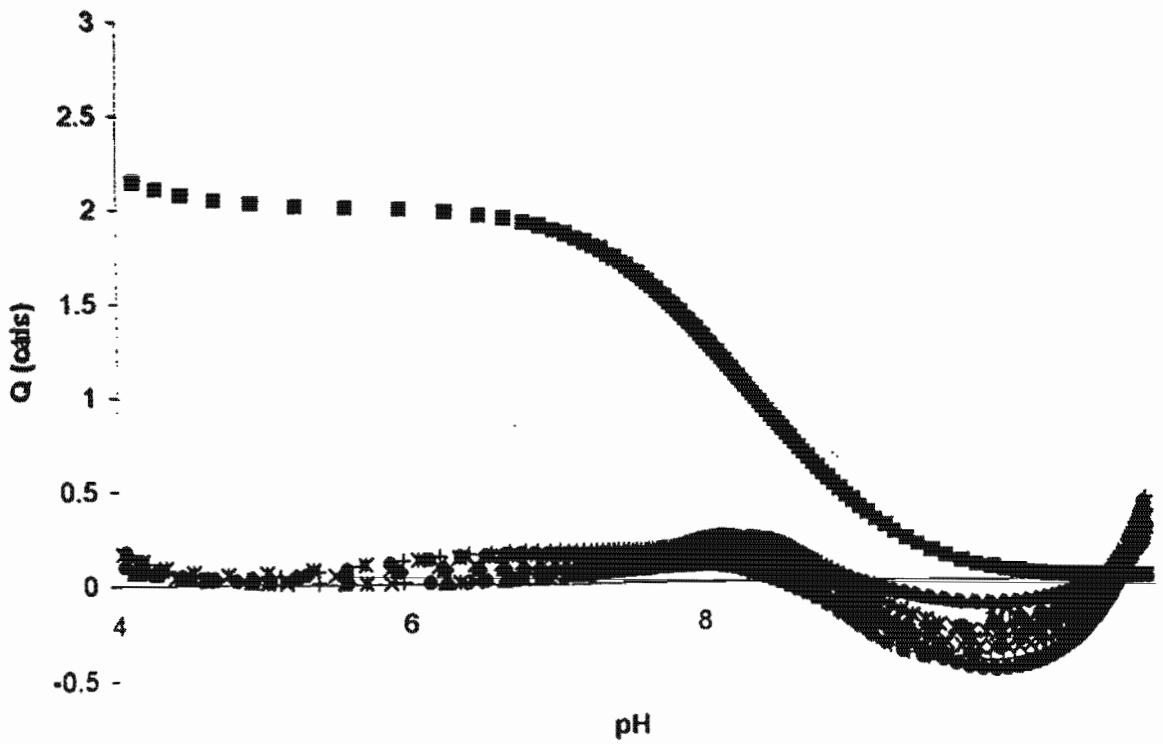

Formation Function Curve ($Z_M$obs) Ca^{2+}-EDA

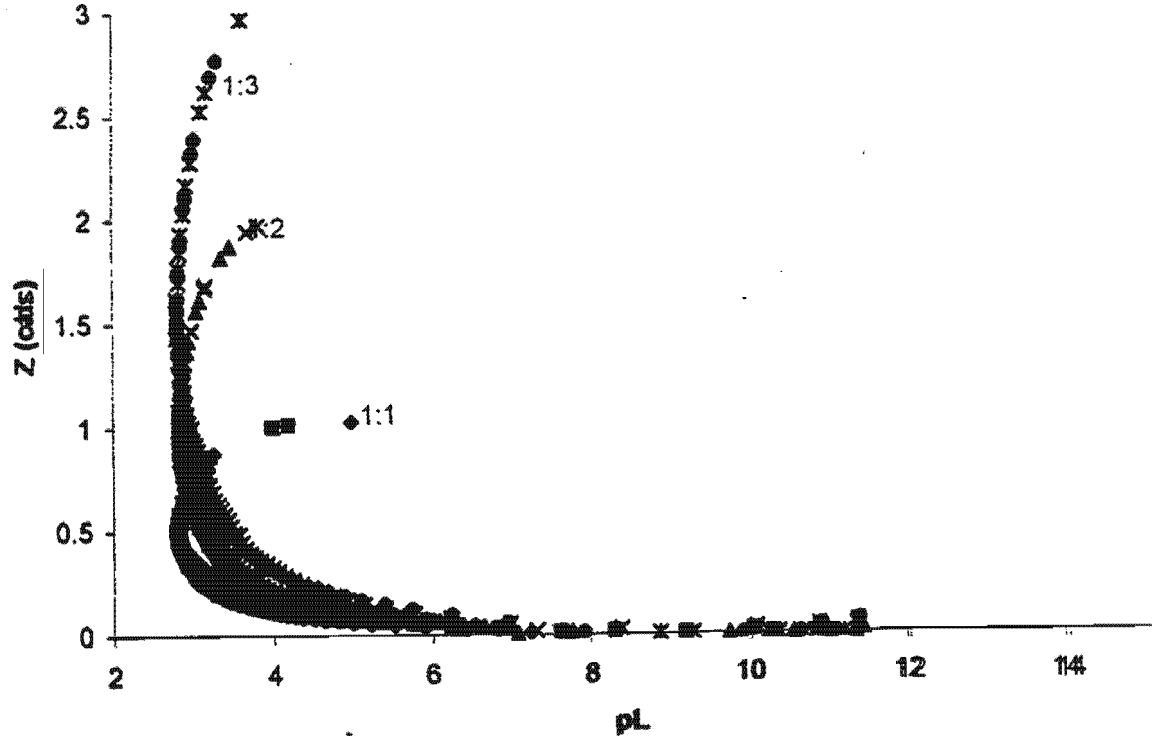

Deprotonation Function Curve ($Q_M$obs) Ca^{2+}-EDA

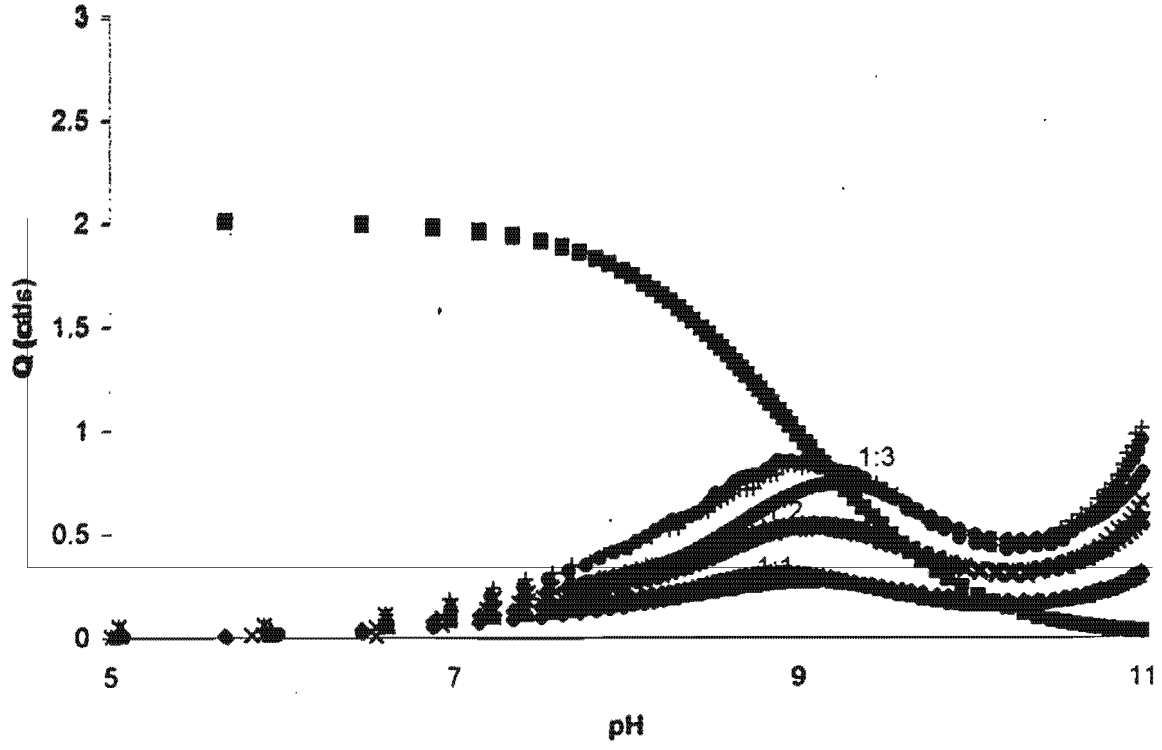

Species Distribution Diagram Ca^{2+}-EDA

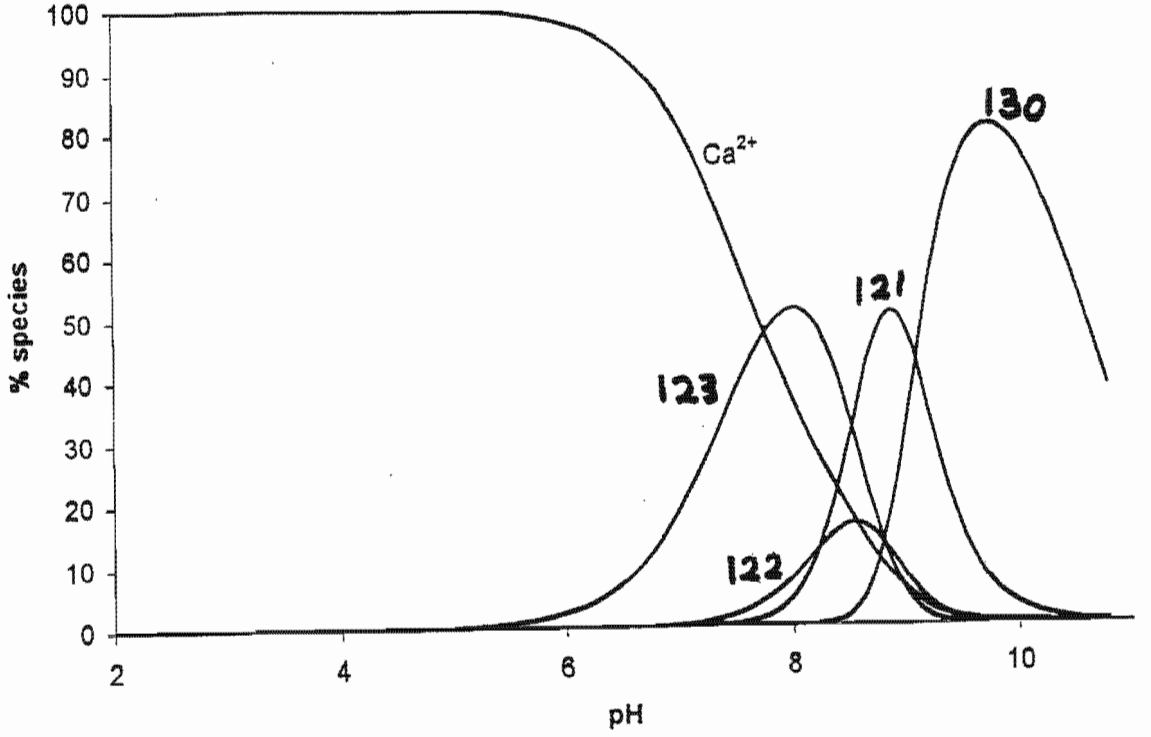

Species Distribution Diagram Ca^{2+}-DME

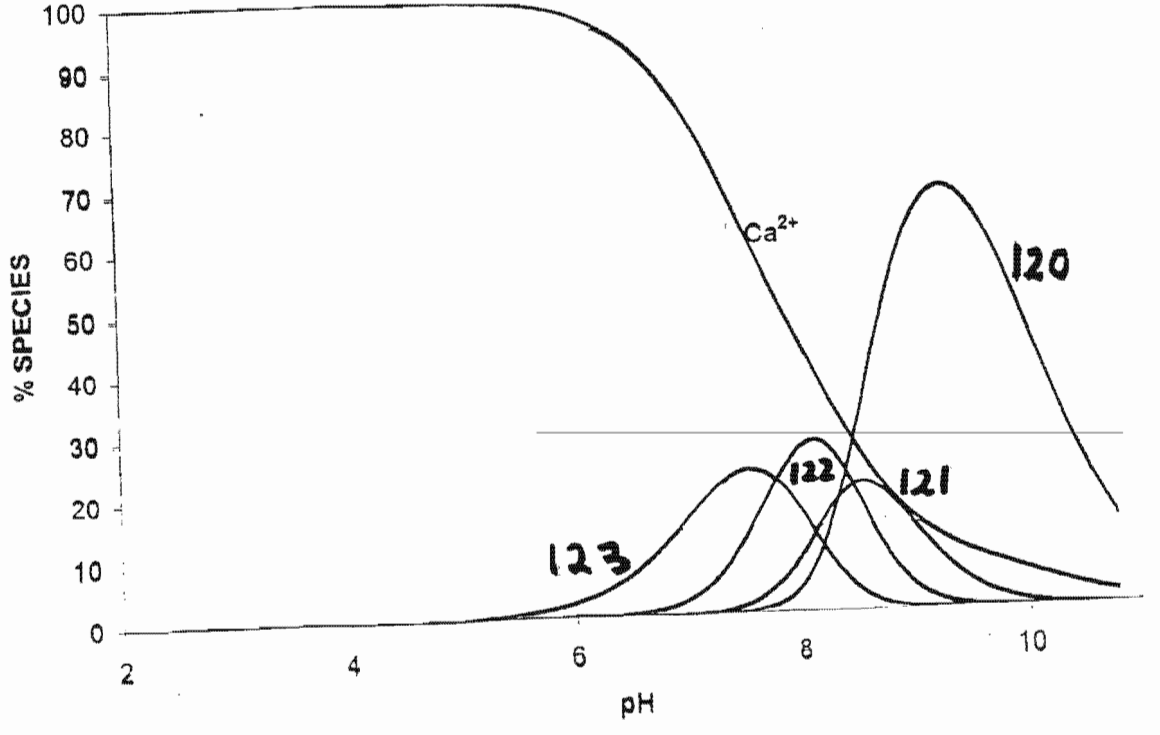

Formation Function Curve ($Z_M$obs) Ca^{2+}-DME

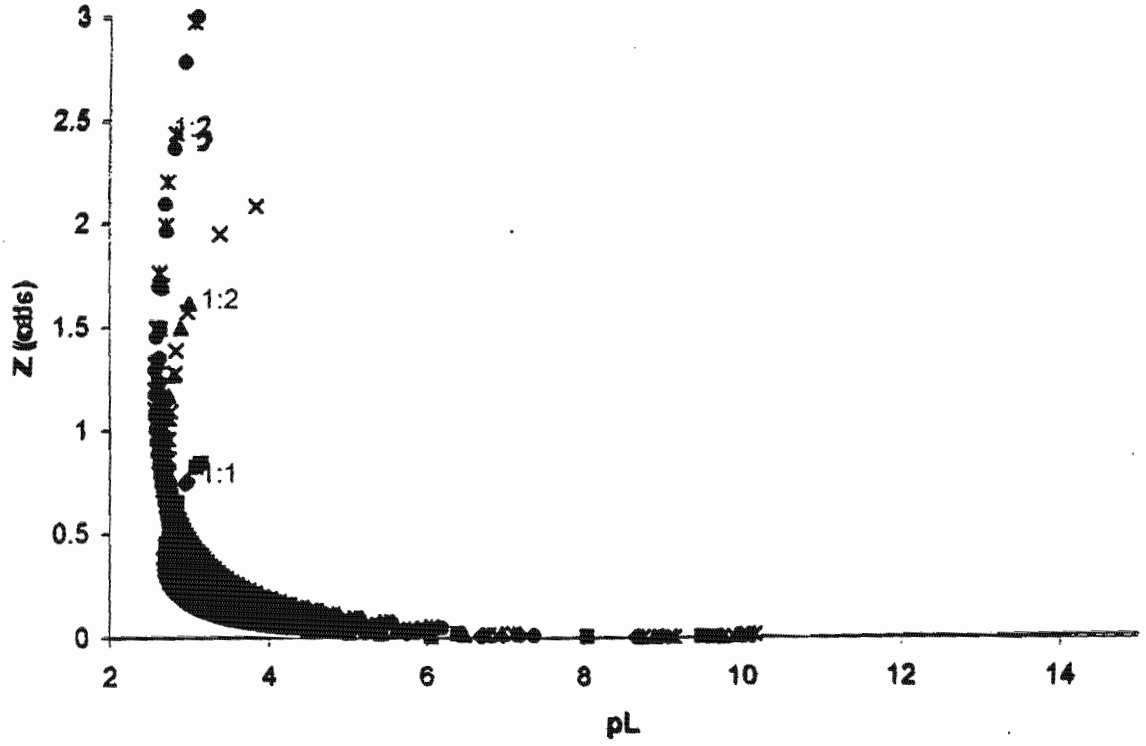

Deprotonation Function Curve ($Q_M$obs) Ca^{2+}-DME

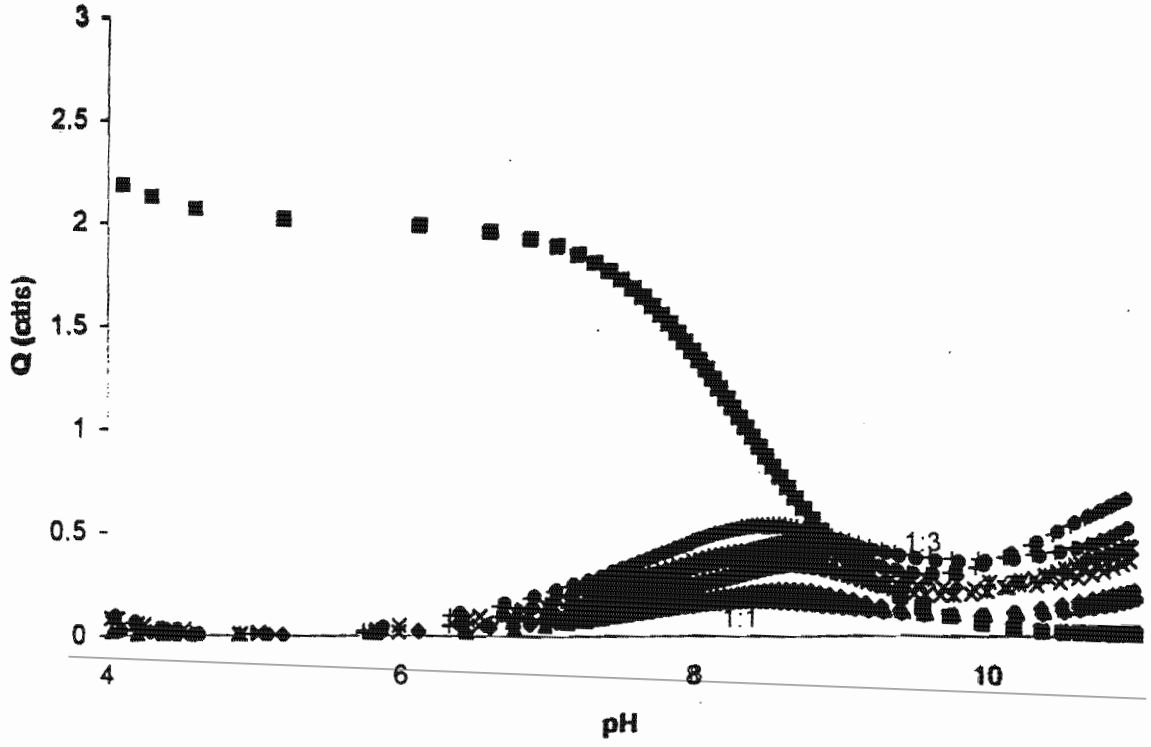

APPENDIX B

Absorption Spectrum of Cu^{2+}-EDA (1:1, Cu^{2+}:EDA) system over 2-11 pH range.

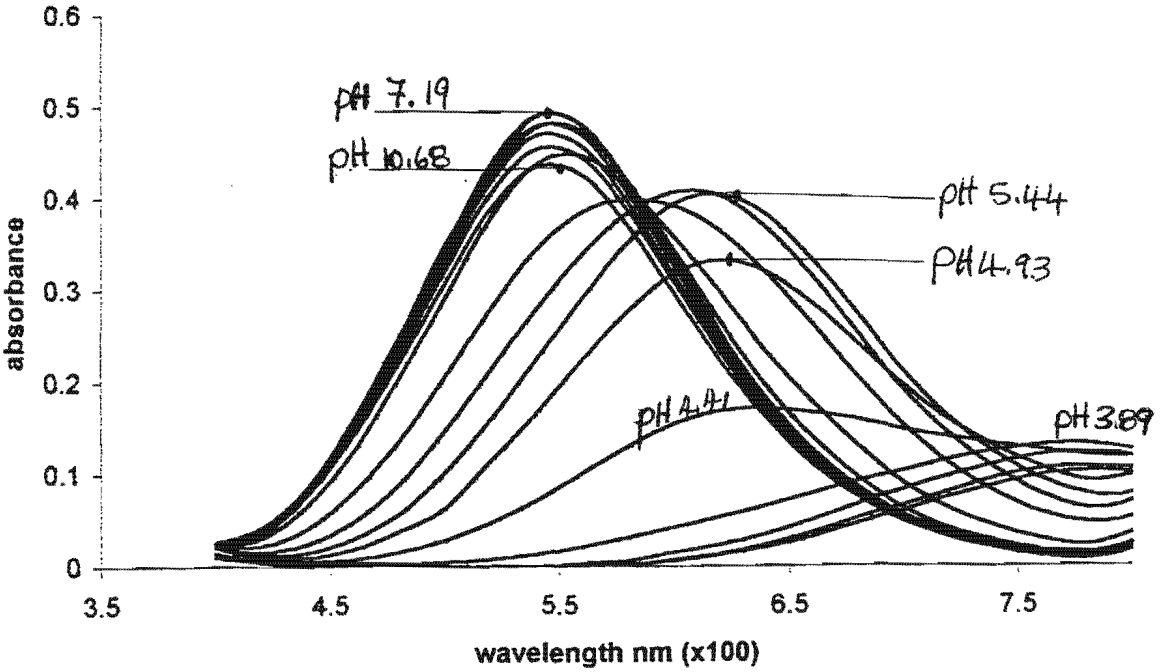

Absorption Spectrum of Cu^{2+}-DME (1:1, Cu^{2+}:DME) system over 2-11 pH range.

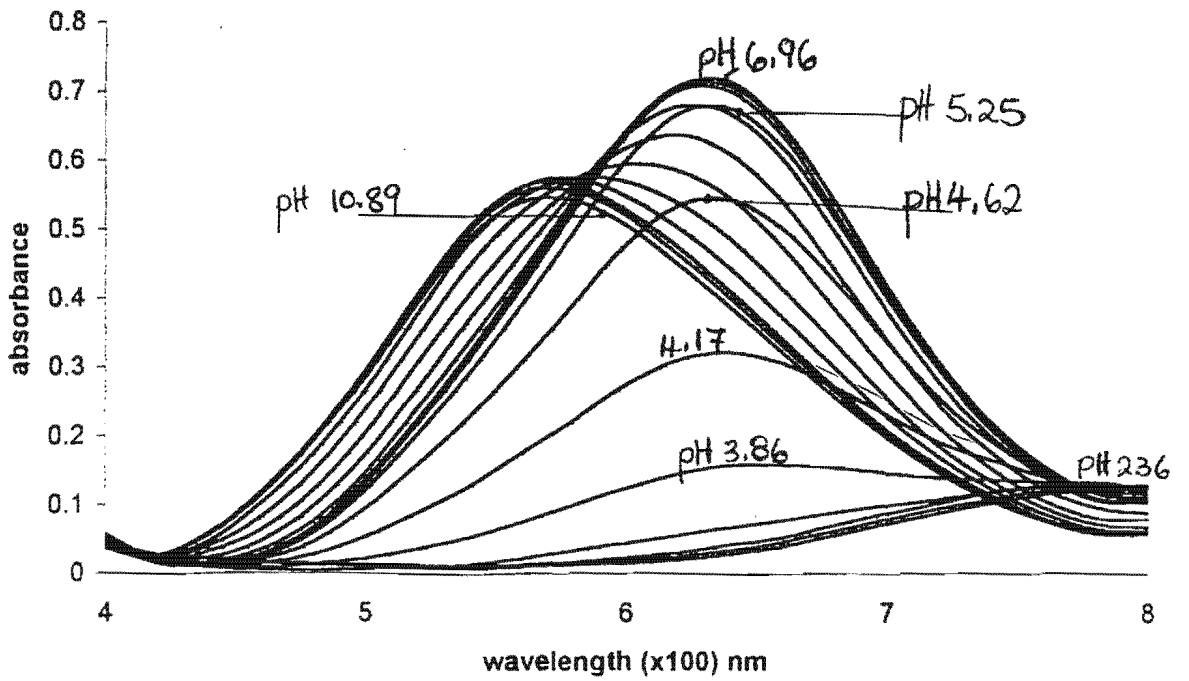

Absorption Spectrum of Cu^{2+}-IDA (1:1, Cu^{2+}:IDA) system over 2-11 pH range.

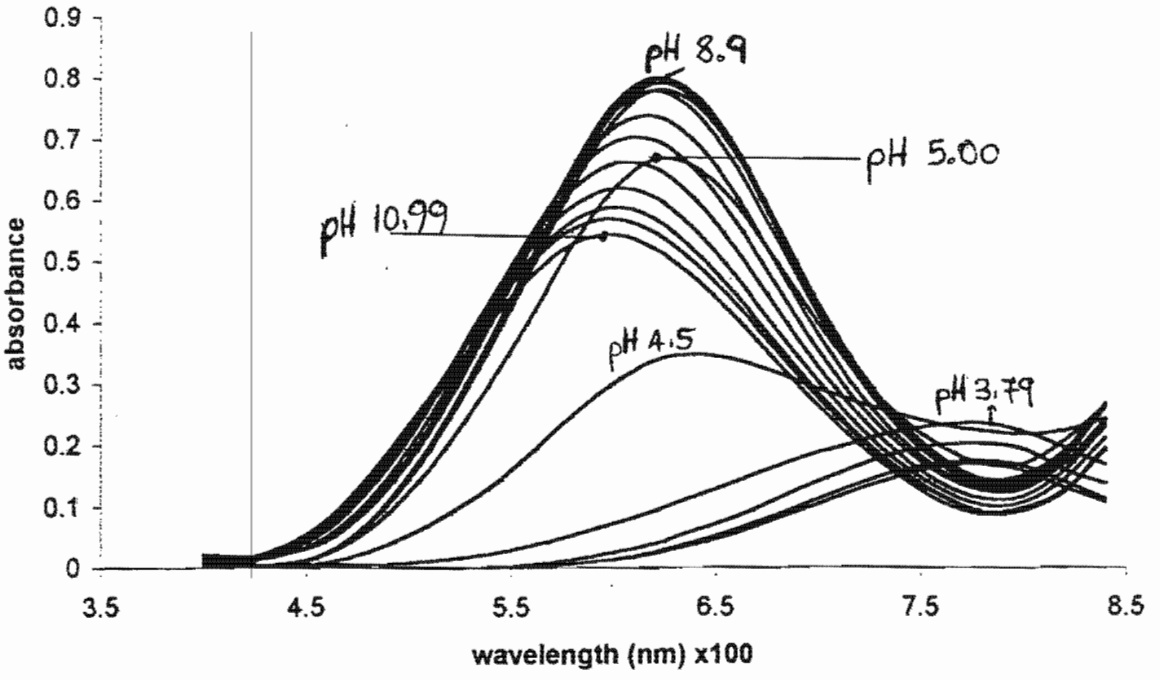

Absorption Spectrum of Cu^{2+}-BID (1:1, Cu^{2+}:BID) system over 2-11 pH range.